Manuscript type: Resource

Title: Differentiation latency, cell division symmetry, and dormancy signatures define fetal liver HSCs at single cell resolution

Authors & Affiliations:
Takashi Ishida[1], Juliane Mercoli[1], Adam M. Heck[1], Ian Phelps[2], Barbara Varnum-Finney[1], Stacey Dozono[1], Cynthia Nourigat-McKay[1], Katie Kraskouskas[1], Rachel Wellington[1], Olivia Waltner[1,3], Dana L Jackson[3], Colleen Delaney[1,4,5], Shahin Rafii[6], Irwin D. Bernstein[1,5], Kimberly A. Aldinger[2,7,8], Birth Defects Research Laboratory (BDRL)[2], Cole Trapnell[3], Helong G. Zhao[1]*, and Brandon Hadland[1,5]*

1. Translational Science and Therapeutics Division, Fred Hutchinson Cancer Center, Seattle, WA, USA.
2. Department of Pediatrics, University of Washington, Seattle, WA
3. Department of Genome Sciences, University of Washington, Seattle, WA, USA.
4. Deverra Therapeutics, Seattle, WA, USA
5. Division of Pediatric Hematology/Oncology, University of Washington, Seattle, WA, USA
6. Division of Regenerative Medicine, Ansary Stem Cell Institute, Department of Medicine, Weill Cornell Medicine, New York, NY, USA.
7. Department of Neurology, University of Washington, Seattle, WA
8. Norcliffe Foundation Center for Integrative Brain Research, Seattle Children's Research Institute, Seattle, WA

*Co-corresponding authors:
Brandon Hadland, M.D, Ph.D.
Fred Hutchinson Cancer Research Center, 1100 Fairview Ave N., Seattle, WA 98109, USA (bhadland@fredhutch.org), Tel: 206.667.1095, Fax: 206.667.6084
Helong G. Zhao, Ph.D.
Fred Hutchinson Cancer Research Center, 1100 Fairview Ave N., Seattle, WA 98109, USA (hzhao2@fredhutch.org)

Summary: 188 words
Manuscript: 7,126 words
Figures: 7; Supplementary Tables: 10; Supplementary Figures: 14

Keywords: hematopoietic stem cell; HSC, fetal liver; FL, multipotent progenitor; MPP, developmental hematopoiesis, niche, microenvironment, single-cell RNA sequencing, self-renewal, differentiation, clonal analysis, cell division symmetry

Summary

Decoding the gene regulatory mechanisms and signaling interactions that orchestrate the self-renewal of hematopoietic stem cells (HSCs) during their expansion in the fetal liver (FL) could unlock novel therapeutic strategies to expand transplantable HSCs, a long-standing challenge. Here, to explore intrinsic and extrinsic regulation of FL-HSC self-renewal at the single cell level, we engineered a culture platform designed to recapitulate the FL endothelial niche, which supports the ex vivo amplification of serially engraftable HSCs. Leveraging this platform in combination with single cell index flow cytometry, live imaging, serial transplantation assays, and single cell RNA-sequencing, we uncovered previously unrecognized heterogeneity within immunophenotypically defined FL-HSCs. Specifically, we demonstrated that differentiation latency, symmetric cell divisions, and transcriptional signatures of biosynthetic dormancy and lipid metabolism are distinguishing properties of rare FL-HSCs capable of serial, long-term multilineage hematopoietic reconstitution. Our findings support a paradigm in which intrinsic programs and extrinsic signals combinatorially facilitate the symmetric self-renewal and expansion of nascent HSCs in the FL niche while delaying their active participation in hematopoiesis. Additionally, our study provides a valuable resource for future investigations into the intrinsic and niche-derived signaling pathways that govern FL-HSC self-renewal.

Introduction

Hematopoietic stem cells (HSCs) have the distinguishing properties of life-long self-renewal and the ability to reconstitute multilineage hematopoiesis upon transplantation. Understanding the biology of HSC development is essential to unlocking methods for de novo HSC generation and expansion to facilitate advances in hematopoietic stem cell transplantation, gene therapies, and disease modeling for blood and immune disorders.

Following their initial emergence in embryonic arteries, HSCs seed the fetal liver (FL), where they have conventionally been thought to both rapidly expand (generating sufficient HSCs to sustain life-long hematopoiesis in the adult) and differentiate (generating mature blood cells essential to support the developing embryo). To facilitate these processes, FL-HSCs have been postulated to exist in a state of proliferative and biosynthetic activation during prenatal development, followed by a transition to a state of biosynthetic dormancy and cell cycle quiescence upon their migration to the bone marrow (BM) perinatally.[1,2]

Several elegant studies using methodologies to track the fate of nascent HSCs and progenitors through development have recently called for a revision of this classical paradigm of developmental hematopoiesis. These studies suggest that distinct waves of HSC-independent progenitors also seed the fetal liver and serve as the primary source of mature blood cells throughout prenatal development, with minimal contribution from HSCs, which are instead reserved to contribute primarily to adult hematopoiesis.[3] Further supporting this novel paradigm, we and others have uncovered distinct ontogenies for oligopotent and even multipotent hematopoietic

84 progenitors that precede HSCs during various waves of endothelial to hematopoietic
85 transition in embryonic blood vessels.[3-5] While some HSC-independent progenitors
86 possess properties that overlap with HSCs, such as multilineage hematopoietic
87 activity, they are generally lacking in durable self-renewal capacity assayed by serial
88 transplantation, the gold standard methodology for defining functional HSCs of
89 relevance for translational applications.

90 Recent studies also suggest that the number of precursors emerging in the
91 embryo that contribute to hematopoiesis in the adult when traced in vivo is
92 substantially larger than the number of engraftable HSCs detected by direct
93 transplantation assays[6,7] and that this compartment of long-lived hematopoietic
94 precursors undergoes only limited expansion in the fetal liver.[8] Lineage barcoding
95 studies in vivo suggest significant heterogeneity in this pool of long-lived precursors
96 in the FL, identifying a distinct population of embryonic multipotent progenitors
97 (eMPPs) independent of HSC origin. Remarkably, eMPPs were found to contribute to
98 mature blood cells in the adult when traced in situ, but lack long-term engraftment
99 properties in transplantation assays essential to classify them as bona fide HSCs.[9] In
100 contrast, another study identified a subset of lymphoid-biased “developmentally-
101 restricted HSCs” in the FL possessing long-term engraftment upon transplantation,
102 yet failing to contribute to adult hematopoiesis in situ,[10] in line with previous work
103 identifying populations of FL-HSCs with distinct engraftment properties.[11]

104 Altogether, these reports highlight substantial heterogeneity of the HSCs
105 and HSCs-independent progenitors that seed the fetal liver in early gestation and
106 contribute to various aspects of hematopoiesis during prenatal development and into

adulthood. Though prior studies have identified surface markers that enable substantial enrichment of engraftable FL-HSCs by FACS to study their properties at a population level, no set of markers has been shown to achieve functional HSC purity. Thus, uncovering the unique phenotypic, functional, and molecular properties of the rare subset with long-term, multilineage engraftment capacity requires studies at a single cell level. Furthermore, a better understanding of how functionally engraftable HSCs undergo maturation and self-renewal in the fetal liver niche could provide insight into engineering more robust protocols for generation of engraftable HSCs in vitro.

To address these issues at single cell level, we developed a serum-free culture platform that mimics the FL vascular niche, which enabled ex vivo amplification of serially engrafting HSCs from individual immunophenotypic FL-HSCs isolated by FACS at early and mid-gestation in the mouse embryo. We leveraged this platform to study the heterogeneity of the FL-HSC compartment by integrating index flow cytometry, live imaging, single cell RNA-sequencing (scRNAseq), and transplantation assays, revealing the distinguishing properties of serially engraftable FL-HSCs and niche signals that contribute to their self-renewal. Altogether, these studies provide a valuable resource for ongoing efforts to understand the ontogeny of functionally transplantable HSCs and recapitulate their development and expansion ex vivo.

127 **Results**

128

129 **Establishment of a clonal HSC amplification platform reveals unique properties**

130 **of serially engrafting FL-HSCs**

131 Aiming to study FL-HSCs at single cell resolution, we first sought to define

132 an immunophenotype sufficient to highly enrich for long-term engrafting HSC activity

133 in both the early (embryonic day (E) 13.5) and mid-gestation (E15.5/16.5) FL at the

134 population level. Using stringent gating for known FL-HSC markers, Endothelial Cell

135 Protein C Receptor (EPCR) and Stem Cell Antigen-1 (SCA1),[12-15] we found that

136 $CD45^{+}DAPI^{-}GR1^{-}F4/80^{-}SCA1^{high}EPCR^{high}$ immunophenotype (hereafter denoted

137 SE^{hi}) efficiently excluded cells expressing other lineage markers as well as CD48,

138 allowing us to simplify the sorting methodology for immunophenotypic FL-HSCs

139 (Figures S1A and B). Since CD150 is not a specific marker of embryonic HSCs until

140 E14.5,[16-18] we excluded CD150 from these initial studies encompassing the early FL.

141 As expected, the SE^{hi} population from both the early and mid-gestation FL provides

142 long-term, multilineage hematopoietic engraftment following transplantation into

143 congenic strain adult mice (Figure S1C).

144 Next, to evaluate functional heterogeneity within the immunophenotypically

145 defined SE^{hi} FL-HSC fraction at the single cell level, we established a coculture

146 platform recapitulating the FL endothelial niche (Figure 1A). Briefly, FL-derived

147 endothelial cells (ECs) were transduced with a lentivirus encoding constitutively

148 active AKT1 (myristoylated AKT1; MyrAKT) (henceforth “FL-AKT-ECs”), which

149 enables EC propagation in serum-free culture while maintaining their endogenous

150 properties, as previously described.[19,20] We first tested immunophenotypically
151 defined HSCs isolated from E15.5/16.5 FL, a developmental stage when engrafting
152 HSCs are most abundant in the FL and are further enriched based on CD150
153 expression.[16,21] $SE^{hi}CD150^{+}$ FL-HSCs were individually index sorted into one well of
154 a 96 well-plate containing FL-AKT-ECs in serum-free media with hematopoietic
155 cytokines (SCF and TPO). In initial experiments, the formation of hematopoietic
156 colonies in coculture was monitored visually over time by microscopy, and a portion
157 of each colony at the time it was initially observed (day 7, 12, or 14) was harvested
158 by pipetting for flow cytometric analysis. Following coculture, most colonies
159 contained cells retaining co-expression of HSC markers EPCR and SCA1 (Figure
160 1B), suggesting maintenance and expansion of HSCs from single SE^{hi} FL cells
161 during culture.[13,14,22] Interestingly, a subset of late-emerging colonies (detected on
162 day 12 and beyond) consisted nearly exclusively of HSC-like $SCA1^{+}EPCR^{+}$ cells,
163 suggesting slower cell cycle kinetics, symmetric expansion, and differentiation
164 latency of this subset during EC coculture (Figure 1B, left panel; Figure S1D). In
165 contrast, most colonies detectable at day 12 and earlier consisted of a mixed
166 population of $SCA1^{+}EPCR^{+}$ HSC-like cells and cells lacking SCA1 and/or EPCR
167 consistent with differentiation to hematopoietic progenitors (Figure 1B, right panel;
168 Figure S1D). These studies reveal significant heterogeneity of immunophenotypic
169 $CD150^{+}SE^{hi}$ FL-HSC behavior when assayed at the single cell level, suggesting
170 intrinsic differences in proliferative potential and propensity for self-renewal verses
171 differentiation during FL-AKT-EC coculture. So as not to exclude late-emerging
172 colonies, colonies were harvested between day 12 and 15 for subsequent

173 experiments.

174 Next, the functional engraftment properties of the progeny of single
175 E15.5/16.5 $SE^{hi}CD150^{+}$ FL-HSCs following coculture was assessed by correlating
176 their immunophenotype (using 50% of cells) with serial transplantation (using the
177 remaining 50% of cells). Although at least short-term engraftment was observed from
178 most colonies tested, colonies providing serial engraftment were exclusively from the
179 subset consisting of nearly homogenous $SCA1^{+}EPCR^{+}$ HSC-like cells (Figure 1C-D).
180 Similar results were observed when assessing single SE^{hi} cells from the early E13.5
181 FL in FL-AKT-EC coculture (Figure 2A), with serial engraftment detected only from a
182 subset of colonies consisting predominantly (>80%) of $SCA1^{+}EPCR^{+}$ cells (Figure
183 2B), which we hereafter refer to as "HSC-like colonies." At both developmental
184 stages, HSC-like colonies contained nearly 100-fold lower average number of total
185 hematopoietic ($CD45^{+}$) cells compared with other colony types (Figure 2C),
186 consistent with relatively lower cell division kinetics. Notably, HSC-like colonies were
187 less frequently generated from SE^{hi} FL cells at E13.5 (mean 17.8% of total SE^{hi} cells
188 sorted) compared with E15.5/16.5 (mean 37.9% of total SE^{hi} cells sorted) (Figure
189 2D). Unlike at E15.5/16.5, E13.5 FL SE^{hi} cells with HSC-like colony potential did not
190 consistently express CD150 (Figures 2E, S1E-F). ESAM (endothelial cell adhesion
191 molecule), another HSC marker,[23] was expressed ubiquitously in FL SE^{hi} cells and
192 thus failed to enrich for HSC-like colony potential at either E13.5 or E15.5/E16.5
193 (Figures 2E, S1E-F).

194 Across multiple independent experiments, the average frequencies of HSC-
195 like colonies generated was: 1 in 5.7 index sorted SE^{hi} cells at E13.5 (range 1 in 4.7

196 to 1 in 6.5, n=3 experiments) and 1 in 2.3 index sorted $SE^{hi}CD150^{+}$ cells at
197 E15.5/16.5 (range 1 in 1.7 to 1 in 4.3, n=5 experiments). Notably, this latter
198 frequency is similar to a previous study, which reported an HSC frequency of 1 in 2.7
199 $CD150^{+}CD48^{+}Sca1^{+}Lineage^{-}Mac\text{-}1^{+}$ cells in the E14.5 FL, based on detection of
200 multilineage engraftment at 16 weeks after limiting dilution transplantation in primary
201 recipients.[16] By more rigorously testing for self-renewing HSC potential by serial
202 transplantation, our current studies suggest the true frequency of bona fide HSCs is
203 significantly lower than that observed by assessing primary transplantation only,
204 which may include short-term engrafting populations. Measuring HSC potential
205 based on serial engraftment, we predict FL-HSC frequency to be approximately 1 in
206 17 SE^{hi} cells at E13.5 and 1 in 5.8 $SE^{hi}CD150^{+}$ FL cells at E15.5/16.5. Together,
207 these studies suggest significant heterogeneity in functional engraftment capacity in
208 even the most stringently immunophenotypically defined FL-HSC populations.
209

210 **Maintenance of ESAM expression identifies HSC-like colonies with serial**
211 **engraftment potential**

212 Since the $SCA1^{+}EPCR^{+}$ HSC-like colonies remain heterogeneous in their
213 engraftment properties (Figure 1D, 2B), we next sought to identify additional surface
214 proteins that may serve as predictive markers of their serial engraftment capacity.
215 Although ESAM was ubiquitously expressed on fresh SE^{hi} FL cells independent of
216 HSC potential (Figure 2E, Figures S1E-F), we hypothesized that maintenance of
217 ESAM expression following in vitro culture might identify $SCA1^{+}EPCR^{+}$ HSC-like
218 colonies with serial engraftment based on prior studies suggesting ESAM as a

219 marker of HSC activity in vitro.[13] To test this, we sorted single E15.5 $SE^{hi}CD150^{+}$ FL-
220 HSCs for coculture with FL-AKT-EC (Figure 3A). Following coculture, we observed
221 heterogeneity of ESAM expression amongst identified $SCA1^{+}EPCR^{+}$ HSC-like
222 colonies (Figure 3B). When we transplanted the remaining cells from each of these
223 HSC-like colonies, we observed long-term, serial multilineage engraftment in HSC-
224 like colonies containing predominantly (>60%) $ESAM^{+}$ cells (hereafter referred to as
225 $ESAM^{+}$ HSC colonies), but not from HSC-like colonies containing predominantly
226 $ESAM^{-}$ cells (Figures 3B and 3C). In an independent experiment from E15.5
227 $SE^{hi}CD150^{+}$ FL-HSCs, ESAM expression in HSC-like colonies also predicted high
228 level donor engraftment of immunophenotypic HSCs ($Lin^{-}SCA1^{+}KIT^{+}CD150^{+}CD48^{-}$)
229 in bone marrow at 24 weeks post-transplant (Figure S2). Notably, when cells from an
230 individual $ESAM^{+}$ HSC colony were transplanted at limiting dilutions, secondary
231 engraftment was observed in multiple recipients, indicating the FL-AKT-EC niche
232 supported expansion of functional long-term $ESAM^{+}$ HSCs from single FL-HSCs
233 (approximately 15 serial-engrafting HSCs generated, range 5-43) (Figure S3).
234 Altogether, these studies establish a novel assay to assess the
235 immunophenotypic properties and engraftment potential of FL-HSCs at single cell
236 resolution in a developmentally relevant ex vivo niche. Specifically, this approach
237 revealed functional heterogeneity in both the immunophenotypic E13.5 SE^{hi} and
238 E15.5/16.5 $SE^{hi}CD150^{+}$ FL-HSC populations at the single cell level based on their
239 differential capacity to generate serially engrafting $ESAM^{+}$ HSC colonies during FL-
240 AKT-EC coculture. Based on homogenous $ESAM^{+}SCA1^{+}EPCR^{+}$ immunophenotype
241 and clonal expansion of serially engrafting HSCs during FL-AKT-EC coculture, these

242 results further suggest that long-term engrafting FL-HSCs are distinctly characterized
243 by latency to differentiate toward progenitors and propensity for symmetric expansion
244 in our ex vivo assay. Remarkably, this differentiation latency and self-renewal
245 behavior of FL-HSCs in vitro is consistent with recent studies that have tracked
246 native FL-HSC fates in the FL niche in vivo.[3,9]
247
248 **Single cell RNA sequencing uncovers transcriptional heterogeneity in**
249 **immunophenotypically defined FL-HSCs**
250 In light of the functional heterogeneity of SE^{hi} FL-HSCs revealed by our
251 single cell assays above, we next sought to explore the corresponding transcriptional
252 heterogeneity of the immunophenotypic SE^{hi} FL-HSC population in the early-stage
253 FL, which may provide insight into the gene regulatory programs responsible for
254 observed differences in self-renewal and engraftment potential of cells in this
255 immunophenotypically homogenous population. To this end, we sorted SE^{hi} cells
256 from freshly isolated FL at E13.5 for scRNAseq (Figures 4A and S4A). After filtering
257 out poor quality cells, we obtained genome-wide transcriptome data for 338 cells.
258 Using the Monocle3 toolkit [24], we performed dimensionality reduction by uniform
259 manifold approximation and projection (UMAP) and unsupervised clustering by the
260 Louvain algorithm to identify distinct cell clusters (Figure 4B). E13.5 SE^{hi} cells
261 globally express *Procr* (EPCR), as expected, as well as other genes associated with
262 HSCs, such as *Hlf, Esam, Mecom*, *Fgd5*, *H19*, and *Cdkn1c,* and mostly lack
263 expression of genes associated with differentiating progenitors and mature blood
264 cells (Figures S4B and S4C). However, the expression levels of HSC-associated

265 transcripts varied among cell clusters across UMAP space, suggesting underlying
266 heterogeneity in the SE^{hi} population. Moreover, although this population is negative
267 for CD48 by flow cytometry (Figure S1A), we observed heterogenous expression of
268 *Cd48* transcript (Figure S4C). *Flt3* expression was also observed heterogeneously
269 (Figure S4C), which may imply presence of previously described eMPP[9] or
270 developmentally-restricted HSCs[10] (known to express *Flt3*) in the SE^{hi} population.
271 Furthermore, while FL-HSCs are generally thought to be proliferative,[1,25] we
272 observed substantial variability in the expressions of genes associated with cell cycle
273 activity within the immunophenotypically defined SE^{hi} FL-HSCs, including a distinct
274 population with low expression of cell cycle genes and low proliferation index, a
275 transcriptional measure of cell cycle activity (Figure S4D).

276 We next examined expression of gene-sets that characterize dormant and
277 serial-engrafting HSCs in adult BM across cell clusters in the SE^{hi} FL-HSC
278 scRNAseq data (Figure 4C, Table S1).[26-29] We observed a marked variation in the
279 expression levels of the adult HSC and dormancy-related gene-sets across the
280 population of SE^{hi} cells, with clusters exhibiting the highest dormancy-associated
281 gene-set scores predominantly localized to regions of UMAP with the lowest
282 expression of genes associated with active cell cycle state and low proliferation
283 index (Figures 4C, 4D and S4D). In contrast, genes characterizing activated
284 HSCs/MPPs in adult BM and MYC target genes that promote biosynthetic and cell
285 cycle activation were lower in this subset (Figure 4C, Table S1).[27,28,30] Interestingly,
286 the expression pattern of genes associated with diapause,[29,31] a reversible
287 embryonic state of dormancy unrelated to hematopoiesis, showed a similar pattern

288 to the HSC dormancy gene-set, as did genes associated with chemokine signaling
289 characteristic of dormant HSCs in adult BM[27] and a gene signature associated with
290 lipid metabolism and dormancy common to embryonic diapause and multiple adult
291 stem cell types[32] (Figure 4C, Table S1).

292 As an orthogonal validation, we carried out an analysis of the same dataset
293 using a Bayesian approach of latent variable modeling (LVM) and feature extraction
294 (MOFA-based framework, MuVI).[33-35] Using the aforementioned gene signatures as
295 the Bayesian priors in LVM, SE^{hi} FL-HSCs were embedded as two distinct islands of
296 cells in latent space (Figure S5A). The isolated minor island (cluster 2, 5, 7) was
297 composed of cells with strong association with serial-engrafting and dormant HSC
298 gene-set features, but negatively correlated with oxidative phosphorylation and
299 MYC-V1 target gene-set features (Figure S5B), supporting the heterogeneity of SE^{hi}
300 FL-HSC observed in our prior analysis.

301 To further characterize transcriptional heterogeneity of the
302 immunophenotypic population of FL-HSCs in an unbiased manner, we performed
303 gene module analysis across cell clusters to determine co-regulated genes (Figures
304 4E, S4E and Table S2). We identified two modules (#1 and #4) of genes with cluster-
305 specific expression patterns that are similar to dormant and serial-engrafting HSC
306 and diapause gene-sets (compare Figure S4E and Figure 4C). Consistent with this
307 observation, genes expressed in these modules include known HSC-specific genes
308 (e.g. *Hlf, Mecom, Mllt3*) (Table S2). Gene Ontology (GO) analysis of genes in these
309 two modules identified terms associated with dormancy in adult HSCs, including
310 stem cell population maintenance, lysosomal transport, protein targeting to

311 lysosome, and positive regulation of catabolic process.[25,36,37] In contrast, GO
312 analysis of genes in module 3 and module 7, which have non-overlapping
313 expression patterns to modules 1 and 4, identified terms associated with activated
314 metabolic and cell cycle states, such as DNA replication initiation,[38,39] ATP
315 biosynthetic process,[40,41] oxidative phosphorylation,[42-44] and translation[45,46] (Table
316 S2). Furthermore, gene-sets specifically related to the cellular metabolism of
317 activated HSCs and MPPs[27,47,48] exhibit similar cluster-specific expression patterns
318 to gene modules 3 and 7 (compare Figure S4E and Figure 4C). To independently
319 verify observed transcriptional heterogeneity in the early fetal liver HSC
320 compartment, we also analyzed published scRNAseq data from E12.5 FL.[49]
321 Extracting HSCs as described in the original article (Figures S6A and S6B), we
322 observed heterogeneity in proliferation index (Figure S6C), gene modules (Figures
323 S6D-F and Table S3) and gene-set scores for HSC self-renewal and dormancy-
324 related signatures (Figure S6G) analogous to that identified in our scRNAseq data.
325 We also performed scRNAseq on HSCs sorted from human FL samples using
326 stringent immunophenotypic markers ($CD34^+CD38^-CD45RA^-CD90^+EPCR^+$) and
327 observed heterogeneous clusters of human FL-HSCs characterized by differences in
328 dormancy-related gene signatures and lipid metabolism, similar to that observed in
329 murine FL-HSCs (Figure S7, Table S4).
330 Collectively, we here observed that immunophenotypically defined FL-HSCs
331 are transcriptionally heterogeneous in their biosynthetic and cell cycle activation
332 states, and we identified a subset exhibiting gene signatures overlapping with
333 dormant adult HSCs, embryonic diapause[29,31] and other dormant stem cell states,[32]

334 particularly those associated with lipid metabolism and lysosomal activity. These
335 results are consistent with our observation that the same immunophenotypic SE^{hi} FL-
336 HSCs exhibit heterogeneous self-renewal, proliferation, differentiation, and
337 engraftment properties revealed by single cell coculture in the FL-AKT-EC niche.
338 Furthermore, the distinct in vitro behavior of the subset of SE^{hi} FL-HSCs with serial
339 engraftment potential (lower proliferation, latency to differentiate, and relatively
340 homogenous $ESAM^{+}SCA1^{+}EPCR^{+}$ HSC immunophenotype) suggests that this
341 subset corresponds to cells in our scRNAseq data characterized by a transcriptional
342 state of relative biosynthetic dormancy and decreased proliferation index.
343

344 **Integrating single cell transcriptomics and transplantation assays from clonal**
345 **progeny of FL-HSCs identifies transcriptional signatures of self-renewing**
346 **HSCs with serial multilineage engraftment**

347 Based on our single cell transcriptomic analysis of freshly isolated SE^{hi} FL-
348 HSCs above, we hypothesized that the subset of HSC-like colonies arising from SE^{hi}
349 FL-HSCs possessing serial engraftment potential could also be distinguished by
350 transcriptional signatures of biosynthetic dormancy. To test this hypothesis, we
351 integrated scRNAseq into our ex vivo platform for clonal analysis of FL-HSCs (Figure
352 5A). Briefly, we index sorted single E13.5 FL SE^{hi} cells into a 96-well plate containing
353 FL-AKT-EC. Following coculture, a portion of each colony (15%) was used for
354 immunophenotyping by flow cytometry to identify HSC-like colonies for further
355 analysis (Figure S8A). A portion of the remaining cells from each of these colonies
356 was used for transplantation (10% per recipient, to three recipients per colony) and

357 for scRNAseq (55%). To minimize batch effects between colonies, we individually
358 labelled each colony with oligonucleotide-barcode-conjugated antibodies to
359 ubiquitous murine cell surface antigens such that cells from each colony could be
360 pooled for downstream steps of scRNAseq.[50] This approach allows us to correlate
361 the functional engraftment properties of each HSC-like colony to the unique
362 transcriptomes of cells in the colony, as well as to the prospectively collected
363 immunophenotype of the individually sorted E13.5 SE^{hi} FL-HSCs from which each
364 HSC-like colony was derived.

365 Using this approach, we found that most identified HSC-like colonies
366 contributed to short-term engraftment whereas colony #2 uniquely contained long-
367 term, multilineage engrafting HSCs by serial transplantation (Figure 5B and S8B).
368 After filtering for poor quality cells, we obtained scRNAseq data for 1,030 cells, which
369 were distinguished by colony of origin after dimensionality reduction by UMAP using
370 the combined scRNAseq data (Figure 5C). Expression of genes associated with
371 HSC state, including *Hlf, Procr, and Mecom*, varied significantly in UMAP space, as
372 did expression of *Cd48* and other genes associated with differentiation of HSCs to
373 multipotent progenitors (Figure S8C). Cells from all HSC-like colonies generally
374 lacked expression of genes associated with more lineage-restricted progenitors and
375 mature blood cells, though a small population of cells expressing markers of
376 granulocyte differentiation (*Elane*) was observed in cells coming primarily from
377 colony #1 (Figures S8C and 5C), which was notably more proliferative than other
378 HSC-like colonies and contained a larger proportion of cells lacking $SCA1^{+}EPCR^{+}$
379 co-expression (Figure S8A).

380 Interestingly, the majority of cells from colony #2 clustered together in
381 regions of UMAP space with the highest expression of HSC-associated genes and
382 absence of genes associated with differentiated progenitors (Figure 5D, S8C).
383 Furthermore, when we examined published adult HSC-specific gene signatures
384 associated with dormancy and serial engraftment,[26-28] we found expression to be
385 significantly higher in cells from colony #2 compared to cells from other types of
386 colonies (Figures 5E, 5F and S8D). Interestingly, cells in colony #2 also exhibited
387 significantly higher expression of genes associated with long-term, multilineage
388 engraftment following in vitro expansion of adult HSCs,[13] diapause,[29,31] lipid
389 metabolism and dormancy common to embryonic diapause and multiple adult stem
390 cell types,[32] and chemokine signaling (Figure S8D). In contrast, MYC target genes
391 that promote biosynthetic and cell cycle activation, as well as gene-sets
392 characterizing differentiated progenitors, were significantly lower in cells from colony
393 #2 (Figures 5G and S8E). Differences in biosynthetic signatures were also confirmed
394 by the comparison of cellular metabolism gene-sets which are reportedly higher in
395 activated HSC/MPPs[27,47,48] (Figure S9A). When performing LVM on cells from these
396 colonies using metabolism-related gene-sets as Bayesian priors, colony #2 stood out
397 from the rest of the colonies in latent embedding as shown on the factor loading dot
398 plot (Figure S10A). Specifically, colony #2 showed a shift away from transcriptomic
399 signature of carbohydrate metabolism and towards that of lipid metabolism (Figures
400 S10A and S10B).
401 To further characterize the transcriptional heterogeneity of HSC-like
402 colonies in an unbiased manner, we performed unsupervised clustering (Figure S9B)

403 and gene module analysis across cell clusters to determine co-regulated genes
404 (Figures 5H and S9C). One of the identified gene modules (module 1) which
405 specifically marks cluster 1 (containing the majority of cells from colony #2) includes
406 known HSC-specific genes such as *Hlf*, *Mecom*, and *Mllt3*, and genes related to
407 autophagy, catabolic processes, epigenetic regulation, and immune/interferon
408 responses based on Gene Ontology (GO) analysis (Table S5). In contrast, non-
409 overlapping gene modules feature active cell cycle genes and genes related to
410 biosynthetic activity (module 2-4), including ribosome biogenesis, translation,
411 mitochondrial activity, and ATP synthesis based on GO analysis (Table S5).
412 Next, to identify genes associated with serial engraftment properties, we
413 determined differentially expressed genes between cells in colony #2 and cells from
414 other HSC colonies lacking serial engraftment (Table S6). Cross-referencing these
415 genes with genes expressed in module 1 (Table S5), we identified 123 common
416 genes representing a gene-set that we termed “serially engrafting FL-HSC genes”
417 (Table S1). Remarkably 40% of the genes identified in our novel gene-set were
418 shared with those in published gene-sets either associated with dormant adult BM
419 HSCs or serially engrafting adult HSCs,[27,28] and these gene-sets marked similar
420 subsets of cells in both our cultured and freshly isolated FL-HSC scRNAseq data
421 (Figures S9D and S9E). Common genes identified include a number of key
422 regulators of adult HSC dormancy and self-renewal, including *Angpt1*, *Mecom*, *Mllt3,*
423 *Cd63,* and *Ndn.*[3,51-56] Interestingly, the *Cxcr4*-expressing subset of hemogenic
424 endothelium (HE) in the E9-9.5 mouse embryo, which we recently demonstrated to
425 contain the majority of HSC-competent HE,[4] also showed significantly higher

426 expression of this gene-set compared with HE lacking *Cxcr4* expression, which can
427 give rise to MPP but largely lack HSC potential (Figure S9F).
428 When we further limited differential expression analysis to cluster #1 (which
429 is appears to be enriched in HSC-specific genes), we identified significantly
430 increased expression of HSC-associated genes including *Mllt3*[54] and *Apoe,*[57] as well
431 as increased expression of gene-sets associated with dormancy and serial
432 engraftment, in cells from colony #2 compared with cells from other colonies (Figure
433 S9G, Table S6). These findings suggest potentially key roles for those genes in
434 maintenance of HSC self-renewal in the FL-AKT-EC niche. Notably, *Esam*
435 expression was also significantly enriched in colony #2 cells compared to cells from
436 other colonies in cluster 1 (Figure S9H), consistent with our finding that ESAM
437 expression in HSC-like colonies predicts serial engraftment potential.
438 In a complementary experiment, we compared ESAM$^+$ HSC colonies to
439 colonies lacking significant ESAM expression by scRNAseq, to determine whether
440 functional differences in engraftment observed between these colony types correlate
441 with differences in their transcriptional properties (Figure S11A). We observed that
442 cells from ESAM$^+$ HSC colonies (1-5) largely localized in UMAP space separately
443 from cells from other colonies (6-7), and that cells from ESAM$^+$ HSC colonies were
444 enriched in self-renewal and dormancy-associated gene signatures (Figure S11B-H).
445 Furthermore, gene module analysis demonstrated enriched expression of HSC-
446 associated genes such as *Apoe, Hlf, Mllt3, Cd63,* and *Mecom* in regions of UMAP
447 space associated with ESAM$^+$ HSC colonies (Figure S11I, Table S7). These results
448 are consistent with the transcriptional differences we observed between HSC-like

449 colonies that differ based on their direct engraftment potential (Figure 5).

450 Taken together, these studies reveal that serially engrafting (ESAM$^+$) HSC
451 colonies are characterized by gene expression patterns associated with dormancy in
452 adult BM HSCs and other stem cells, including lower biosynthetic/MYC pathway
453 activation, a shift toward lipid metabolism, and decreased cell cycle activity.[27] The
454 finding that this gene expression profile also characterizes a subset of freshly
455 isolated E13.5 SE^{hi} FL-HSCs as well as HSC-competent HE in the early embryo[4]
456 suggests a conserved gene expression program of biosynthetic dormancy
457 established in early embryonic development may be essential for initiating and
458 maintaining HSC fate.

459

460 **Single cell transcriptomic analysis identifies candidate signaling interactions**
461 **supporting FL-HSC self-renewal in the FL-AKT-EC niche**

462 FL-AKT-ECs provide a niche sufficient to support expansion of FL-HSCs,
463 revealing that the subset of immunophenotypic SE^{hi} FL-HSCs with serial engraftment
464 potential are intrinsically primed for differentiation latency and symmetric self-renewal
465 behavior. To elucidate potential extrinsic signaling interactions regulating the process
466 of FL-HSC self-renewal, we first integrated scRNAseq data from FL-AKT-ECs and
467 serially engrafting HSCs (from HSC colony #2, Figure 5B), and broadly identified
468 candidate ligand-receptor interactions using a comprehensive database of curated
469 pairs of ligands and receptors[58,59] (Table S8). Since FL-ATK-EC-conditioned media
470 was insufficient to support the generation of ESAM$^+$ HSC colonies (Figure S12),
471 suggesting that direct contact with FL-AKT-ECs is indispensable for FL-HSC self-

472 renewal, we included both soluble and transmembrane ligands expressed by FL-
473 AKT-EC. This unbiased analysis identified an extensive list of potential signaling
474 interactions, many of which have been previously shown to regulate various aspects
475 of HSC self-renewal in the context of embryonic development and/or the adult BM,
476 including those involving Notch, TGF-β, Wnt/β-catenin, integrins, and
477 cytokines/chemokines (SCF, CXCL12, IGF1).

478 To further define the pathways that may be specifically required for HSC
479 self-renewal in the FL-AKT-EC niche, we applied NicheNet,[60] a computational
480 algorithm that identifies ligand-receptor pairs from scRNAseq data based on
481 knowledge of downstream signaling pathways and gene regulatory networks.
482 Integrating scRNAseq data from FL-AKT-EC and HSC-like colonies (Figure 6A),
483 NicheNet identified candidate ligand-receptor signaling interactions prioritized based
484 on likelihood of accounting for genes significantly enriched in serially engrafting FL-
485 HSCs (from colony #2) compared with cells from other HSC-like colonies in our
486 scRNAseq data (Figures 6B-D). Multiple ligand-receptor pairs and downstream
487 pathways were identified, including *tgfb1* (TGFβ1), a well-established regulator of
488 HSC quiescence in adult BM,[61,62] transmembrane and extracellular cell adhesion
489 molecules (egs. *Icam1, Col4a1, Lamb2*) that bind and activate integrin receptors
490 (*Itgb1, Itgav*) essential for colonization of HSCs to the FL[63] and for regulating the size
491 of the FL-HSC pool[64], *Selp* (P-selectin), implicated in HSC expansion in the zebrafish
492 caudal hematopoietic territory (CHT, equivalent to the mammalian FL),[65] and *Jam3*,
493 encoding a cell surface adhesion protein implicated in HSC maintenance in the adult
494 BM.[66] Numerous ligand-receptor signals not previously implicated in HSC self-

495 renewal or fate determination were also identified. Notably, a large proportion of
496 identified interactions were predicted to contribute to regulating downstream genes
497 that are essential to HSC dormancy and self-renewal, particularly *Mecom*, *Prdm16*,
498 and *Angpt1*.[3,51,52,67] To further validate that our findings in the ex vivo FL-AKT-EC
499 niche reflect signals endogenous to FL endothelial cells in vivo, we repeated this
500 ligand-receptor analysis using published scRNAseq data from E14 FL-ECs,[68]
501 demonstrating substantial overlap in identified signaling interactions (Figure S13,
502 Table S9). These results suggest that combinatorial ligand-receptor interactions
503 between niche FL-ECs and FL-HSCs involving numerous, integrated signaling
504 pathways are likely essential to the self-renewal of serially engrafting HSCs in vitro
505 (Graphical abstract). Altogether, our ex vivo clonal FL-HSC expansion platform and
506 correlative single cell transcriptomic data provide a valuable resource for future
507 studies to determine how these complex receptor-ligand interactions in the FL
508 vascular niche coordinately regulate downstream transcriptional programs essential
509 to FL-HSC self-renewal.
510

511 **Live imaging in the FL-AKT-EC niche reveals FL-HSC undergo predominantly**
512 **symmetric cell divisions**

513 Adult murine and human HSCs can undergo asymmetric cell divisions in
514 which the paired daughter cells inherit differential activation states, with the more
515 dormant cell maintaining HSC fate necessary for self-renewal while the activated cell
516 adopts a progenitor state necessary to actively contribute to hematopoiesis.[36,69] Our
517 immunophenotypic, functional, and transcriptomic analysis of FL-HSCs supports a

518 distinct model in which serially engrafting HSCs predominantly undergo symmetric
519 self-renewal and homogenous expansion in the FL-EC niche, giving rise to daughter
520 HSCs that maintain a relatively dormant biosynthetic state and delayed differentiation
521 to progenitors. Based on this model, we predict that FL-HSCs should be
522 distinguishable based on symmetric cell division behavior observed during coculture
523 with FL-AKT-EC in vitro. To test this prediction, we index sorted single SE^{hi} FL cells
524 (co-stained with CellTrace-Far Red) to FL-AKT-EC and observed their initial cell
525 divisions by live imaging to measure relative fluorescence intensity (total protein
526 content) of daughter cells as a marker of division symmetry (Figure 7A). Consistent
527 with our hypothesis, we found that $ESAM^{+}$ HSC colonies were derived from SE^{hi} FL
528 cells observed to almost exclusively undergo symmetric cell division (ratio of
529 CellTrace fluorescence intensity between daughter cells ~1) whereas other colony
530 types were derived from cells that underwent a broader distribution of symmetric and
531 asymmetric divisions (ratio of CellTrace fluorescence intensity between daughter
532 cells of <1) (Figure 7B-C).

533 Lysosome-associated membrane protein 3 (Lamp3, or CD63), a tetraspanin
534 with roles in lysosomal trafficking, cholesterol transport, and extracellular vesicle
535 (EV) formation, was found to be highly enriched in serially engrafting FL-HSCs
536 based on our transcriptomic analysis. CD63 has been implicated in HSC cell division
537 symmetry[70] and is functionally involved in HSC self-renewal and dormancy through
538 interactions with the TGF-β pathway.[28,55] A recent study has also suggested a role for
539 CD63 in HSC self-renewal via autocrine signals mediated by HSC-derived EVs
540 downstream of NADPH-driven cholesterol biosynthesis.[71] Consistent with

541 observations that CD63 is expressed on dormant adult HSCs with enhanced
542 reconstitution potential, we observed that CD63 expression was enriched in primary
543 E13.5 FL-HSPCs expressing the highest levels of EPCR (Figures 7D and S14A) and
544 that ESAM^{+} HSC colonies were primarily derived from the CD63^{+} fraction of SE^{hi} FL-
545 HSCs based on index flow cytometry analysis (Figure 7E and S14B). Together, these
546 results suggest that SE^{hi} FL-HSCs with serial engraftment potential are characterized
547 by increased CD63 expression and by their specific propensity for symmetric cell
548 division. Collectively, our findings support a paradigm in which FL-HSCs are
549 maintained in a relatively biosynthetically dormant, slow cycling state characterized
550 by symmetric self-renewal and differentiation latency, which is supported by signals
551 from the FL vascular niche (Figure 7F). Critically, this stage-specific behavior may
552 function to expand the HSC pool during fetal development while delaying their
553 contribution to active hematopoiesis until after birth, when HSCs have transitioned
554 from the FL and to the bone marrow niche.

555 **Discussion**

556 Here we establish a novel ex vivo platform that supports the expansion of
557 serially engrafting HSCs from individually sorted FL-HSCs. This platform provides a
558 powerful tool to analyze the intrinsic properties of functionally validated FL-HSCs at
559 single cell resolution, as well as the extrinsic niche-derived signals enabling HSC
560 self-renewal in vitro. To this end, we leveraged this platform to resolve heterogeneity
561 in immunophenotypically defined FL-HSCs by simultaneously integrating index flow
562 cytometry, live imaging, single cell transcriptomics, and transplantation assays. In so
563 doing, we identified a rare subset of FL-HSCs with serial engraftment potential that
564 are characterized by propensity for symmetric cell divisions, differentiation latency,
565 and transcriptional signatures of lipid metabolism and biosynthetic dormancy.

566 Notably, the observed behavior and transcriptional profiles of serially
567 engrafting FL-HSCs in our study contrast with previous paradigms proposing that FL-
568 HSCs reside in a state of heightened biosynthetic and proliferative activity necessary
569 to simultaneously expand their total numbers (providing sufficient HSCs for the adult)
570 and differentiate to progenitors (providing functional blood cells for fetal
571 development). Instead, our findings support a shift in this paradigm in line with
572 several recent studies that have traced the origin and evolution of HSCs and HSC-
573 independent progenitors from early embryonic development to adulthood by various
574 clonal assays and lineage tracing methodologies in vitro and in vivo.[3-5,9,72] Together,
575 these studies suggest that functional, long-term engrafting HSCs and HSC-
576 independent embryonic multipotent progenitors (eMPP) emerge from distinct
577 populations of HE, that HSCs contribute minimally to differentiating progenitors and

578 mature blood cells prenatally, and that eMPP contribute prenatally as well as
579 postnatally to lifelong multilineage hematopoiesis natively in vivo but fail to provide
580 long-term, multilineage hematopoietic engraftment as measured by transplantation
581 assays. Remarkably, our platform revealed intrinsic behaviors of individual FL-HSCs
582 in vitro that recapitulated their predicted behaviors consistent with these recent
583 studies in vivo.[3,9,72] Specifically, the rare subset of immunophenotypic (SE^{hi}) FL-
584 HSCs at early and mid-gestation with serial engraftment potential gave rise to
585 colonies that consisted of fewer total cell numbers, homogenously expressed
586 immunophenotypic markers of HSCs (i.e. EPCR, SCA1, ESAM), and supported
587 serial engraftment in multiple mice transplanted from a single colony, suggesting
588 symmetric self-renewal and constrained proliferative activity in vitro. Moreover,
589 serially engrafting FL-HSC colonies demonstrated differentiation latency in vitro,
590 failing to generate differentiated progenitors or mature blood cells based on
591 immunophenotypic and transcriptomic analysis after extended coculture (12-15
592 days), which would temporally correspond to the postnatal period in vivo. Together,
593 our data suggest the immunophenotypic (SE^{hi}) FL-HSC compartment is
594 heterogeneous, with only a minor subset representing functional, serially engrafting
595 HSCs (Figure 7F). Based on their in vitro behavior and clonal engraftment
596 properties, we postulate that the remaining cells in this compartment may include a
597 spectrum of separately emerging, HSC-independent lineages with multilineage
598 hematopoietic potential but with minimal or restricted (short-term or lineage biased)
599 engraftment potential, including recently described eMPP (that lack engraftment
600 potential based on transplantation assays)[9] and “developmentally restricted” HSCs

601 (that reconstitute multilineage hematopoiesis upon transplantation but with lymphoid
602 biased engraftment).[10]

603 By integrating single cell transcriptomics into our platform, we also
604 determined the unique transcriptional properties of serially engrafting FL-HSCs
605 during the process of self-renewal in the ex vivo FL-AKT-EC niche. Surprisingly, this
606 revealed a transcriptional signature of relative biosynthetic dormancy that overlaps
607 with signatures of highly dormant and serially engrafting HSCs in the adult BM,[8] as
608 well as HSC-competent HE in the early embryo.[4] Together, these studies support a
609 novel paradigm in which HSC fate across prenatal development is linked to a state of
610 relative dormancy that enables limited symmetric stem cell self-renewal while
611 preventing excessive proliferation and differentiation to multilineage blood cells
612 (Figure 7F). Crucially, this mechanism would serve to minimize metabolic,
613 proteotoxic, and genotoxic stress during HSC development that could contribute to
614 hematopoietic dysfunction later in adult life. Furthermore, these cell intrinsic
615 dormancy-related programs may synergize with extrinsic mechanisms in the FL, for
616 example niche-derived antioxidant systems that minimize oxidative stress[73] and
617 exogenous bile acids that alleviate endoplasmic reticulum stress,[74] to protect self-
618 renewing HSCs during their regulated expansion in the FL.

619 Studies of HSC development in the FL niche in vivo have been challenging
620 due to the relative scarcity of functional, long-term engrafting HSCs amongst a sea
621 of differentiating progenitors in the FL and the lack of markers that can prospectively
622 identify FL-HSCs at single cell resolution with high specificity. By providing a culture
623 system to functionally validate and characterize single FL-HSCs in vitro, our platform

624 offers a complementary approach that provides several advantages and overcomes
625 many challenges to studying FL-HSCs in vivo. We defined a combination of
626 immunophenotypic markers in vitro (SCA1, EPCR, ESAM) sufficient to predict FL-
627 HSCs expanded in vitro with serial engraftment potential in vivo, in line with previous
628 studies that have identified these surface proteins as markers of HSC potential
629 following in vitro culture.[13,22,75] Our platform thus provides a means to screen more
630 rapidly for functional HSC potential at the single cell level while reducing the need for
631 resource-intensive transplantation in mouse models, which remains the gold
632 standard to validate the engraftment potential of HSCs. Incorporating single cell
633 index sorting into the platform, we also provide a means to retrospectively screen for
634 immunophenotypic markers or other properties that can be captured by FACS (such
635 as measures of metabolic activity, ROS, etc) which may predict engraftment
636 potential. In the present study, for example, we demonstrated that functional FL-
637 HSCs from the primary FL at E13.5 are enriched by CD63 surface expression,
638 consistent with previous studies in adult HSCs.[55] Our platform also facilitates direct
639 visualization of HSCs actively self-renewing in a developmentally relevant ex vivo
640 niche, enabling longitudinal observations of their behavior and interactions with niche
641 cells, which is not currently possible in vivo due to technical limitations and lack of
642 markers that can reliably identify functional FL-HSCs at single cell resolution in situ.
643 Here we leveraged this capability, by further incorporating live fluorescence probes,
644 to measure cell division symmetry in paired daughter cells, demonstrating that FL-
645 HSCs are distinguished by exclusive symmetric cell division behaviors. Building on
646 this work, our current efforts are utilizing machine learning approaches to determine

647 whether additional aspects of cell morphology, motility, or other properties captured
648 during live imaging in this platform can predict HSC fate, which may provide
649 unprecedented insight into the distinct behaviors of FL-HSCs and their interaction
650 with niche ECs.

651 Since the FL-AKT-EC niche was sufficient to support the in vitro self-
652 renewal of serial engrafting FL-HSCs, we also leveraged the platform to identify
653 potential niche signaling interactions that regulate the process of FL-HSC self-
654 renewal, using complementary scRNAseq data from the FL-AKT-EC and FL-HSCs
655 expanded in vitro. To this end, NicheNet[76], a scRNAseq package which can infer and
656 prioritize receptor-ligand pairs based on downstream gene expression changes in
657 receiving cells, enabled identification of the signaling interactions between self-
658 renewing HSCs and our engineered vascular environment that could account for
659 genes identified as significantly enriched in engrafting HSC colonies verses
660 immunophenotypically similar HSC-like colonies lacking long-term engraftment.
661 Interestingly, TGFβ1, a key signaling molecule regulating dormancy in adult BM
662 HSCs,[61,62,77] was identified as one of the top 3 ligands in this analysis, with
663 measurable regulatory potential for a large portion of differentially expressed genes
664 in self-renewing HSCs in vitro (Figures 6C and 6D). This finding is consistent with
665 the observation that serial engrafting FL-HSCs in our study were specifically
666 enriched in transcriptional signatures associated with biosynthetic dormancy that are
667 shared with adult BM HSCs. Thus, it is tempting to speculate a role for TGFβ
668 signaling in the FL by regulating a relative state of dormancy in FL-HSCs. However,

669 NicheNet also predicted signals involving multiple pathways that interact with TGFβ,
670 including both positive and negative regulators and Smad7 (which can act via
671 negative feedback on TGFβ/Activin pathways), suggesting fine tuning of TGFβ-
672 mediated signals may be essential to achieve the appropriate balance of dormancy,
673 allowing for FL-HSC expansion through controlled, symmetric self-renewal, while
674 inhibiting excessive proliferation and differentiation. In addition to regulators of the
675 TGFβ pathway, other signaling interactions and pathways identified by NicheNet
676 have also been specifically implicated in HSC maintenance and self-renewal,
677 including several intercellular and ECM adhesive interactions involving integrins, P-
678 selectin, and JAM-C.[64-66] Interestingly, the top ligand identified by NicheNet analysis,
679 ApoE, has been postulated to regulate HSC quiescence via modulation of
680 lipid/cholesterol efflux and oxidative stress.[78-80] Indeed, mitochondrial fatty acid
681 oxidation (FAO) is essential for adult HSC self-renewal[81,82] and ex vivo maintenance
682 of engrafting HSCs has been shown to be dependent on exogenous cholesterol/fatty
683 acids that may serve as a source of eicosanoid signaling molecules and other lipid-
684 derivatives essential to HSC function.[83] Moreover, a recent study showed that FAO-
685 generated NADPH fuels cholesterol biosynthesis in HSCs, which is essential for
686 HSC self-renewal through both cell autonomous mechanisms and through HSC-
687 niche interactions mediated by extracellular vesicles.[71] Altogether, these results
688 predict that complex, combinatorial interactions involving both EC niche-derived
689 signals and cell intrinsic properties of FL-HSCs synergistically contribute to
690 regulating the relative biosynthetic dormancy and cell cycle activity required for HSC
691 self-renewal (Graphical abstract).

692 In summary, using a novel in vitro assay to assess for functional FL-HSCs
693 at single cell resolution, we report here previously unrecognized heterogeneity of
694 immunophenotypic FL-HSCs, revealing a subset of serially engraftable FL-HSCs
695 characterized by intrinsic propensity for symmetric self-renewal, differentiation
696 latency, and biosynthetic dormancy that is concomitantly dependent on critical
697 extrinsic signals from the FL vascular niche. These findings support a paradigm shift
698 in line with other recent studies that suggest prenatal hematopoiesis is largely
699 supplied by HSC-independent progenitors whereas FL-HSCs are preserved to
700 undergo limited self-renewal without differentiation during development to generate
701 the adult HSC pool. Interestingly, we show that the minor subset of serially
702 transplantable FL-HSCs exhibit transcriptional profiles overlapping with those of
703 dormant and serially-engrafting adult HSCs, including biosynthetic dormancy, lipid
704 metabolism/FAO, lysosomal activity, and autophagy. However, adult HSCs are
705 largely quiescent (cell cycle inactive) at homeostasis and, when activated by
706 physiologic stress, can undergo asymmetric cell divisions to simultaneously self-
707 renew and contribute progenitors to active hematopoiesis. Our studies demonstrate
708 that FL-HSCs, in contrast, predominantly undergo symmetric self-renewal without
709 progenitor differentiation. Future studies unlocking the mechanisms by which FL-
710 HSCs are transiently locked into symmetric expansion, including roles for intrinsic
711 factors and extrinsic factors from the FL niche, may facilitate efforts to engineer and
712 expand engrafting HSCs in vitro for transplantation, gene editing, and cellular
713 therapies. Our novel platform and transcriptomic data provide a valuable resource for

714 such future exploration of the intricate interactions between intrinsic and extrinsic

715 signaling networks regulating FL-HSC self-renewal at unprecedented resolution.

716 **Acknowledgments**

717 Studies involving mouse models in this manuscript were supported by the American
718 Society of Hematology Scholar Award (to B.H.), the NIH under NHLBI
719 (K08HL140143 and R01HL168110 to B.H.), and the NIH under NIDDK
720 (RC2DK114777 to I.D.B., C.T., S.R., and B.H. and U24DK126127 sub-award to
721 H.G.Z.). This work was also supported by the Flow Cytometry Shared Resource, the
722 Cellular Imaging Shared Resource (RRID:SCR_022609), the Genomics &
723 Bioinformatics Shared Resource of the Fred Hutch/University of Washington/Seattle
724 Children's Cancer Consortium (NCI grant P30 CA015704), and the University of
725 Washington Birth Defects Research Laboratory (BDRL) (NICHD grant
726 R24HD000836). T.I is supported for overseas medical research by Takeda Science
727 Foundation, The Nakatomi Foundation and Kitasato University School of Medicine
728 Alumni Association. The graphical abstract was created with BioRender.

729

730 **Author contributions**

731 Study design, experiments, collection of data and interpretation: T.I, H.G.Z, J.M, A.H,
732 B.V, S.D, C.N.-M, K.K, R.W, O.W, C.D, D.L.J, I.P, K.A.A, S.R., C.T, I.D.B., and B.H.
733 Original writing: T.I, A.H, B.V, H.G.Z and B.H. Article revision and editing: all authors.
734 Supervision: B.H and H.G.Z.

735

736 **Declaration of interests**

737 Authors declare no conflicting financial interest related to studies reported in this
738 manuscript.

739 **Figures**

Figure 1

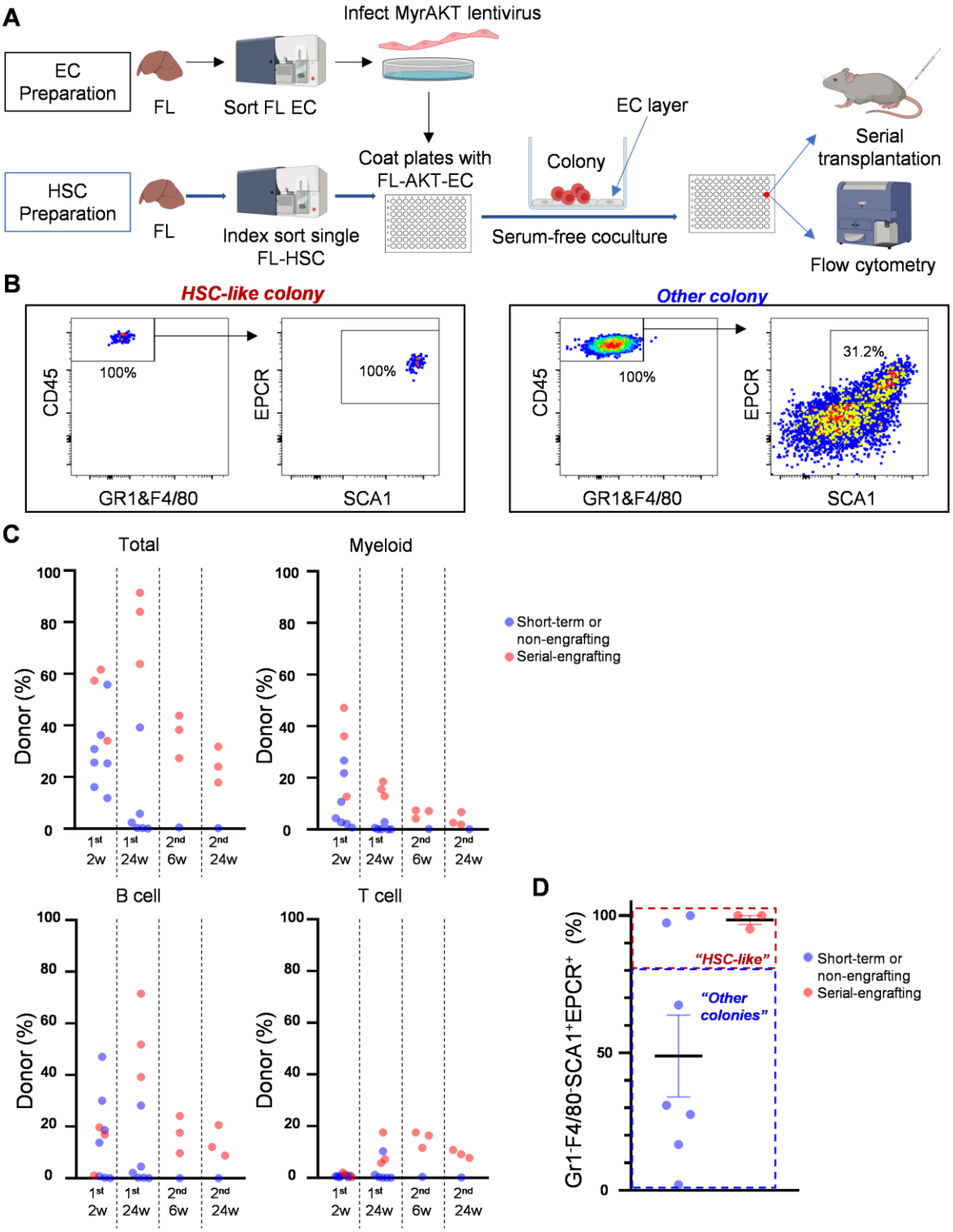

740

741 **Figure 1: Establishment of a FL vascular niche platform supporting ex vivo**
742 **amplification of clonal FL-HSCs.**
743 **(A)** Overview of methodology. Sorted FL-derived ECs were infected with lentivirus
744 encoding myristoylated AKT (myrAKT) to generate FL-AKT-ECs. Single FL-HSCs
745 were sorted into each well of a 96 well-plate coated with FL-AKT-EC in serum free
746 media with hematopoietic cytokines (SCF, TPO). Following a period of coculture,
747 emerging colonies were assessed by flow cytometry for immunophenotype and by
748 serial transplantation to measure long-term hematopoietic engraftment (See
749 Materials & Methods for details).
750 **(B)** Representative immunophenotypes of colonies emerging from single E16.5
751 $SE^{hi}CD150^{+}$ FL-HSC following coculture with FL-AKT-EC. Colonies were analyzed
752 on day 15 by flow cytometry. Shown is expression of EPCR and SCA1 within cells
753 gated as $CD45^{+}GR1^{-}F4/80^{-}$, after exclusion of dead cells ($DAPI^{+}$) and VE-cadherin^{+}
754 FL-AKT-EC.
755 **(C)** Donor chimerism (total, myeloid, B cell, and T cell) in peripheral blood of primary
756 and secondary recipients transplanted with the progeny of single E16.5 FL-HSCs
757 following coculture with FL-AKT-ECs. 50% of cells from each colony were analyzed
758 by flow cytometry and a portion of the remaining cells (25-50%) was used for
759 transplantation (n=10).
760 **(D)** Frequency of $GR1^{-}F4/80^{-}SCA1^{+}EPCR^{+}$ cells (amongst total viable $CD45^{+}$ cells)
761 in individual colonies possessing serial multilineage engraftment (red) (n=3) or
762 lacking serial multilineage engraftment (blue) (n=7). “HSC-like” colonies were defined
763 as colonies with frequency of >80% $GR1^{-}F4/80^{-}SCA1^{+}EPCR^{+}$ amongst total viable
764 $CD45^{+}$ cells (defined to encompass all colonies possessing serial multilineage
765 engraftment).

Figure 2

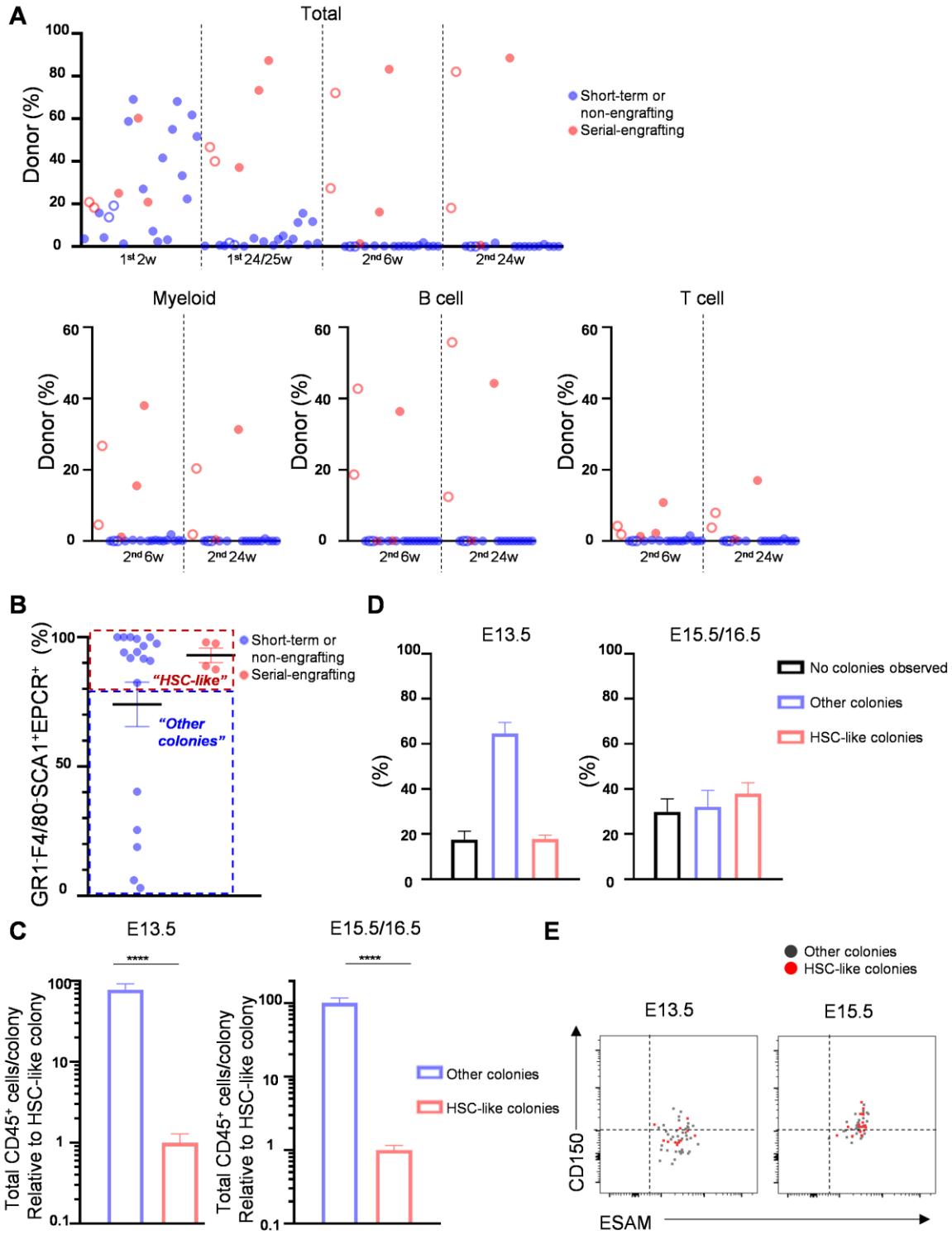
A
Total
Donor (%)
Short-term or non-engrafting
Serial-engrafting
1st 2w
1st 24/25w
2nd 6w
2nd 24w
Myeloid
B cell
T cell
B
GR1-F4/80-SCA1+EPCR+ (%)
"HSC-like"
"Other colonies"
D
E13.5
E15.5/16.5
(%)
No colonies observed
Other colonies
HSC-like colonies
C
Total CD45+ cells/colony Relative to HSC-like colony
****
E
CD150
ESAM
E15.5

766

767 **Figure 2: SE^{hi} FL-HSCs demonstrate heterogeneity in functional engraftment,**
768 **proliferation, and immunophenotype following FL-AKT-EC coculture.**
769 **(A)** Donor chimerism (total, myeloid, B cell, and T cell) in peripheral blood of primary
770 and secondary recipients transplanted with the progeny of single E13.5 SE^{hi} FL-
771 HSCs following coculture with FL-AKT-ECs. 50% of cells from each colony were
772 analyzed by flow cytometry and the remaining cells were used for transplantation
773 (n=22 total colonies transplanted to n=24 total recipients; results pooled from 3
774 independent experiments). Two colonies (open circles) were each transplanted to 2
775 recipients.
776 **(B)** Frequency of GR1^{-}F4/80^{-}SCA1^{+}EPCR^{+} cells (amongst total viable CD45^{+} cells)
777 in individual colonies possessing serial multilineage engraftment (red) (n=4) or
778 lacking serial multilineage engraftment (blue) (n=18). “HSC-like” colonies were
779 defined as colonies with frequency of >80% GR1^{-}F4/80^{-}SCA1^{+}EPCR^{+} amongst total
780 viable CD45^{+} cells (defined to encompass all colonies possessing serial multilineage
781 engraftment).
782 **(C)** Total viable CD45+ cells per colony determined by flow cytometry following
783 coculture of single E13.5 or E15.5/16.5 SE^{hi} FL-HSCs with FL-AKT-ECs. Cell
784 numbers were normalized to HSC-like colonies for each experiment. (E13.5: n=32
785 HSC-like colonies, n=119 other colonies, from 3 independent experiments;
786 E15.5/16.5: n=95 HSC colonies, n=80 other colonies, from 5 independent
787 experiments). ****P<0.0001 (Mann-Whitney test). Data are expressed as
788 mean±SEM.
789 **(D)** Frequency of colony types observed following coculture of single E13.5 (3
790 independent experiments) or E15.5/16.5 SE^{hi} (5 independent experiments) FL-HSCs
791 with FL-AKT-ECs. Data are expressed as mean±SEM.
792 **(E)** Expression of ESAM and CD150 by index analysis of E13.5 (left) and E15.5
793 (right) SE^{hi} FL-HSCs giving rise to immunophenotypic HSC-like colonies (red) or
794 other colonies (gray) following FL-AKT-EC coculture.

Figure 3

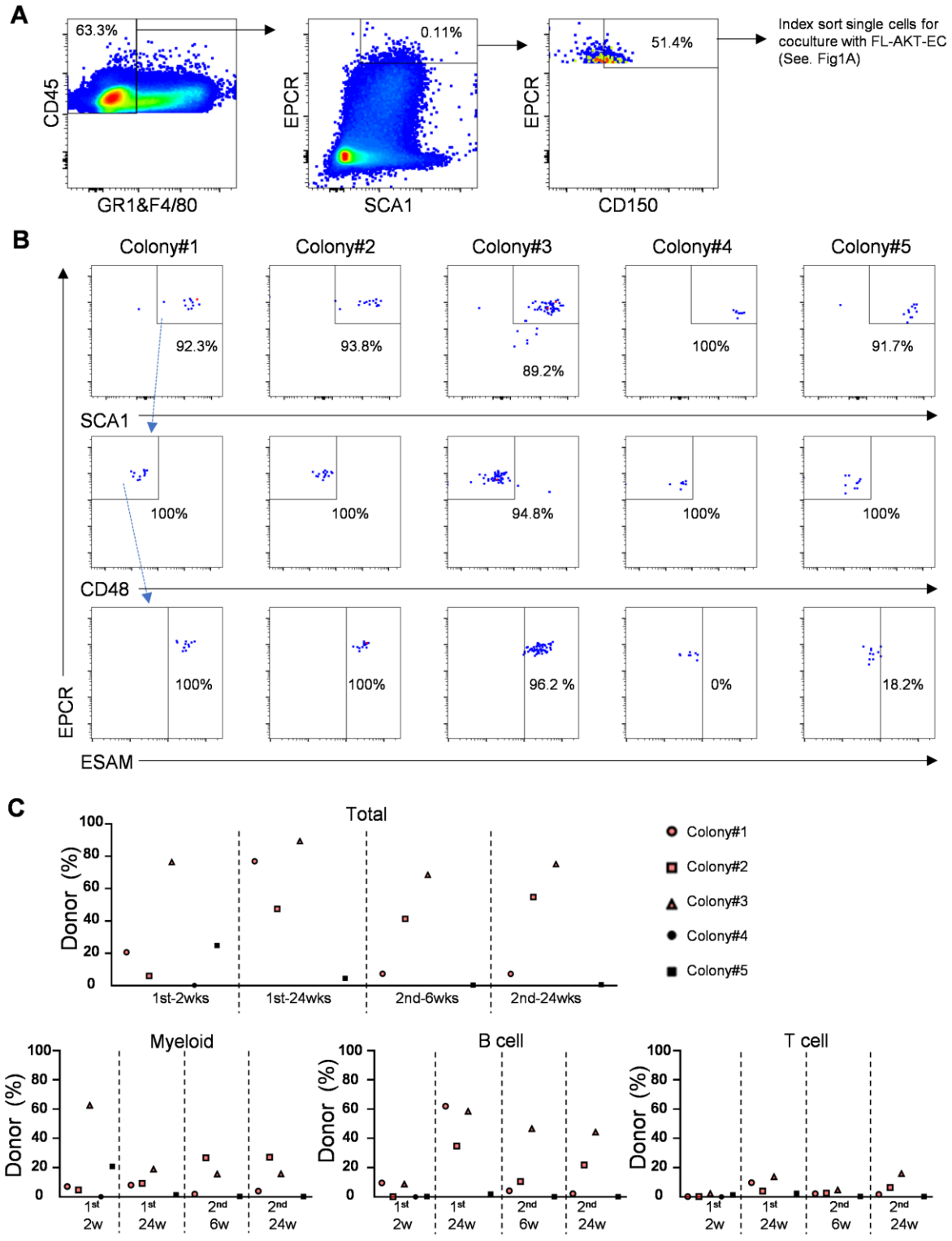
A
63.3%
CD45
GR1&F4/80
0.11%
EPCR
SCA1
51.4%
EPCR
CD150
Index sort single cells for coculture with FL-AKT-EC (See. Fig1A)
B
Colony#1
Colony#2
Colony#3
Colony#4
Colony#5
92.3%
93.8%
89.2%
100%
91.7%
SCA1
100%
100%
94.8%
100%
100%
CD48
100%
100%
96.2 %
0%
18.2%
EPCR
ESAM
C
Total
Donor (%)
1st-2wks
1st-24wks
2nd-6wks
2nd-24wks
Colony#1
Colony#2
Colony#3
Colony#4
Colony#5
Myeloid
B cell
T cell
1st 2w
1st 24w
2nd 6w
2nd 24w

795

796 **Figure 3: ESAM-expressing HSC colonies exhibit serial hematopoietic**
797 **reconstitution capacity.**
798 **(A)** Single cell sorting strategy of E15.5 $SE^{hi}CD150^{+}$ FL-HSCs for coculture with FL-
799 AKT-EC.
800 **(B)** Expression of CD48 and ESAM in 5 HSC-like colonies analyzed by flow
801 cytometry following 15 days of coculture. 50% of the cells from each colony were
802 used for flow cytometry and the remaining cells were used for transplantation. (HSC-
803 like colonies were defined as containing >80% $CD48^{-}SCA1^{+}EPCR^{+}$ cells amongst
804 total viable $CD45^{+}$ cells).
805 **(C)** Donor chimerism (total, myeloid, B cell, and T cell) in peripheral blood of primary
806 and secondary recipients transplanted with cells from each of the HSC-like colonies
807 shown in B (n=5).

Figure 4

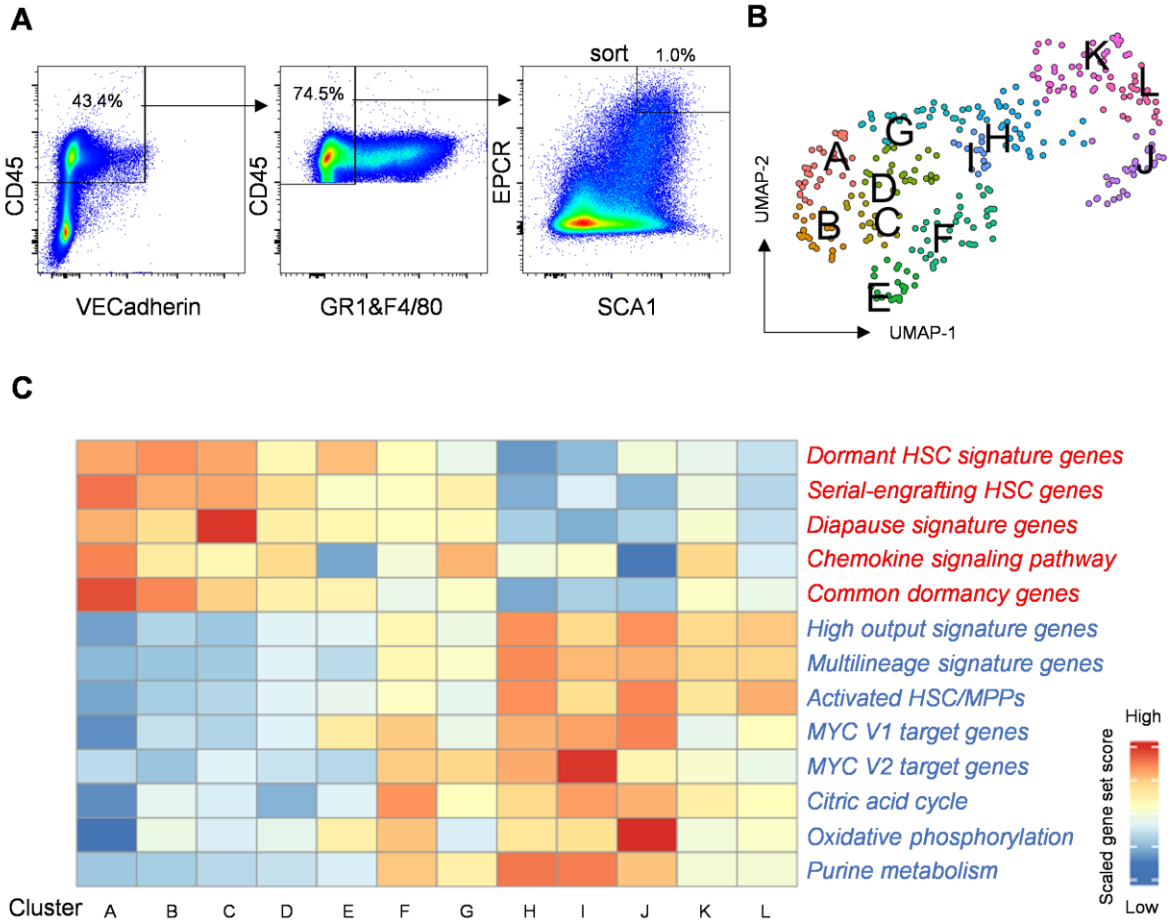
A
43.4%
CD45
VECadherin
74.5%
CD45
GR1&F4/80
sort
1.0%
EPCR
SCA1
B
UMAP-2
UMAP-1
A
B
C
D
E
F
G
H
I
J
K
L
C
Dormant HSC signature genes
Serial-engrafting HSC genes
Diapause signature genes
Chemokine signaling pathway
Common dormancy genes
High output signature genes
Multilineage signature genes
Activated HSC/MPPs
MYC V1 target genes
MYC V2 target genes
Citric acid cycle
Oxidative phosphorylation
Purine metabolism
Cluster
A B C D E F G H I J K L
Scaled gene set score
High
Low
D
Dormant HSC signature genes
Serial-engrafting HSC genes
UMAP-2
UMAP-1
Expression
High
Low
E
Module1
Hlf
H19
Tcf15
Hmga2
Module3
Myc
Dkc1
Mrpl12
Module4
Mecom
Mllt3
Kmt2a
Mpl
Module7
Cdk4
Eif4e
Mrpl1
UMAP-2
UMAP-1
Expression
High
Low

808

809 **Figure 4: Single cell RNA sequencing reveals transcriptional heterogeneity**
810 **amongst immunophenotypically-defined SE^{hi} FL-HSCs.**
811 **(A)** Sorting strategy for SE^{hi} FL-HSCs from freshly isolated E13.5 FL used for
812 scRNAseq.
813 **(B)** Unsupervised clustering of E13.5 SE^{hi} FL-HSC scRNAseq data in UMAP.
814 **(C)** Heatmap of gene-set scores by cluster for genes associated with adult HSC
815 dormancy,[27] serial-engrafting HSCs,[28] diapause,[29,31] chemokine signaling
816 (WP_CHEMOKINE_SIGNALING_PATHWAY), and a common stem cell dormancy
817 state associated with lipid metabolism,[32] or genes associated with activated
818 HSC/MPP states including high output and multilineage signatures,[27,28,84] Myc
819 pathway activation (Hallmark Myc Target Genes V1, V2), and metabolic activity
820 (WP_TCA_CYCLE, HALLMARK_OXIDATIVE_PHOSPHORYLATION,
821 WP_PURINE_METABOLISM) .
822 **(D)** Gene-set expression heatmaps for dormant HSC signature genes and serial-
823 engrafting HSC signature genes.[27,28]
824 **(E)** Expression heatmaps for modules of co-regulated genes determined using
825 Louvain community analysis in Monocle3. Gene modules 1, 3, 4 and 7 are shown with
826 representative genes identified in each module.

Figure 5

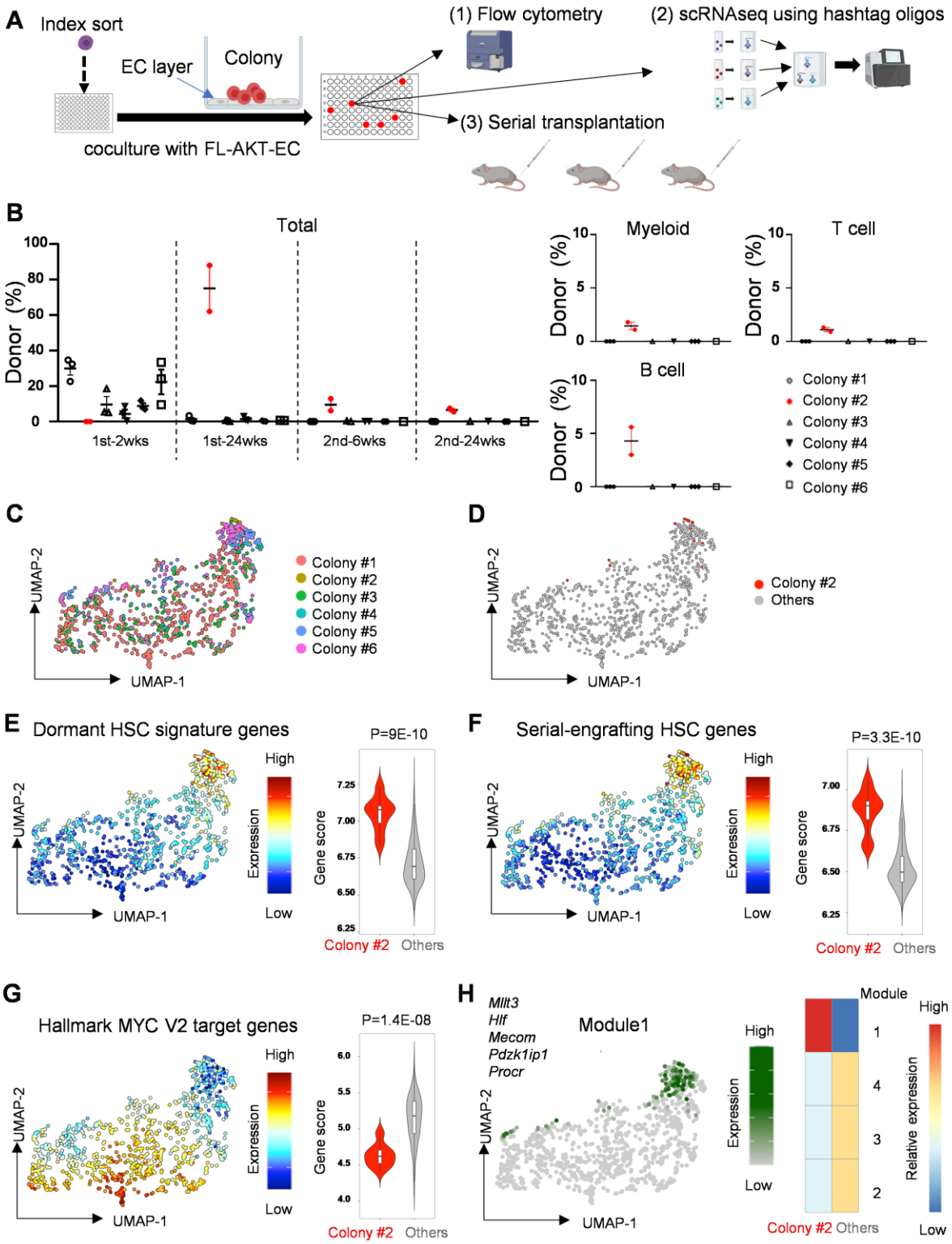
A
Index sort
EC layer
Colony
coculture with FL-AKT-EC
(1) Flow cytometry
(2) scRNAseq using hashtag oligos
(3) Serial transplantation
B
Total
Donor (%)
1st-2wks
1st-24wks
2nd-6wks
2nd-24wks
Myeloid
T cell
B cell
Colony #1
Colony #2
Colony #3
Colony #4
Colony #5
Colony #6
C
UMAP-2
UMAP-1
D
Colony #2
Others
E
Dormant HSC signature genes
P=9E-10
High
Low
Expression
Gene score
Colony #2
Others
F
Serial-engrafting HSC genes
P=3.3E-10
G
Hallmark MYC V2 target genes
P=1.4E-08
H
Mllt3
Hlf
Mecom
Pdzk1ip1
Procr
Module1
Module
Relative expression

827

Figure 5: Analysis of clonal progeny of single FL-HSCs by integrating scRNAseq, flow cytometry, and transplantation reveals transcriptional and functional heterogeneity of HSC colonies.

(A) Overview of the experiment design. 15% of each well was used for flow cytometric analysis, 55% for scRNAseq, and 30% for serial transplantation (10% to each of 3 recipient mice).

(B) Donor chimerism in peripheral blood of primary and secondary recipients transplanted with the progeny of single E13.5 SE^{hi} cells following coculture with FL-AKT-ECs. Left: Total donor chimerism at indicated timepoints following primary and secondary transplant. Right: Donor myeloid, B cell, and T cell contribution at 24 weeks in secondary recipients. (n=3 mice transplanted for each colony).

(C) UMAP analysis with cells labeled based on colony of origin (colony #1: 513 cells, colony #2: 16 cells, colony #3: 202 cells, colony #4: 44 cells, colony #5: 102 cells, colony #6: 153 cells).

(D) UMAP of cells grouped by engraftment properties (serially engrafting colony #2 verses all other colonies lacking serial engraftment).

(E) Heatmap of gene-set scores characterizing dormant adult HSCs.[27] Violin plots of gene-set scores by colony type. p values indicate Wilcoxon rank-sum test.

(F) Heatmap of gene-set scores characterizing serial-engrafting HSCs.[28] Violin plots of gene-set scores by colony type. p values indicate Wilcoxon rank-sum test.

(G) Heatmap of gene-set scores for Myc target genes (HALLMARK_MYC_TARGETS_V2). Violin plots of gene-set scores by colony type. p values indicate Wilcoxon rank-sum test.

(H) Expression heatmaps for modules of co-regulated genes determined using Louvain community analysis. Gene modules 1 is shown in UMAP with representative genes (left). Heatmap of expression of gene modules by colony type (right).

Figure 6

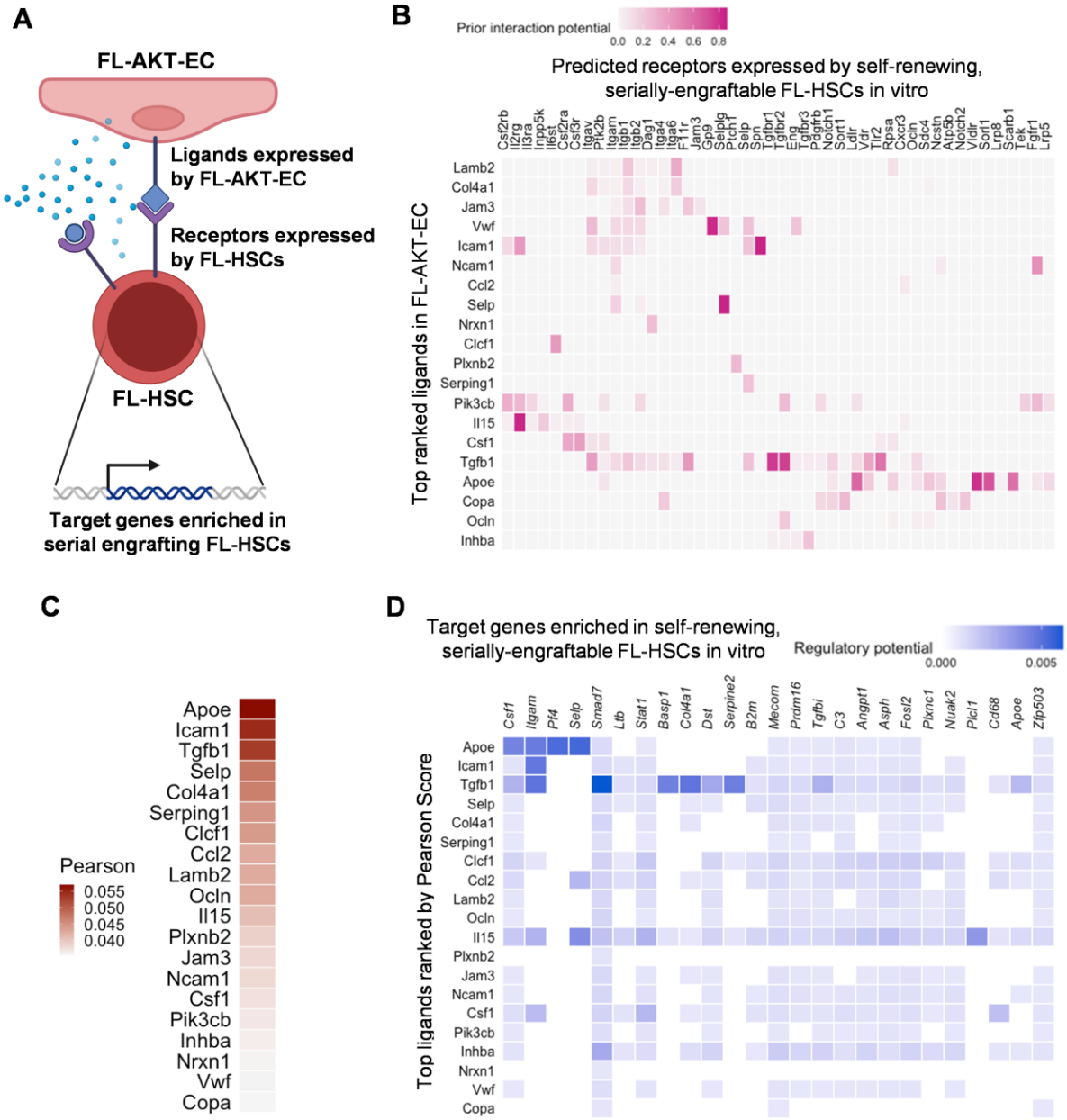
A
FL-AKT-EC
Ligands expressed by FL-AKT-EC
Receptors expressed by FL-HSCs
FL-HSC
Target genes enriched in serial engrafting FL-HSCs
B
Prior interaction potential
0.0 0.2 0.4 0.6 0.8
Predicted receptors expressed by self-renewing, serially-engraftable FL-HSCs in vitro
Top ranked ligands in FL-AKT-EC
Lamb2
Col4a1
Jam3
Vwf
Icam1
Ncam1
Ccl2
Selp
Nrxn1
Clcf1
Plxnb2
Serping1
Pik3cb
Il15
Csf1
Tgfb1
Apoe
Copa
Ocln
Inhba
C
Pearson
0.055
0.050
0.045
0.040
Apoe
Icam1
Tgfb1
Selp
Col4a1
Serping1
Clcf1
Ccl2
Lamb2
Ocln
Il15
Plxnb2
Jam3
Ncam1
Csf1
Pik3cb
Inhba
Nrxn1
Vwf
Copa
D
Target genes enriched in self-renewing, serially-engraftable FL-HSCs in vitro
Regulatory potential
0.000
0.005
Top ligands ranked by Pearson Score
Csf1
Itgam
Pf4
Selp
Smad7
Ltb
Stat1
Basp1
Col4a1
Dst
Serpine2
B2m
Mecom
Prdm16
Tgfbi
C3
Angpt1
Asph
Fosl2
Plxnc1
Nuak2
Plcl1
Cd68
Apoe
Zfp503
Apoe
Icam1
Tgfb1
Selp
Col4a1
Serping1
Clcf1
Ccl2
Lamb2
Ocln
Il15
Plxnb2
Jam3
Ncam1
Csf1
Pik3cb
Inhba
Nrxn1
Vwf
Copa

854

855 **Figure 6: Complementary analysis of scRNAseq data identifies candidate**
856 **receptor-ligand interactions regulating self-renewal of serially engrafting FL-**
857 **HSCs in the FL-AKT-EC niche.**
858 **(A)** Model for analysis of receptor-ligand interactions by NicheNet.[76]
859 **(B)** Heatmap showing candidate ligands (expressed by FL-AKT-EC) interacting with
860 receptors (expressed by cells in serially engrafting HSC colony #2) inferred by
861 NicheNet.
862 **(C)** Heatmap showing candidate ligands (expressed by FL-AKT-EC) ranked by
863 Pearson correlation.
864 **(D)** Heatmap showing the regulatory potential between the top ranked ligands
865 (expressed by FL-AKT-EC) and downstream genes whose expression is enriched in
866 cells from serially engrafting HSC colony (#2) compared to cells from other HSC-like
867 colonies lacking serial engraftment.

Figure 7

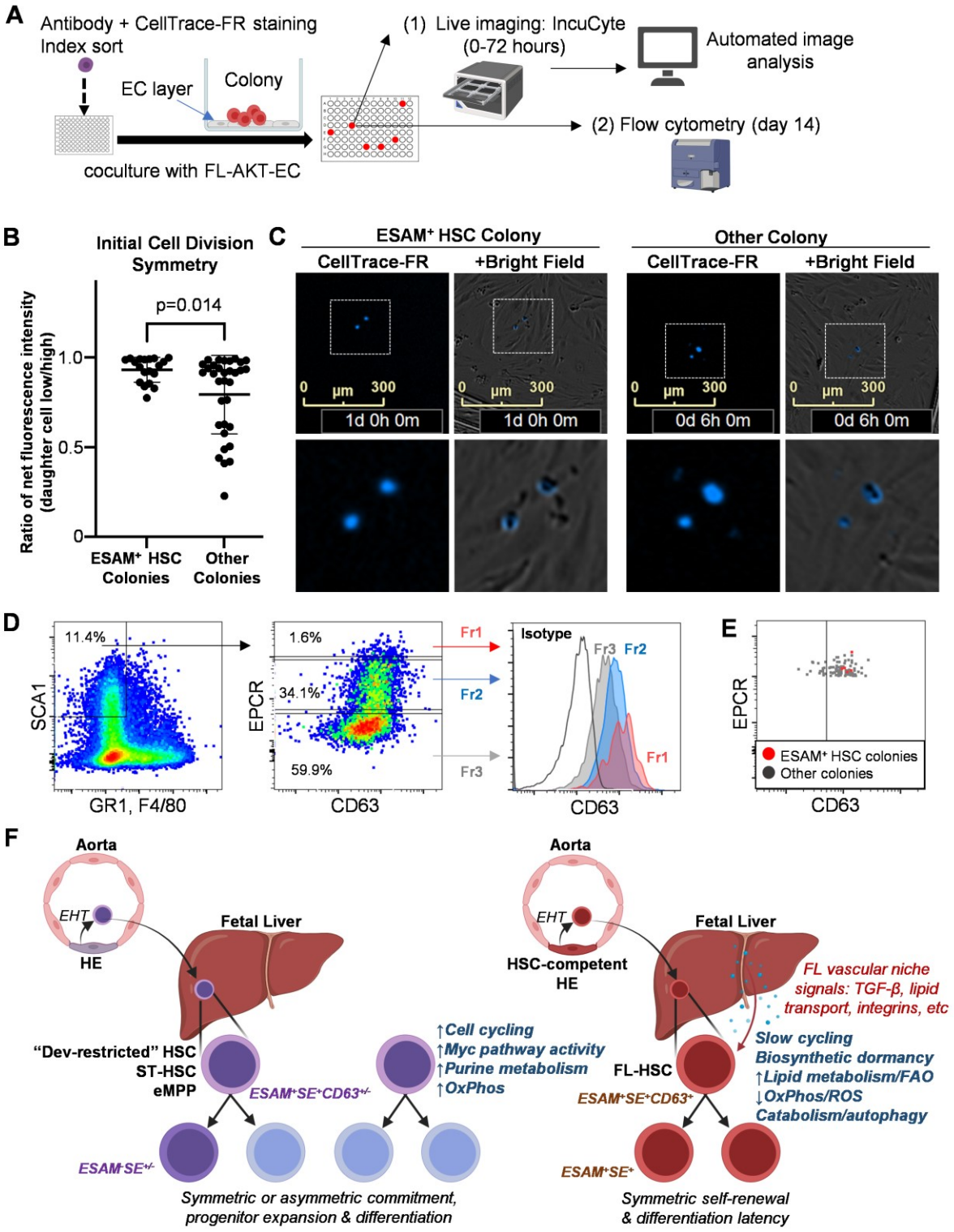
A
Antibody + CellTrace-FR staining
Index sort
EC layer
Colony
coculture with FL-AKT-EC
(1) Live imaging: IncuCyte
(0-72 hours)
Automated image
analysis
(2) Flow cytometry (day 14)
B
Initial Cell Division
Symmetry
p=0.014
Ratio of net fluorescence intensity
(daughter cell low/high)
1.0
0.5
0
ESAM+ HSC
Colonies
Other
Colonies
C
ESAM+ HSC Colony
Other Colony
CellTrace-FR
+Bright Field
CellTrace-FR
+Bright Field
0 µm 300
1d 0h 0m
1d 0h 0m
0d 6h 0m
0d 6h 0m
D
11.4%
SCA1
GR1, F4/80
1.6%
34.1%
59.9%
EPCR
CD63
Fr1
Fr2
Fr3
Isotype
Fr3
Fr2
Fr1
CD63
E
EPCR
ESAM+ HSC colonies
Other colonies
CD63
F
Aorta
EHT
HE
Fetal Liver
"Dev-restricted" HSC
ST-HSC
eMPP
ESAM+SE+CD63+/-
ESAM-SE+/-
↑Cell cycling
↑Myc pathway activity
↑Purine metabolism
↑OxPhos
Symmetric or asymmetric commitment,
progenitor expansion & differentiation
Aorta
EHT
HSC-competent
HE
Fetal Liver
FL vascular niche
signals: TGF-β, lipid
transport, integrins, etc
FL-HSC
ESAM+SE+CD63+
Slow cycling
Biosynthetic dormancy
↑Lipid metabolism/FAO
↓OxPhos/ROS
Catabolism/autophagy
ESAM+SE+
Symmetric self-renewal
& differentiation latency

868

869 **Figure 7: Live imaging reveals FL-HSCs are characterized by symmetric cell**
870 **divisions.**
871 **(A)** Overview of the experiment design. E15.5/15.6 SE^{hi} FL cells co-stained with
872 CellTrace-FR were individually index sorted to FL-AKT-EC and cell divisions
873 monitored by live imaging for initial 48 hours of coculture. At day 14, colonies were
874 harvested and analyzed by flow cytometry.
875 **(B)** Cell division symmetry measured by ratio of fluorescence intensity of CellTrace-
876 FR inherited by daughter cells amongst SE^{hi} FL cells after first cell division that either
877 generated $ESAM^+$ HSC colonies or other colony types (n = 118 colonies pooled from
878 two independent experiments). Error bars represent standard deviation.
879 **(C)** CellTrace-FR and brightfield images of initial cell division in a representative
880 $ESAM^+$ HSC colony (symmetric division) and other colony type (asymmetric division).
881 **(D)** Relative expression of CD63 in E13.5 FL $CD45^+GR1^-F4/80^-SCA1^+$ HSPCs
882 divided by EPCR expression. Fr1: EPCR high (red), Fr2: EPCR medium (blue), Fr3:
883 EPCR low (gray). Fr: Fraction.
884 **(E)** Expression of CD63 by index analysis of E13.5 SE^{hi} FL-HSCs giving rise to
885 immunophenotypic $ESAM^+$ HSC colonies (red) or other colony types (gray) following
886 FL-AKT-EC coculture.
887 **(F)** Summary model. The FL SE^{hi} compartment comprises a heterogeneous population
888 of HSC-independent hematopoietic descendants (including embryonic multipotent
889 progenitors, eMPP,[9] short-term and developmentally-restricted HSCs[10], which may
890 actively contribute to prenatal hematopoiesis) and functionally competent (serially
891 transplantable) FL-HSCs, which are preserved for adult hematopoiesis. FL-HSCs
892 exhibit distinctly dormant biosynthetic and metabolic states, symmetric self-renewal
893 behavior, reduced cell cycle kinetics, and differentiation latency, facilitating the
894 regulated expansion of the HSC pool in the context of supportive signals from the FL
895 vascular niche.

896 **STAR★Methods**

897 **Resource availability**

898 **Lead contact**

899 Further information and requests for resources and reagents should be directed to

900 and will be fulfilled by the lead contact, Brandon Hadland (bhadland@fredhutch.org).

901

902 **Materials availability**

903 FL-AKT-EC are available upon request.

904

905 **Experimental model and subject details**

906 **Mice**

907 Wild type C57Bl6/J7 (CD45.2) and congenic C57BL/6.SJL-Ly5.1-Pep3b (CD45.1)

908 mice were bred at the Fred Hutchinson Cancer Research Center. Male and female

909 C57Bl6/J7 CD45.2 mice at 8-12 weeks of age were used for timed matings and

910 transplantation experiments. All animal studies were conducted in accordance with

911 the NIH guidelines for humane treatment of animals and were approved by the

912 Institutional Animal Care and Use Committee at the Fred Hutchinson Cancer Center.

913

914 **Methods details**

915 **Dissection of embryos and cell sorting**

916 Embryos were harvested from pregnant females and washed with PBS containing

917 2% FBS to minimize contaminating maternal tissues. Embryo age was determined

918 by the date of observed maternal plugging and further confirmed by the following

919 morphologic criteria. E13.5: Four lobes in the liver and retinal pigmentation were
920 observed, digits were not completely separated but showed indentations. E15.5:
921 Four lobes in the liver and retinal pigmentation were observed, digits were separated
922 clearly and appeared unparallel. E16.5: Four lobes in the liver and retinal
923 pigmentation were observed, digits were separated clearly and appeared parallel.
924 Fetal livers were dissected under an inverted microscope using fine forceps, pooled
925 in 10 ml conical tubes, and dissociated to a single cell suspension in 2% or 10% FBS
926 with PBS by vigorous pipetting followed by passage through a 70um strainer to
927 isolate single cells. Samples were then washed in PBS and resuspended in red
928 blood cell lysis buffer (4L water, 33.2g Ammonium chloride (Fisher #6613), 4g
929 sodium bicarbonate (Sigma Aldrich, S5761), and EDTA (0.1488g, Acros Organics,
930 147855000) or 200 uL/L of 0.5 M EDTA (Invitrogen, 15575-038)) for 5 minutes at
931 room temperature. Cells were washed once more, pre-incubated with anti-mouse
932 CD16/32 (FcRII blocker, BD Biosciences Cat#553141), and stained with the
933 following monoclonal anti-mouse antibodies as described in results: GR1 FITC
934 (clone RB6-8C5, BD Biosciences, RRID: AB_394643), F4/80 FITC (clone BM8,
935 Biolegend, RRID: AB_893502), CD201/EPCR PE (clone eBio1560, eBioscience,
936 RRID: AB_914317), CD45 Peridinin-Chlorophyll-Protein (PerCP) Cyanine 5.5 (clone
937 30-F11, Invitrogen, RRID: AB_906233), SCA1 APC (clone D7, eBioscience, RRID:
938 AB_469488), CD144 PE-cyanine7 (PE-Cy7) (clone eBioBV13, eBioscience, RRID:
939 AB_2573402), CD150 biotin (clone TC15-12F12.2, Biolegend, RRID: AB_345278),
940 Streptavidin APC-eFluor780(eBioscience, RRID: AB_10366688) or Streptavidin
941 APC-cyanine7(APC-Cy7) (BD Biosciences, RRID: AB_10054651), GR1

942 APCeFluor780 (clone RB6-8C5, eBioscience, RRID: AB_1518804), F4/80
943 APCeFluor780 (clone BM8, eBioscience, RRID: AB_2735036), CD150 PerCP-
944 Cyanine 5.5 (clone TC5-12F12.2, Biolegend, RRID: AB_2303663), CD45 PE-Cy7
945 (clone 30-F11, BD Biosciences, RRID: AB_394489), ESAM FITC (clone 1GB/ESAM,
946 Biolegend, RRID: AB_2044017). CD201 PerCP-eFluor710 (clone eBio1560,
947 Invitrogen, RRID: AB_10718383), CD63 PE (clone NVG-2, Biolegend, RRID:
948 AB_11203532). DAPI (Millipore, Cat#268298) was used to exclude dead cells. In
949 some experiments, FL cells were also stained with CellTrace Far Red
950 (ThermoFisher, Cat#C34564) following the manufacturer's protocol. Cells were
951 sorted by either BD FACSymphony6 or Aria II equipped with BD FACS Diva
952 Software with index sorting capability (Becton Dickinson). For index-sorted single
953 cells, sorting was performed in single cell mode with maximum purity mask settings
954 to minimize contaminating cells.
955
956 **Flow cytometric analysis of fresh FL cells**
957 For the phenotyping of freshly isolated FL, harvested FL cells were subjected to red
958 blood cell lysis (as described above), pre-incubated with anti-mouse CD16/32 (FcRII
959 blocker), and stained with the following monoclonal anti-mouse antibodies: GR1
960 APCeFluor780 (clone RB6-8C5, eBioscience, RRID: AB_1518804), F4/80
961 APCeFluor780 (clone BM8, eBioscience, RRID: AB_2735036), CD201 PE (clone
962 eBio1560, eBioscience, RRID: AB_914317), SCA1 APC (clone D7, eBioscience,
963 RRID: AB_469488), CD45 PE-Cy7 (clone 30-F11, BD Biosciences, RRID:
964 AB_394489), TER119 FITC (clone TER119, eBiosceicne, RRID: AB_465311), CD2

965 FITC (clone RM2-5, eBioscience, RRID: AB_464874), CD5 FITC (clone 53-7.3,
966 eBioscience, RRID: AB_464909), CD8a FITC (clone 53-6.7, eBioscience, RRID:
967 AB_469897), B220 FITC (clone RA3-6B2, BD Biosciences, RRID: AB_394618),
968 CD48 FITC (clone HM48-1, eBioscience, RRID: AB_465078). DAPI was used to
969 exclude dead cells. Cells were analyzed by BD FACSymphony S6 equipped with BD
970 FACS Diva Software (Becton Dickinson) and further analyzed by Flow Jo software.
971

972 **Generation of FL-derived Akt-EC (FL-AKT-EC)**

973 FL-AKT-EC were generated as previously described for similar EC lines derived from
974 murine AGM,[19,20] which is further detailed in a protocol available at Nature Protocol
975 Exchange (https://protocolexchange.researchsquare.com/article/pex-986/v1). Briefly,
976 FL tissues were dissected from pooled E12 embryos and VECadherin^{+}CD45^{-}CD41^{-}
977 Ter119^{-} cells were isolated by FACS. Sorted cells (>50,000 cells) were cultured on
978 48-well tissue culture plates coated with RetroNectin (r-fibronectin CH-296; Takara
979 Bio Inc.) in EC media; Iscove's Modified Dulbecco's Medium (Gibco), 20% FBS
980 (HyClone, fisher scientific), 1%Penicillin/streptomycin (Gibco), 1%L-glutamine
981 (STEMCELL Technologies), heparin 0.1 mg/ml (Sigma-Aldrich), endothelial mitogen
982 100 µg/ml (Biomedical Technologies)*, VEGF (50 ng/ml; PeproTech), CHIR009921
983 (5 µM; Stemgent), and SB431542 (10 µM; R&D Systems). *EC mitogen no longer
984 available (currently substituting rmVEGF-10ng/ml, rmFGF-10ng/ml, rmIGF-1-
985 10ng/ml, and rmEGF-10ng/ml). Following 1–2 days culture, colonies of ECs were
986 transduced by lentivirus with constitutively active murine AKT (PGK.myr-AKT) as
987 previously reported.[19] Cells were serially split, expanded in EC media and then

988 frozen down for future use.

989

990 **FL-AKT-EC coculture**

991 For coculture experiments, FL-AKT-ECs at passage 12 or less were plated at a
992 density of 1 × 10^4 cells per well on 96-well plates 1-2 days prior to use. Prior to
993 coculture, FL-AKT-EC layers were washed with serum-free media (X-VIVO20
994 (Lonza). For single cell index coculture, FL-HSCs (from donor CD45.2 mice) were
995 individually index sorted to each well of 96-well containing FL-AKT-EC in serum-free
996 coculture media consisting of X-VIVO 20 with recombinant cytokines (PeproTech):
997 murine stem cell factor (SCF) at 100 ng/ml and thrombopoietin (TPO) at 20 ng/ml.
998 Formation of hematopoietic colonies in coculture was monitored visually over time by
999 microscopy and following various periods of coculture as indicated, a portion of cells
1000 (as indicated for each experiment) were harvested by pipetting for phenotypic
1001 analysis by flow cytometry, and in some experiments, remaining cells were used for
1002 confirmatory transplantation assays and/or scRNAseq (described below). Based on
1003 initial observations of the kinetics of colony emergence (Figure S1D), we assayed
1004 the immunophenotype of colonies between day 12-15 to ensure capture of the entire
1005 array of colony types simultaneously for the remaining experiments. When the
1006 number of viable $CD45^+$ cell recorded by flow cytometry was <2, the well was
1007 classified as “no colony.” Based on initial experiments correlating colony
1008 immunophenotype with engraftment properties, colonies with greater than 80% $GR1^-$
1009 $F4/80^-SCA1^+EPCR^+$ or $CD48^-SCA1^+EPCR^+$ cells amongst total viable $CD45^+$ cells
1010 were retrospectively classified as “HSC-like colonies.” Hematopoietic colonies with

1011 all other immunophenotypes were classified as “other colonies.” For experiments
1012 using conditioned media, X-VIVO 20 media supplemented with SCF and TPO was
1013 continuously exposed to FL-AKT-ECs (conditioned media) plated in T75 flasks.
1014 Index-sorted FL-HSCs were replenished with conditioned media every 48 hours
1015 during coculture.
1016
1017 **Flow cytometric analysis of colonies**
1018 Following coculture, a fraction of the generated hematopoietic progeny in each 96-
1019 well was harvested by pipetting from the EC layer for analysis of surface phenotype
1020 by flow cytometry (unless otherwise indicated, 50% of cells generated following
1021 single cell index culture on FL-AKT-EC were used for flow cytometry). Cells were
1022 spun and re-suspended in PBS with 2% FBS, pre-incubated with anti-mouse
1023 CD16/CD32 (FcRII block) and then stained with the following anti-mouse monoclonal
1024 antibodies: GR1 FITC (clone RB6-8C5, BD Biosciences, RRID: AB_394643), F4/80
1025 FITC (clone BM8, Biolegend, RRID: AB_893502), CD201 PE (clone eBio1560,
1026 eBioscience, RRID: AB_914317), CD45 PerCP-Cyanine5.5 (clone 30-F11,
1027 Invitrogen, RRID: AB_906233), SCA1 APC (clone D7, eBioscience, RRID:
1028 AB_469488), CD144 PE-Cy7 (clone eBioBV13, eBioscience, RRID: AB_2573402),
1029 CD45 PE-Cy7 (clone 30-F11, BD Biosciences, RRID: AB_394489), ESAM FITC
1030 (clone 1GB/ESAM, Biolegend, RRID: AB_2044017), SCA1 Alexa Fluor700 (clone
1031 D7, eBioscience, RRID: AB_657836), CD201 PerCPeFluor710(clone eBio1560,
1032 Invitrogen, RRID: AB_10718383), CD48 APC (clone HM48-1, Invitrogen, RRID:
1033 AB_469408), GR1 APCeFluor780 (clone RB6-8C5, eBioscience, RRID:

1034 AB_1518804), F4/80 APCeFluor780 (clone BM8, eBioscience, RRID: AB_2735036).
1035 DAPI was used to exclude dead cells. Cells were analyzed by either BD FACS Canto
1036 II or BD FACS LSR Fortessa equipped with BD FACS Diva Software (Becton
1037 Dickinson) and further analyzed by Flow Jo ver.10 software. For index sort analysis,
1038 Flow Jo Plugin v3.0.6 and R4.2.2 were used.
1039

1040 **Live-cell imaging and image data analysis**

1041 Live-cell imaging of colony formation from single index-sorted cells was carried out
1042 on the Incucyte SX5 incubator microscope system. Brightfield and fluorescent
1043 (Celltrace-Far Red) images of whole wells were captured every 3 hours during the
1044 initial incubation period (48-96 hours). For image analysis, raw image data were
1045 exported as tiff files after background reduction, which were then used as input for a
1046 custom-developed cell tracing program in Python. The code of the celltracing
1047 program has been deposited in our lab's Github directory for open access. In brief,
1048 the program reads in the whole time series of each well at once, identifies cell
1049 objects by fluorescent signal (CellTrace-Far Red), tracks cell divisions and
1050 hierarchical orders, and extracts parameters (eg. cell volume and cell-cell distance)
1051 for output. Python packages used in the program include *skimage*, *cv2*, *numpy*,
1052 *scipy*, *os*, and *glob*. More information about the program is available in its description
1053 on Github.
1054

1055 **Transplantation assays**

1056 Recipient C57BL/6.SJL-Ly5.1-Pep3b (CD45.1) mice (6-12 weeks) were lethally

1057 irradiated with 1,000cGy using a Cesium source, and transplanted via tail vein
1058 injection. Whole bone marrow $1x10^5$ cells from C57BL/6.SJL-Ly5.1-Pep3b (CD45.1)
1059 were used for hematopoietic rescue. For single cell index assays, a fraction of the
1060 colonies harvested by pipetting was used for flow cytometric analysis (described
1061 above) and the remaining cells (or a fraction indicated in each experiment) were
1062 used for transplantation. For some experiments, a portion of the cells (as indicated
1063 for each experiment) was also used for scRNAseq studies. In limit-dilution
1064 experiments, residual (50%) cells from a single colony were serially diluted and used
1065 for transplantation. ELDA software (http://bioinf.wehi.edu.au/software/elda/) was
1066 used to calculate the number and frequency of HSCs per colony based on the
1067 fraction of mice demonstrating serial-engraftment at each dilution.[85] Secondary
1068 transplants were performed after 24 weeks using $2x10^6$ whole bone marrow cells
1069 collected from primary recipients transplanted to lethally irradiated C57BL/6.SJL-
1070 Ly5.1-Pep3b (CD45.1) secondary recipients via the tail vein. Serial, long-term
1071 multilineage engraftment was strictly defined as donor (CD45.2) contribution to the
1072 peripheral blood with detectable contribution (>0.1%) to each lineage of donor
1073 myeloid (Gr-1 and F4/80), B cells (CD19) and T-cells (CD3) at 24 weeks post-
1074 transplant in both primary and secondary recipients. Transplant data is summarized
1075 in Table S10. We observed in initial experiments that recipients without detectable
1076 multilineage donor engraftment at 24 weeks post-transplant in primary recipients
1077 failed to provide multilineage engraftment in secondary recipients; thus, for
1078 remaining experiments, mice failing to demonstrate multilineage engraftment in
1079 primary recipients at 24 weeks were not subject to secondary transplantation.

1080 Recipient mice that died before the final timepoint analyzed for engraftment were
1081 censored for analysis of long-term serial engraftment potential but peripheral blood
1082 engraftment for these mice is shown at the ultimate timepoint analyzed before death
1083 in relevant figures (as shown in Table S10 for all transplant data).
1084
1085 **Analysis of donor chimerism in recipient mice**
1086 Leukocytes from peripheral blood samples collected by retro-orbital bleeding were
1087 analyzed at the indicated time points. Lineage-specific staining for donor (CD45.2)
1088 and recipient/hematopoietic rescue (CD45.1) cells from peripheral blood was
1089 performed as previously described [20], using anti-mouse monoclonal antibodies: CD3
1090 FITC (clone 17A2, BD Pharmingen, RRID: AB_395698), F4/80 PE (clone BM8,
1091 Invitrogen, RRID: AB_465923), GR1 PerCP-Cyanine 5.5 (clone RB6-8C5, BD
1092 Phrmingen, RRID: AB_394334), CD45.1 PE-Cy7 (clone A20, eBioscience,
1093 RRID:AB_469629), CD19 APC (clone 1D3/CD19, Biolegend, RRID: AB_2629839),
1094 CD45.2 APCeFluor780 (clone 104, Invitrogen, RRID: AB_1272175).
1095 Bone marrow was collected from primary recipient femur, fibula and tibiae and
1096 treated with red blood cell lysis buffer for 5 minutes at room temperature. Cells were
1097 then washed and stained using anti-mouse monoclonal antibodies: CD45.1 Brilliant
1098 Violet 510 (clone A20, BD Pharmingen, RRID: AB_2739150), CD45.2 FITC (clone
1099 104, BD Pharmingen, RRID: AB_395041), CD2 PE (clone RM2-5, BD Pharmingen,
1100 RRID: AB_2073810), CD5 PE (clone 53-7.3, Biolegend, RRID: AB_312737), CD8a
1101 PE (clone 53-6.7, BD Pharmingen, RRID: AB_394571), GR1 PE (clone RB6-8C5,
1102 BD Pharmingen, RRID: AB_394644), TER119 PE (clone TER-119, eBioscience,

1103 RRID: AB_466043), CD11b PE (clone M1/70, BD Biosciences, RRID: AB_394775),
1104 B220 PE (clone RA3-6 B2, BD Pharmingen, RRID: AB_394620), CD150 PerCP-
1105 Cyanine 5.5 (clone TC5-12F12.2, Biolegend, RRID: AB_2303663), SCA1 APC
1106 (clone D7, eBioscience, RRID: AB_469488), CD117 APCeFluor780 (clone 2B8,
1107 eBioscience, RRID: AB_1272177), CD48 PE-Cy7 (clone HM48-1, Biolegend, RRID:
1108 AB_2075049). DAPI was used to exclude dead cells. Cells were analyzed by BD
1109 FACS Canto II equipped with BD FACS Diva Software (Becton Dickinson) and
1110 further analyzed by Flow Jo software.
1111

1112 **Single cell RNA sequence experiments**

1113 **Freshly isolated FL-HSC and FL-AKT-EC**

1114 For single cell RNA sequencing (scRNAseq) studies, freshly sorted DAPI^{-}
1115 VECadherin$^{-/low}$CD45^{+}Gr1^{-}F4/80^{-}Sca1^{high}EPCR^{high} (SE^{hi}) cells derived from E13.5
1116 murine fetal liver samples were subject to scRNAseq experiment. Sorted cells (3050
1117 total) were washed twice and resuspended with PBS containing 0.04% ultrapure
1118 BSA (Invitrogen) on ice.
1119 For FL-AKT-EC, confluent ECs in a 6-well plate were cultured in serum-free
1120 coculture media (described above) overnight, harvested by treatment with TrypLE
1121 Express (Gibco), then resuspended in PBS/10% FBS at 4°C, washed twice and
1122 resuspended PBS with 0.04% ultrapure BSA in on ice. A portion of cells (targeting
1123 3,500 cells) were subject to downstream scRNAseq assay.
1124 Cell suspensions were loaded into the Chromium Single Cell Chip G (10X
1125 Genomics) and processed in the Chromium single cell controller (10X Genomics).

1126 The 10X Genomics Version 3.1 single cell 3' kit was used to prepare single cell
1127 mRNA libraries with the Index Kit T Set A, according to manufacturer
1128 protocols. Sequencing was performed for pooled libraries from each sample on an
1129 Illumina NextSeq 500 using the 75 cycle, high output kit, targeting a minimum of
1130 100,000 reads per cell.
1131

1132 **Cocultured FL-HSC colonies**

1133 For scRNAseq of colonies emerging following coculture, a portion of each colony
1134 was used for flow cytometry and transplantation, as indicated in each experiment,
1135 and the remaining used for scRNAseq. TotalSeq™-B0301-307 anti-mouse Hashtag
1136 Antibodies (clones M1/42; 30-F11; Biolegend, RRID: AB_ 2814067-2814072) were
1137 used to label individual colonies for multiplexing,[50] at a concentration of 125 mg/ml
1138 (determined by titration of PE-conjugated antibodies of the identical clones), per
1139 manufacturer (10X Genomics) protocols. Cells labeled with hashing antibodies were
1140 pooled, loaded into the Chromium Single Cell Chip G (10X Genomics), and
1141 processed in the Chromium single cell controller (10X Genomics). Single cell mRNA
1142 libraries were prepared using the 10X Chromium Next GEM Single Cell3' Reagent
1143 Kits version 3.1 with Feature Barcoding technology for Cell Surface Protein, per
1144 manufacturer protocols. Sequencing was performed for pooled libraries from each
1145 sample on an Illumina NextSeq 500 using the 75 cycle, high output kit, targeting a
1146 minimum of 35,000 reads per cell.
1147

1148 **Human FL-HSCs**

1149 Human fetal livers were obtained by the Birth Defects Research Laboratory at the
1150 University of Washington following ethics board approval and maternal written
1151 consent. This study was performed in accordance with ethical and legal guidelines of
1152 the University of Washington institutional review board. Specimen age is denoted in
1153 post conception days, two weeks less than gestational age, as determined by fetal
1154 foot length measurement. Liver tissue was transferred into sterile C Tube (Miltenyi
1155 Biotec, 130-093-237) with 10 mL of cold 10% FBS in PBS and dissociated using the
1156 gentleMACS Octo Dissociator (Miltenyi Biotec, 165 rpm for 36 seconds at room
1157 temperature). The cell suspension was filtered through a 70uM cell strainer and
1158 washed 3 times with 1 mL 10% FBS in PBS. Cells were centrifuged, resuspended in
1159 5mL RBC lysis buffer (2.0L Sterile Water, 16.6g Ammonium Chloride, 2.0g Sodium
1160 Bicarbonate, 74.4mg EDTA) and incubated at room temperature for 5 minutes. The
1161 suspension was centrifuged, resuspend with 4 mL 10% FBS in PBS, and again
1162 filtered through a 70 uM cell strainer. After centrifugation, the pellet was
1163 resuspended in 4 mL MACs buffer (MACS BSA Stock Solution Miltenyi Biotec 130-
1164 091-376, in autoMACs Rinsing Solution, Miltenyi Biotec 130-091-222) for CD34
1165 enrichment using CD34 selection beads/kit (Miltenyi Biotech, 130-100-453)
1166 according to the manufacturer protocol. CD34-enriched cells were cryopreserved at
1167 a density of $1X10^6$/ml in freezing media (90% FBS/10% DMSO) or Cryo-stor CS 10
1168 (Sigma, C2874). Prior to FACS, frozen samples were thawed in 37C water bath,
1169 washed with PBS with 10% FBS, and incubated with the following anti-human
1170 antibodies; APC-conjugated CD34 (clone 8G12, BD Biosciences, PRID:AB_400514),
1171 BV421-conjugated CD90 (clone 5E10, BD Biosciences, RRID:AB_2737651), PE-

1172 conjugated CD201 (clone RCR-401, Biolegend, RRID:AB_10900806), PE-Cyanine7-
1173 conjugated CD38 (clone HIT2, eBioscience, RRID:AB_1724057) and APC-
1174 eFour780-conjugated CD45RA(clone HI100, eBioscience, RRID:AB_1085364).
1175 DAPI staining was used to exclude dead cells. All reagents for cell staining were
1176 diluted in PBS with 10% FBS and staining was carried out on ice for 30 minutes.
1177 Cells were sorted to enrich for HSCs as $CD34^{+}CD38^{-}CD45RA^{-}CD90^{+}EPCR^{+}$ on a
1178 BD FACSymphonyS6 equipped with BD FACSDiva Software. Sorted cells were
1179 washed with PBS containing 0.04% ultrapure BSA (Invitrogen) and re-suspended in
1180 0.04% ultrapure BSA in PBS on ice. Cells were processed using the Chromium Next
1181 GEM Single Cell 5' Reagent Kits v2 (Dual Index) (10X Genomics, PN-1000265) in
1182 accordance with the manufacturers protocol. Briefly, GEMs were generated using
1183 Chromium Next GEM Chip K (10X Genomics, PN-1000182) and processed in the
1184 Chromium Controller, targeting 1,000 to 2,500 cells per lane. Following GEM-RT
1185 clean-up and cDNA amplification, 5' genex expression dual index library construction
1186 was performed using the Dual Index plate TT Set A. Libraries were pooled and
1187 sequenced by the Northwest Genomics Center on an Illumina NovaSeq 6000 using
1188 the SP 100 cycle, high output kit.
1189

1190 **Single cell transcriptome computational analysis and quality control**

1191 The Cell Ranger pipeline v6.1.2 (10X Genomics) was used to align reads to
1192 the mm10 reference genome (for mouse samples) or to the GChr38 reference
1193 genome (for human samples) to generate the feature barcode matrix, filtering low-
1194 quality cells using default parameters. Monocle3 (v.3.1.2.9) was used for

1195 downstream analysis, combining read-depth normalized data for each group of
1196 samples.[24,86] Uniform Manifold Approximation (UMAP) was used for dimensionality
1197 reduction.[87] The data was mapped onto the top principal components (default
1198 settings). The alignCDS() function was applied to remove batch effects between
1199 samples using a “mutual nearest neighbor” algorithm, Batchelor (v.1.2.4).[88]
1200 Clustering was performed using the Louvain method implemented in
1201 Monocle3.[89] Cells with high mitochondrial genes were excluded (>10% in HSC
1202 colonies and FL-AKT-EC or >5% in fresh FL-HSCs), as were cells with low genes
1203 per cell (<1,000) and cells with low UMI per cell (UMI<10,000 for scRNAseq data in
1204 fresh FL-HSCs or UMI<3,000 for scRNAseq data in HSC colonies). Outlying clusters
1205 of cells identified as non-hematopoietic populations (lacking expression of *Ptprc*, a
1206 pan-hematopoietic gene, and expressing either *Cdh5*, an EC-specific gene, or *Hbb-*
1207 *bt*, a globin gene expressed by red blood cells) were removed for downstream
1208 analysis. The m3addon package was used to demultiplex the hashed samples in
1209 conjunction with Monocle3. Cells unique to each hashtag-oligo were assigned to the
1210 corresponding original colony names.
1211 The number of UMIs and genes expressed per cell are as follows. Figure 4: UMI
1212 (median 39120, mean 40290, range 10074-92208) and genes expressed (median
1213 6088, mean 5923, range 2513-8768). Figure 5: UMI (median: 18267, mean:19908,
1214 range 3821-49485) and genes expressed (median: 4465, mean: 4435, range 1819-
1215 6694). Figure S11: UMI (median 15701, mean 15595, range 4601-29149) and genes
1216 expressed (median 3701, mean 3599, range 1473-4970).
1217

1218 **Gene module analysis**

1219 The graph_test function and the find_gene_modules function in Monocle3 were used
1220 to find genes that vary across clusters and cell types, and to group genes that have
1221 similar patterns of expressions into modules. Module genes with q-value<0.05 were
1222 selected.

1223

1224 **Differential gene expression analysis**

1225 A quasipoisson distribution was used to evaluate the differential expression with the
1226 fit_model() and coefficient_table() functions in Monocle3. A q-value for multiple
1227 hypothesis testing was calculated by the Benjamini and Hochberg correction
1228 method, and q<0.05 was considered as statistically significant.

1229

1230 **Gene-set scores**

1231 Gene-set scores were calculated as the log-transformed sum of the size factor-
1232 normalized expression for each gene[90] from published signature gene-sets (Table
1233 S1) as well as the Molecular Signatures Database (https://www.gsea-
1234 msigdb.org/gsea/msigdb/index.jsp) including: Dormant HSC signature genes,[27]
1235 Serial-engrafting HSC signature genes,[28] diapause signature genes,[29,31] Low output
1236 signature genes,[28] MolO genes,[26] REPOPSIG genes,[13] High output signature
1237 genes,[28] Multilineage signature genes,[28] common stem cell dormancy genes
1238 associated with lipid metabolism,[32] Hallmark Myc target genes (https://www.gsea-
1239 msigdb.org/gsea/msigdb/mouse/geneset/HALLMARK_MYC_TARGETS_V1.html,
1240 https://www.gsea-

1241 msigdb.org/gsea/msigdb/mouse/geneset/HALLMARK_MYC_TARGETS_V2.html),
1242 Activated HSC/MPPs, [27,84] WP_PURINE_METABOLISM (https://www.gsea-
1243 msigdb.org/gsea/msigdb/mouse/geneset/WP_PURINE_METABOLISM.html),
1244 WP_TCA_CYCLE (https://www.gsea-
1245 msigdb.org/gsea/msigdb/mouse/geneset/WP_TCA_CYCLE.html),
1246 HALLMARK_OXIDATIVE_PHOSPHORYLATION (https://www.gsea-
1247 msigdb.org/gsea/msigdb/mouse/geneset/HALLMARK_OXIDATIVE_PHOSPHORYL
1248 ATION.html), WP_MRNA_PROCESSING (https://www.gsea-
1249 msigdb.org/gsea/msigdb/mouse/geneset/WP_MRNA_PROCESSING.html),
1250 REACTOME_TRANSLATION (https://www.gsea-
1251 msigdb.org/gsea/msigdb/mouse/geneset/REACTOME_TRANSLATION.html).
1252 Wilcoxon Rank Sum Test (ggupbr package v0.4.0) was used to calculate p values.
1253

1254 **Identification of genes encoding surface proteins**

1255 To identify genes encoding putative surface proteins in scRNAseq analysis, we
1256 cross-referenced to CPSA validated surface protein[91]
1257 (http://wlab.ethz.ch/cspa/#downloads). Only those with CSPA category defined as 1-
1258 High confidence were included.
1259

1260 **Gene Ontology (GO) analysis**

1261 Gene enrichment analysis was performed using an online functional annotations
1262 tool, The AmiGO v2.5.13[92-94] (http://geneontology.org/docs/go-citation-policy/), with
1263 the 'GO biological process complete' algorithm.

1264

1265 **NicheNet**

1266 The nichenetr package[60]

1267 (https://github.com/saeyslab/nichenetr/blob/master/vignettes/ligand_activity_geneset.

1268 md) was applied to scRNAseq data to identify receptor-ligand interaction between

1269 FL-AKT-EC or primary FL-EC and cells in the serially engrafting HSC colony (#2). All

1270 genes expressed in cells from HSC colonies (colonies #1-6) were used as the

1271 background gene-set, and genes that were significantly enriched in serially-

1272 engrafting HSC colony #2 (Table S6) were used as the gene-set of interest (i.e.,

1273 genes in the receiver cell population that are potentially affected by ligands).

1274

1275 **Latent variable modeling with encoded domain knowledge (MuVI)**

1276 Latent variable modeling with gene ontology or pathway gene-sets as Bayesian

1277 priors were performed using the MuVI package[35] (https://github.com/MLO-lab/MuVI),

1278 with relevant published gene-sets (Table S10) or gene-sets downloaded from

1279 Molecular Signatures Database (https://www.gsea-msigdb.org/gsea/msigdb).

1280 scRNAseq count matrix from relevant experiments were used as input for the 'rna'

1281 view and MuVI was run on a single view. Max training number was 2,000 epochs,

1282 batch size was 2,000, learning rate was 0.003, 3 dense factors (random priors) were

1283 included in the mask. UMAP projection, leiden clustering, and plotting were

1284 performed using incorporated analysis and plotting modules of MuVI that are based

1285 on Scanpy (https://scanpy.readthedocs.io/).

1286

1287 **Quantification and Statistical analysis**

1288 Wilcoxon signed-rank testing was used for comparison of gene-set scores in
1289 scRNAseq studies. Mann-Whitney testing was used where indicated. One-way-
1290 ANOVA with Dunnett's multiple comparisons test was used in statistical analysis for
1291 the comparison between multiple cohorts. A p-value < 0.05 was considered
1292 statistically significant. GraphPad Prism (GraphPad Software, La Jolla, CA) was
1293 used for all statistical analysis except for scRNAseq studies.

1294

1295 **Graphics**

1296 Some figures were created using BioRender.com.

1297

1298 **Data and Code Availability**

1299 - Raw sequencing data and Monocle3 cell data sets have been deposited at
1300 NCBI GEO (accession number GSE233031) and are publicly available as of
1301 the date of publication.
1302 - All original code generated during this study has been deposited at Github
1303 and is publicly available as of the date of publication. Github repository:
1304 https://github.com/FredHutch/Ishida-etal-2023.
1305 - Any additional information required to reanalyze the data reported in this
1306 paper is available from the lead contact (Brandon Hadland,
1307 bhadland@fredhutch.org) upon request.

1308

1309

1310 **Supplementary Information**

1311 **Table S1:** Gene-sets used for this study

1312 **Table S2:** Gene modules and related gene ontology analysis of scRNAseq data from
1313 freshly isolated E13.5 FL-HSCs (related to Figure 4).

1314 **Table S3:** Gene module analysis of scRNAseq data from E12.5 FL-HSCs (published
1315 data set, GEO GSE180050) (related to Figure S6).

1316 **Table S4:** Gene module analysis of scRNAseq data from human FL-HSCs (related
1317 to Figure S7).

1318 **Table S5:** Gene modules and related gene ontology analysis scRNAseq data from
1319 cocultured HSC colonies (related to Figure 5).

1320 **Table S6:** Genes differentially expressed by serially engrafting HSC colony (#2)
1321 versus HSC-like colonies lacking long-term engraftment potential (related to Figure
1322 5).

1323 **Table S7:** Gene module analysis of scRNAseq data from cocultured HSC-like
1324 colonies divided by ESAM expression (related to Figure S11).

1325 **Table S8:** Receptor-ligand pairs inferred by a comprehensive database of curated
1326 pairs of ligands and receptors (using scRNAseq data from FL-AKT-EC and HSC-like
1327 colonies) (related to Figure 6).

1328 **Table S9:** Receptor-ligand pairs inferred by a comprehensive database of curated
1329 pairs of ligands and receptors (using published scRNAseq data from FL-EC: GEO
1330 GSE174209) (related to Figure S13).

1331 **Table S10:** Summary of transplant data

1332

References

1. Bowie, M.B., McKnight, K.D., Kent, D.G., McCaffrey, L., Hoodless, P.A., and Eaves, C.J. (2006). Hematopoietic stem cells proliferate until after birth and show a reversible phase-specific engraftment defect. The Journal of clinical investigation *116*, 2808-2816. 10.1172/jci28310.
2. Bowie, M.B., Kent, D.G., Dykstra, B., McKnight, K.D., McCaffrey, L., Hoodless, P.A., and Eaves, C.J. (2007). Identification of a new intrinsically timed developmental checkpoint that reprograms key hematopoietic stem cell properties. Proceedings of the National Academy of Sciences of the United States of America *104*, 5878-5882. 10.1073/pnas.0700460104.
3. Yokomizo, T., Ideue, T., Morino-Koga, S., Tham, C.Y., Sato, T., Takeda, N., Kubota, Y., Kurokawa, M., Komatsu, N., Ogawa, M., et al. (2022). Independent origins of fetal liver haematopoietic stem and progenitor cells. Nature *609*, 779-784. 10.1038/s41586-022-05203-0.
4. Dignum, T., Varnum-Finney, B., Srivatsan, S.R., Dozono, S., Waltner, O., Heck, A.M., Ishida, T., Nourigat-McKay, C., Jackson, D.L., Rafii, S., et al. (2021). Multipotent progenitors and hematopoietic stem cells arise independently from hemogenic endothelium in the mouse embryo. Cell Rep *36*, 109675. 10.1016/j.celrep.2021.109675.
5. Ulloa, B.A., Habbsa, S.S., Potts, K.S., Lewis, A., McKinstry, M., Payne, S.G., Flores, J.C., Nizhnik, A., Feliz Norberto, M., Mosimann, C., and Bowman, T.V. (2021). Definitive hematopoietic stem cells minimally contribute to embryonic hematopoiesis. Cell Reports *36*, 109703. 10.1016/j.celrep.2021.109703.
6. Ganuza, M., Hall, T., Finkelstein, D., Chabot, A., Kang, G., and McKinney-Freeman, S. (2017). Lifelong haematopoiesis is established by hundreds of precursors throughout mammalian ontogeny. Nature cell biology *19*, 1153-1163. 10.1038/ncb3607.
7. Pei, W., Feyerabend, T.B., Rössler, J., Wang, X., Postrach, D., Busch, K., Rode, I., Klapproth, K., Dietlein, N., Quedenau, C., et al. (2017). Polylox barcoding reveals haematopoietic stem cell fates realized in vivo. Nature *548*, 456-460. 10.1038/nature23653.
8. Ganuza, M., Hall, T., Myers, J., Nevitt, C., Sánchez-Lanzas, R., Chabot, A., Ding, J., Kooienga, E., Caprio, C., Finkelstein, D., et al. (2022). Murine foetal liver supports limited detectable expansion of life-long haematopoietic

progenitors. Nature cell biology *24*, 1475-1486. 10.1038/s41556-022-00999-5.

9. Patel, S.H., Christodoulou, C., Weinreb, C., Yu, Q., da Rocha, E.L., Pepe-Mooney, B.J., Bowling, S., Li, L., Osorio, F.G., Daley, G.Q., and Camargo, F.D. (2022). Lifelong multilineage contribution by embryonic-born blood progenitors. Nature *606*, 747-753. 10.1038/s41586-022-04804-z.

10. Beaudin, A.E., Boyer, S.W., Perez-Cunningham, J., Hernandez, G.E., Derderian, S.C., Jujjavarapu, C., Aaserude, E., MacKenzie, T., and Forsberg, E.C. (2016). A Transient Developmental Hematopoietic Stem Cell Gives Rise to Innate-like B and T Cells. Cell stem cell *19*, 768-783. 10.1016/j.stem.2016.08.013.

11. Benz, C., Copley, M.R., Kent, D.G., Wohrer, S., Cortes, A., Aghaeepour, N., Ma, E., Mader, H., Rowe, K., Day, C., et al. (2012). Hematopoietic stem cell subtypes expand differentially during development and display distinct lymphopoietic programs. Cell stem cell *10*, 273-283. 10.1016/j.stem.2012.02.007.

12. Iwasaki, H., Arai, F., Kubota, Y., Dahl, M., and Suda, T. (2010). Endothelial protein C receptor-expressing hematopoietic stem cells reside in the perisinusoidal niche in fetal liver. Blood *116*, 544-553. 10.1182/blood-2009-08-240903.

13. Che, J.L.C., Bode, D., Kucinski, I., Cull, A.H., Bain, F., Becker, H.J., Jassinskaja, M., Barile, M., Boyd, G., Belmonte, M., et al. (2022). Identification and characterization of in vitro expanded hematopoietic stem cells. *23*, e55502. https://doi.org/10.15252/embr.202255502.

14. Hadland, B.K., Varnum-Finney, B., Mandal, P.K., Rossi, D.J., Poulos, M.G., Butler, J.M., Rafii, S., Yoder, M.C., Yoshimoto, M., and Bernstein, I.D. (2017). A Common Origin for B-1a and B-2 Lymphocytes in Clonal Pre- Hematopoietic Stem Cells. Stem Cell Reports *8*, 1563-1572. 10.1016/j.stemcr.2017.04.007.

15. McKinney-Freeman, S.L., Naveiras, O., Yates, F., Loewer, S., Philitas, M., Curran, M., Park, P.J., and Daley, G.Q. (2009). Surface antigen phenotypes of hematopoietic stem cells from embryos and murine embryonic stem cells. Blood *114*, 268-278. 10.1182/blood-2008-12-193888 %J Blood.

16. Kim, I., He, S., Yilmaz, O.H., Kiel, M.J., and Morrison, S.J. (2006). Enhanced purification of fetal liver hematopoietic stem cells using SLAM family receptors. Blood *108*, 737-744. 10.1182/blood-2005-10-4135.

17. Papathanasiou, P., Attema, J.L., Karsunky, H., Xu, J., Smale, S.T., and Weissman, I.L. (2009). Evaluation of the long-term reconstituting subset of hematopoietic stem cells with CD150. Stem Cells *27*, 2498-2508. 10.1002/stem.170.
18. McKinney-Freeman, S.L., Naveiras, O., Yates, F., Loewer, S., Philitas, M., Curran, M., Park, P.J., and Daley, G.Q. (2009). Surface antigen phenotypes of hematopoietic stem cells from embryos and murine embryonic stem cells. Blood *114*, 268-278. 10.1182/blood-2008-12-193888.
19. Kobayashi, H., Butler, J.M., O'Donnell, R., Kobayashi, M., Ding, B.S., Bonner, B., Chiu, V.K., Nolan, D.J., Shido, K., Benjamin, L., and Rafii, S. (2010). Angiocrine factors from Akt-activated endothelial cells balance self-renewal and differentiation of haematopoietic stem cells. Nature cell biology *12*, 1046-1056. 10.1038/ncb2108.
20. Hadland, B.K., Varnum-Finney, B., Poulos, M.G., Moon, R.T., Butler, J.M., Rafii, S., and Bernstein, I.D. (2015). Endothelium and NOTCH specify and amplify aorta-gonad-mesonephros-derived hematopoietic stem cells. J Clin Invest *125*, 2032-2045. 10.1172/jci80137.
21. Ema, H., and Nakauchi, H. (2000). Expansion of hematopoietic stem cells in the developing liver of a mouse embryo. Blood *95*, 2284-2288.
22. Hadland, B.K., Varnum-Finney, B., Nourigat-Mckay, C., Flowers, D., and Bernstein, I.D. (2018). Clonal Analysis of Embryonic Hematopoietic Stem Cell Precursors Using Single Cell Index Sorting Combined with Endothelial Cell Niche Co-culture. JoVE, e56973. doi:10.3791/56973.
23. Yokota, T., Oritani, K., Butz, S., Kokame, K., Kincade, P.W., Miyata, T., Vestweber, D., and Kanakura, Y. (2009). The endothelial antigen ESAM marks primitive hematopoietic progenitors throughout life in mice. Blood *113*, 2914-2923. 10.1182/blood-2008-07-167106.
24. Cao, J., Spielmann, M., Qiu, X., Huang, X., Ibrahim, D.M., Hill, A.J., Zhang, F., Mundlos, S., Christiansen, L., Steemers, F.J., et al. (2019). The single-cell transcriptional landscape of mammalian organogenesis. Nature *566*, 496-502. 10.1038/s41586-019-0969-x.
25. Nakamura-Ishizu, A., Ito, K., and Suda, T. (2020). Hematopoietic Stem Cell Metabolism during Development and Aging. Developmental Cell *54*, 239-255. https://doi.org/10.1016/j.devcel.2020.06.029.

26. Wilson, N.K., Kent, D.G., Buettner, F., Shehata, M., Macaulay, I.C., Calero-Nieto, F.J., Sánchez Castillo, M., Oedekoven, C.A., Diamanti, E., Schulte, R., et al. (2015). Combined Single-Cell Functional and Gene Expression Analysis Resolves Heterogeneity within Stem Cell Populations. Cell stem cell *16*, 712-724. 10.1016/j.stem.2015.04.004.
27. Cabezas-Wallscheid, N., Buettner, F., Sommerkamp, P., Klimmeck, D., Ladel, L., Thalheimer, F.B., Pastor-Flores, D., Roma, L.P., Renders, S., Zeisberger, P., et al. (2017). Vitamin A-Retinoic Acid Signaling Regulates Hematopoietic Stem Cell Dormancy. Cell *169*, 807-823.e819. 10.1016/j.cell.2017.04.018.
28. Rodriguez-Fraticelli, A.E., Weinreb, C., Wang, S.W., Migueles, R.P., Jankovic, M., Usart, M., Klein, A.M., Lowell, S., and Camargo, F.D. (2020). Single-cell lineage tracing unveils a role for TCF15 in haematopoiesis. Nature *583*, 585-589. 10.1038/s41586-020-2503-6.
29. Boroviak, T., Loos, R., Lombard, P., Okahara, J., Behr, R., Sasaki, E., Nichols, J., Smith, A., and Bertone, P. (2015). Lineage-Specific Profiling Delineates the Emergence and Progression of Naive Pluripotency in Mammalian Embryogenesis. Dev Cell *35*, 366-382. 10.1016/j.devcel.2015.10.011.
30. Liberzon, A., Birger, C., Thorvaldsdóttir, H., Ghandi, M., Mesirov, J.P., and Tamayo, P. (2015). The Molecular Signatures Database (MSigDB) hallmark gene set collection. Cell systems *1*, 417-425. 10.1016/j.cels.2015.12.004.
31. Duy, C., Li, M., Teater, M., Meydan, C., Garrett-Bakelman, F.E., Lee, T.C., Chin, C.R., Durmaz, C., Kawabata, K.C., Dhimolea, E., et al. (2021). Chemotherapy Induces Senescence-Like Resilient Cells Capable of Initiating AML Recurrence. Cancer Discovery *11*, 1542-1561. 10.1158/2159-8290.Cd-20-1375.
32. van der Weijden, V.A., Stötzel, M., Iyer, D.P., Fauler, B., Gralinska, E., Shahraz, M., Meierhofer, D., Vingron, M., Rulands, S., Alexandrov, T., et al. (2024). FOXO1-mediated lipid metabolism maintains mammalian embryos in dormancy. Nat Cell Biol *26*, 181-193. 10.1038/s41556-023-01325-3.
33. Argelaguet, R., Velten, B., Arnol, D., Dietrich, S., Zenz, T., Marioni, J.C., Buettner, F., Huber, W., and Stegle, O. (2018). Multi-Omics Factor Analysis-a framework for unsupervised integration of multi-omics data sets. Mol Syst Biol *14*, e8124. 10.15252/msb.20178124.
34. Qoku, A., Katsaouni, N., Flinner, N., Buettner, F., and Schulz, M.H. (2023). Multimodal analysis methods in predictive biomedicine. Comput Struct

Biotechnol J *21*, 5829-5838. 10.1016/j.csbj.2023.11.011.

35. Qoku, A., and Buettner, F. (2023). Encoding Domain Knowledge in Multi-view Latent Variable Models: A Bayesian Approach with Structured Sparsity. In 206. (Proceedings of Machine Learning Research), pp. 11545-11562.

36. Loeffler, D., Wehling, A., Schneiter, F., Zhang, Y., Müller-Bötticher, N., Hoppe, P.S., Hilsenbeck, O., Kokkaliaris, K.D., Endele, M., and Schroeder, T. (2019). Asymmetric lysosome inheritance predicts activation of haematopoietic stem cells. Nature *573*, 426-429. 10.1038/s41586-019-1531-6.

37. García-Prat, L., Kaufmann, K.B., Schneiter, F., Voisin, V., Murison, A., Chen, J., Chan-Seng-Yue, M., Gan, O.I., McLeod, J.L., Smith, S.A., et al. (2021). TFEB-mediated endolysosomal activity controls human hematopoietic stem cell fate. Cell Stem Cell *28*, 1838-1850.e1810. 10.1016/j.stem.2021.07.003.

38. Alvarez, S., Díaz, M., Flach, J., Rodriguez-Acebes, S., López-Contreras, A.J., Martínez, D., Cañamero, M., Fernández-Capetillo, O., Isern, J., Passegué, E., and Méndez, J. (2015). Replication stress caused by low MCM expression limits fetal erythropoiesis and hematopoietic stem cell functionality. Nature Communications *6*, 8548. 10.1038/ncomms9548.

39. Flach, J., Bakker, S.T., Mohrin, M., Conroy, P.C., Pietras, E.M., Reynaud, D., Alvarez, S., Diolaiti, M.E., Ugarte, F., Forsberg, E.C., et al. (2014). Replication stress is a potent driver of functional decline in ageing haematopoietic stem cells. Nature *512*, 198-202. 10.1038/nature13619.

40. Inoue, S.-I., Noda, S., Kashima, K., Nakada, K., Hayashi, J.-I., and Miyoshi, H. (2010). Mitochondrial respiration defects modulate differentiation but not proliferation of hematopoietic stem and progenitor cells. FEBS Letters *584*, 3402-3409. https://doi.org/10.1016/j.febslet.2010.06.036.

41. Simsek, T., Kocabas, F., Zheng, J., DeBerardinis, R.J., Mahmoud, A.I., Olson, E.N., Schneider, J.W., Zhang, C.C., and Sadek, H.A. (2010). The Distinct Metabolic Profile of Hematopoietic Stem Cells Reflects Their Location in a Hypoxic Niche. Cell stem cell *7*, 380-390. https://doi.org/10.1016/j.stem.2010.07.011.

42. Tothova, Z., Kollipara, R., Huntly, B.J., Lee, B.H., Castrillon, D.H., Cullen, D.E., McDowell, E.P., Lazo-Kallanian, S., Williams, I.R., Sears, C., et al. (2007). FoxOs are critical mediators of hematopoietic stem cell resistance to physiologic oxidative stress. Cell *128*, 325-339. 10.1016/j.cell.2007.01.003.

43. Abbas, H.A., Maccio, D.R., Coskun, S., Jackson, J.G., Hazen, A.L., Sills, T.M., You, M.J., Hirschi, K.K., and Lozano, G. (2010). Mdm2 is required for survival of hematopoietic stem cells/progenitors via dampening of ROS-induced p53 activity. Cell stem cell *7*, 606-617. 10.1016/j.stem.2010.09.013.

44. Maryanovich, M., Zaltsman, Y., Ruggiero, A., Goldman, A., Shachnai, L., Zaidman, S.L., Porat, Z., Golan, K., Lapidot, T., and Gross, A. (2015). An MTCH2 pathway repressing mitochondria metabolism regulates haematopoietic stem cell fate. Nature Communications *6*, 7901. 10.1038/ncomms8901.

45. Keyvani Chahi, A., Belew, M.S., Xu, J., Chen, H.T.T., Rentas, S., Voisin, V., Krivdova, G., Lechman, E., Marhon, S.A., De Carvalho, D.D., et al. (2022). PLAG1 dampens protein synthesis to promote human hematopoietic stem cell self-renewal. Blood *140*, 992-1008. 10.1182/blood.2021014698 %J Blood.

46. Kruta, M., Sunshine, M.J., Chua, B.A., Fu, Y., Chawla, A., Dillingham, C.H., Hidalgo San Jose, L., De Jong, B., Zhou, F.J., and Signer, R.A.J. (2021). Hsf1 promotes hematopoietic stem cell fitness and proteostasis in response to ex vivo culture stress and aging. Cell stem cell *28*, 1950-1965.e1956. 10.1016/j.stem.2021.07.009.

47. Karigane, D., Kobayashi, H., Morikawa, T., Ootomo, Y., Sakai, M., Nagamatsu, G., Kubota, Y., Goda, N., Matsumoto, M., Nishimura, Emi K., et al. (2016). p38α Activates Purine Metabolism to Initiate Hematopoietic Stem/Progenitor Cell Cycling in Response to Stress. Cell stem cell *19*, 192-204. https://doi.org/10.1016/j.stem.2016.05.013.

48. Takubo, K., Nagamatsu, G., Kobayashi, Chiharu I., Nakamura-Ishizu, A., Kobayashi, H., Ikeda, E., Goda, N., Rahimi, Y., Johnson, Randall S., Soga, T., et al. (2013). Regulation of Glycolysis by Pdk Functions as a Metabolic Checkpoint for Cell Cycle Quiescence in Hematopoietic Stem Cells. Cell stem cell *12*, 49-61. https://doi.org/10.1016/j.stem.2012.10.011.

49. Ceccacci, E., Villa, E., Santoro, F., Minucci, S., Ruhrberg, C., and Fantin, A. (2023). A Refined Single Cell Landscape of Haematopoiesis in the Mouse Foetal Liver. Journal of Developmental Biology *11*, 15.

50. Stoeckius, M., Zheng, S., Houck-Loomis, B., Hao, S., Yeung, B.Z., Mauck, W.M., Smibert, P., and Satija, R. (2018). Cell Hashing with barcoded antibodies enables multiplexing and doublet detection for single cell genomics. Genome

1537 Biology *19*, 224. 10.1186/s13059-018-1603-1.
1538 51. Arai, F., Hirao, A., Ohmura, M., Sato, H., Matsuoka, S., Takubo, K., Ito, K., Koh,
1539 G.Y., and Suda, T. (2004). Tie2/angiopoietin-1 signaling regulates
1540 hematopoietic stem cell quiescence in the bone marrow niche. Cell *118*, 149-
1541 161. 10.1016/j.cell.2004.07.004.
1542 52. Kataoka, K., Sato, T., Yoshimi, A., Goyama, S., Tsuruta, T., Kobayashi, H.,
1543 Shimabe, M., Arai, S., Nakagawa, M., Imai, Y., et al. (2011). Evi1 is essential for
1544 hematopoietic stem cell self-renewal, and its expression marks hematopoietic
1545 cells with long-term multilineage repopulating activity. J Exp Med *208*, 2403-
1546 2416. 10.1084/jem.20110447.
1547 53. Kustikova, O.S., Schwarzer, A., Stahlhut, M., Brugman, M.H., Neumann, T.,
1548 Yang, M., Li, Z., Schambach, A., Heinz, N., Gerdes, S., et al. (2013). Activation
1549 of Evi1 inhibits cell cycle progression and differentiation of hematopoietic
1550 progenitor cells. Leukemia *27*, 1127-1138. 10.1038/leu.2012.355.
1551 54. Calvanese, V., Nguyen, A.T., Bolan, T.J., Vavilina, A., Su, T., Lee, L.K., Wang,
1552 Y., Lay, F.D., Magnusson, M., Crooks, G.M., et al. (2019). MLLT3 governs
1553 human haematopoietic stem-cell self-renewal and engraftment. Nature *576*,
1554 281-286. 10.1038/s41586-019-1790-2.
1555 55. Hu, M., Lu, Y., Wang, S., Zhang, Z., Qi, Y., Chen, N., Shen, M., Chen, F., Chen,
1556 M., Yang, L., et al. (2022). CD63 acts as a functional marker in maintaining
1557 hematopoietic stem cell quiescence through supporting TGFβ signaling in mice.
1558 Cell Death & Differentiation *29*, 178-191. 10.1038/s41418-021-00848-2.
1559 56. Asai, T., Liu, Y., Di Giandomenico, S., Bae, N., Ndiaye-Lobry, D., Deblasio, A.,
1560 Menendez, S., Antipin, Y., Reva, B., Wevrick, R., and Nimer, S.D. (2012).
1561 Necdin, a p53 target gene, regulates the quiescence and response to genotoxic
1562 stress of hematopoietic stem/progenitor cells. Blood *120*, 1601-1612.
1563 10.1182/blood-2011-11-393983.
1564 57. Murphy, A.J., Akhtari, M., Tolani, S., Pagler, T., Bijl, N., Kuo, C.-L., Wang, M.,
1565 Sanson, M., Abramowicz, S., Welch, C., et al. (2011). ApoE regulates
1566 hematopoietic stem cell proliferation, monocytosis, and monocyte accumulation
1567 in atherosclerotic lesions in mice. The Journal of Clinical Investigation *121*,
1568 4138-4149. 10.1172/JCI57559.
1569 58. Hadland, B., Varnum-Finney, B., Dozono, S., Dignum, T., Nourigat-McKay, C.,
1570 Heck, A.M., Ishida, T., Jackson, D.L., Itkin, T., Butler, J.M., et al. (2022).

Engineering a niche supporting hematopoietic stem cell development using integrated single-cell transcriptomics. Nat Commun *13*, 1584. 10.1038/s41467-022-28781-z.

59. Ramilowski, J.A., Goldberg, T., Harshbarger, J., Kloppmann, E., Lizio, M., Satagopam, V.P., Itoh, M., Kawaji, H., Carninci, P., Rost, B., and Forrest, A.R. (2015). A draft network of ligand-receptor-mediated multicellular signalling in human. Nat Commun *6*, 7866. 10.1038/ncomms8866.

60. Browaeys, R., Saelens, W., and Saeys, Y. (2020). NicheNet: modeling intercellular communication by linking ligands to target genes. Nature Methods *17*, 159-162. 10.1038/s41592-019-0667-5.

61. Yamazaki, S., Iwama, A., Takayanagi, S., Eto, K., Ema, H., and Nakauchi, H. (2009). TGF-beta as a candidate bone marrow niche signal to induce hematopoietic stem cell hibernation. Blood *113*, 1250-1256. 10.1182/blood-2008-04-146480.

62. Yamazaki, S., Ema, H., Karlsson, G., Yamaguchi, T., Miyoshi, H., Shioda, S., Taketo, Makoto M., Karlsson, S., Iwama, A., and Nakauchi, H. (2011). Nonmyelinating Schwann Cells Maintain Hematopoietic Stem Cell Hibernation in the Bone Marrow Niche. Cell *147*, 1146-1158. https://doi.org/10.1016/j.cell.2011.09.053.

63. Potocnik, A.J., Brakebusch, C., and Fässler, R. (2000). Fetal and adult hematopoietic stem cells require beta1 integrin function for colonizing fetal liver, spleen, and bone marrow. Immunity *12*, 653-663. 10.1016/s1074-7613(00)80216-2.

64. Biswas, A., Roy, I.M., Babu, P.C., Manesia, J., Schouteden, S., Vijayakurup, V., Anto, R.J., Huelsken, J., Lacy-Hulbert, A., Verfaillie, C.M., and Khurana, S. (2020). The Periostin/Integrin-αv Axis Regulates the Size of Hematopoietic Stem Cell Pool in the Fetal Liver. Stem Cell Reports *15*, 340-357. 10.1016/j.stemcr.2020.06.022.

65. Esain, V., Kwan, W., Carroll, K.J., Cortes, M., Liu, S.Y., Frechette, G.M., Sheward, L.M., Nissim, S., Goessling, W., and North, T.E. (2015). Cannabinoid Receptor-2 Regulates Embryonic Hematopoietic Stem Cell Development via Prostaglandin E2 and P-Selectin Activity. Stem Cells *33*, 2596-2612. 10.1002/stem.2044.

66. Arcangeli, M.L., Frontera, V., Bardin, F., Obrados, E., Adams, S., Chabannon,

1605 C., Schiff, C., Mancini, S.J., Adams, R.H., and Aurrand-Lions, M. (2011). JAM-
1606 B regulates maintenance of hematopoietic stem cells in the bone marrow. Blood
1607 *118*, 4609-4619. 10.1182/blood-2010-12-323972.
1608 67. Gudmundsson, K.O., Nguyen, N., Oakley, K., Han, Y., Gudmundsdottir, B., Liu,
1609 P., Tessarollo, L., Jenkins, N.A., Copeland, N.G., and Du, Y. (2020). Prdm16 is
1610 a critical regulator of adult long-term hematopoietic stem cell quiescence. Proc
1611 Natl Acad Sci U S A *117*, 31945-31953. 10.1073/pnas.2017626117.
1612 68. Gómez-Salinero, J.M., Izzo, F., Lin, Y., Houghton, S., Itkin, T., Geng, F., Bram,
1613 Y., Adelson, R.P., Lu, T.M., Inghirami, G., et al. (2022). Specification of fetal liver
1614 endothelial progenitors to functional zonated adult sinusoids requires c-Maf
1615 induction. Cell Stem Cell *29*, 593-609.e597. 10.1016/j.stem.2022.03.002.
1616 69. Loeffler, D., Schneiter, F., Wang, W., Wehling, A., Kull, T., Lengerke, C., Manz,
1617 M.G., and Schroeder, T. (2022). Asymmetric organelle inheritance predicts
1618 human blood stem cell fate. Blood *139*, 2011-2023. 10.1182/blood.2020009778.
1619 70. Giebel, B., and Beckmann, J. (2007). Asymmetric cell divisions of human
1620 hematopoietic stem and progenitor cells meet endosomes. Cell Cycle *6*, 2201-
1621 2204. 10.4161/cc.6.18.4658.
1622 71. Bonora, M., Morganti, C., van Gastel, N., Ito, K., Calura, E., Zanolla, I., Ferroni,
1623 L., Zhang, Y., Jung, Y., Sales, G., et al. (2024). A mitochondrial NADPH-
1624 cholesterol axis regulates extracellular vesicle biogenesis to support
1625 hematopoietic stem cell fate. Cell Stem Cell *31*, 359-377.e310.
1626 10.1016/j.stem.2024.02.004.
1627 72. Kobayashi, M., Wei, H., Yamanashi, T., Azevedo Portilho, N., Cornelius, S.,
1628 Valiente, N., Nishida, C., Cheng, H., Latorre, A., Zheng, W.J., et al. (2023).
1629 HSC-independent definitive hematopoiesis persists into adult life. Cell Rep *42*,
1630 112239. 10.1016/j.celrep.2023.112239.
1631 73. Cacialli, P., Mahony, C.B., Petzold, T., Bordignon, P., Rougemont, A.-L., and
1632 Bertrand, J.Y. (2021). A connexin/ifi30 pathway bridges HSCs with their niche
1633 to dampen oxidative stress. Nature Communications *12*, 4484.
1634 10.1038/s41467-021-24831-0.
1635 74. Sigurdsson, V., Takei, H., Soboleva, S., Radulovic, V., Galeev, R., Siva, K.,
1636 Leeb-Lundberg, L.M.F., Iida, T., Nittono, H., and Miharada, K. (2016). Bile Acids
1637 Protect Expanding Hematopoietic Stem Cells from Unfolded Protein Stress in
1638 Fetal Liver. Cell Stem Cell *18*, 522-532.

https://doi.org/10.1016/j.stem.2016.01.002.

75. Fares, I., Chagraoui, J., Lehnertz, B., MacRae, T., Mayotte, N., Tomellini, E., Aubert, L., Roux, P.P., and Sauvageau, G. (2017). EPCR expression marks UM171-expanded CD34(+) cord blood stem cells. Blood *129*, 3344-3351. 10.1182/blood-2016-11-750729.

76. Browaeys, R., Saelens, W., and Saeys, Y. (2020). NicheNet: modeling intercellular communication by linking ligands to target genes. Nat Methods *17*, 159-162. 10.1038/s41592-019-0667-5.

77. Termini, C.M., Pang, A., Li, M., Fang, T., Chang, V.Y., and Chute, J.P. (2022). Syndecan-2 enriches for hematopoietic stem cells and regulates stem cell repopulating capacity. Blood *139*, 188-204. 10.1182/blood.2020010447 %J Blood.

78. Murphy, A.J., Akhtari, M., Tolani, S., Pagler, T., Bijl, N., Kuo, C.L., Wang, M., Sanson, M., Abramowicz, S., Welch, C., et al. (2011). ApoE regulates hematopoietic stem cell proliferation, monocytosis, and monocyte accumulation in atherosclerotic lesions in mice. J Clin Invest *121*, 4138-4149. 10.1172/jci57559.

79. Aires, R., Porto, M.L., de Assis, L.M., Pereira, P.A.N., Carvalho, G.R., Côco, L.Z., Vasquez, E.C., Pereira, T.M.C., Campagnaro, B.P., and Meyrelles, S.S. (2021). DNA damage and aging on hematopoietic stem cells: Impact of oxidative stress in ApoE. Exp Gerontol *156*, 111607. 10.1016/j.exger.2021.111607.

80. Tie, G., Messina, K.E., Yan, J., Messina, J.A., and Messina, L.M. (2014). Hypercholesterolemia induces oxidant stress that accelerates the ageing of hematopoietic stem cells. J Am Heart Assoc *3*, e000241. 10.1161/JAHA.113.000241.

81. Ito, K., Carracedo, A., Weiss, D., Arai, F., Ala, U., Avigan, D.E., Schafer, Z.T., Evans, R.M., Suda, T., Lee, C.H., and Pandolfi, P.P. (2012). A PML–PPAR-δ pathway for fatty acid oxidation regulates hematopoietic stem cell maintenance. Nat Med *18*, 1350-1358. 10.1038/nm.2882.

82. Ito, K., Turcotte, R., Cui, J., Zimmerman, S.E., Pinho, S., Mizoguchi, T., Arai, F., Runnels, J.M., Alt, C., Teruya-Feldstein, J., et al. (2016). Self-renewal of a purified Tie2+ hematopoietic stem cell population relies on mitochondrial clearance. Science *354*, 1156-1160. 10.1126/science.aaf5530.

83. Kobayashi, H., Morikawa, T., Okinaga, A., Hamano, F., Hashidate-Yoshida, T., Watanuki, S., Hishikawa, D., Shindou, H., Arai, F., Kabe, Y., et al. (2019). Environmental Optimization Enables Maintenance of Quiescent Hematopoietic Stem Cells Ex Vivo. Cell Rep *28*, 145-158.e149. 10.1016/j.celrep.2019.06.008.
84. Schönberger, K., Obier, N., Romero-Mulero, M.C., Cauchy, P., Mess, J., Pavlovich, P.V., Zhang, Y.W., Mitterer, M., Rettkowski, J., Lalioti, M.E., et al. (2021). Multilayer omics analysis reveals a non-classical retinoic acid signaling axis that regulates hematopoietic stem cell identity. Cell Stem Cell. 10.1016/j.stem.2021.10.002.
85. Hu, Y., and Smyth, G.K. (2009). ELDA: extreme limiting dilution analysis for comparing depleted and enriched populations in stem cell and other assays. J Immunol Methods *347*, 70-78. 10.1016/j.jim.2009.06.008.
86. Trapnell, C., Cacchiarelli, D., Grimsby, J., Pokharel, P., Li, S., Morse, M., Lennon, N.J., Livak, K.J., Mikkelsen, T.S., and Rinn, J.L. (2014). The dynamics and regulators of cell fate decisions are revealed by pseudotemporal ordering of single cells. Nature Biotechnology *32*, 381-386. 10.1038/nbt.2859.
87. Armstrong, G., Martino, C., Rahman, G., Gonzalez, A., Vázquez-Baeza, Y., Mishne, G., and Knight, R. (2021). Uniform Manifold Approximation and Projection (UMAP) Reveals Composite Patterns and Resolves Visualization Artifacts in Microbiome Data. mSystems, e0069121. 10.1128/mSystems.00691-21.
88. Haghverdi, L., Lun, A.T.L., Morgan, M.D., and Marioni, J.C. (2018). Batch effects in single-cell RNA-sequencing data are corrected by matching mutual nearest neighbors. Nat Biotechnol *36*, 421-427. 10.1038/nbt.4091.
89. Levine, J.H., Simonds, E.F., Bendall, S.C., Davis, K.L., Amir el, A.D., Tadmor, M.D., Litvin, O., Fienberg, H.G., Jager, A., Zunder, E.R., et al. (2015). Data-Driven Phenotypic Dissection of AML Reveals Progenitor-like Cells that Correlate with Prognosis. Cell *162*, 184-197. 10.1016/j.cell.2015.05.047.
90. Saunders, L.M., Mishra, A.K., Aman, A.J., Lewis, V.M., Toomey, M.B., Packer, J.S., Qiu, X., McFaline-Figueroa, J.L., Corbo, J.C., Trapnell, C., and Parichy, D.M. (2019). Thyroid hormone regulates distinct paths to maturation in pigment cell lineages. Elife *8*. 10.7554/eLife.45181.
91. Bausch-Fluck, D., Hofmann, A., Bock, T., Frei, A.P., Cerciello, F., Jacobs, A., Moest, H., Omasits, U., Gundry, R.L., Yoon, C., et al. (2015). A mass

spectrometric-derived cell surface protein atlas. PLoS One *10*, e0121314. 10.1371/journal.pone.0121314.

92. Carbon, S., Ireland, A., Mungall, C.J., Shu, S., Marshall, B., and Lewis, S. (2009). AmiGO: online access to ontology and annotation data. Bioinformatics *25*, 288-289. 10.1093/bioinformatics/btn615.

93. Ashburner, M., Ball, C.A., Blake, J.A., Botstein, D., Butler, H., Cherry, J.M., Davis, A.P., Dolinski, K., Dwight, S.S., Eppig, J.T., et al. (2000). Gene ontology: tool for the unification of biology. The Gene Ontology Consortium. Nat Genet *25*, 25-29. 10.1038/75556.

94. Gene Ontology, C. (2021). The Gene Ontology resource: enriching a GOld mine. Nucleic Acids Res *49*, D325-D334. 10.1093/nar/gkaa1113.

Supplemental Information

Figure S1.

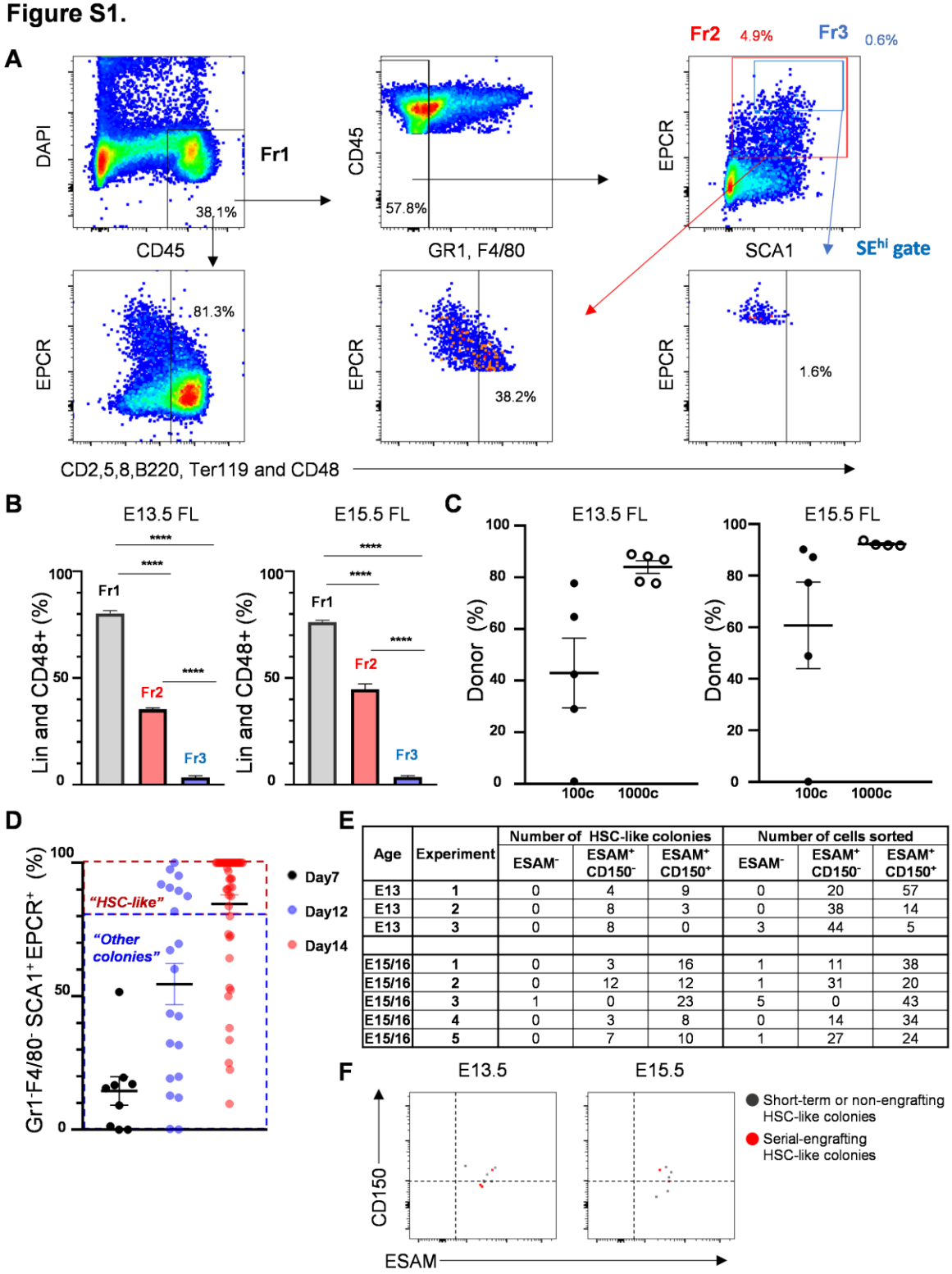

Age	Experiment	Number of HSC-like colonies			Number of cells sorted		
		ESAM⁻	ESAM⁺ CD150⁻	ESAM⁺ CD150⁺	ESAM⁻	ESAM⁺ CD150⁻	ESAM⁺ CD150⁺
E13	1	0	4	9	0	20	57
E13	2	0	8	3	0	38	14
E13	3	0	8	0	3	44	5
E15/16	1	0	3	16	1	11	38
E15/16	2	0	12	12	1	31	20
E15/16	3	1	0	23	5	0	43
E15/16	4	0	3	8	0	14	34
E15/16	5	0	7	10	1	27	24

Figure S1: Gating strategy and index sorting of FL-HSCs. (Related to Figure 1 and Figure 2)

(A) Expression of lineage markers (CD2, 5, 8, B220, Ter119) and CD48 in each gated fraction from freshly isolated E13.5 FL were analyzed by flow cytometry. Representative flow cytometry analysis is shown. Fr: Fraction

(B) Frequency of cells expressing CD2, 5, 8, B220, Ter119 and CD48 in each fraction from freshly isolated E13.5 (left) and E15.5 (right) FL. N=6 (3 embryos from 2 different litters). Lin: Lineage (CD2, CD5, CD8, B220 and TER119). ****P<0.0001 (One-way ANOVA with Dunnett's multiple comparisons test).

(C) $CD45^{+}GR1^{-}F4/80^{-}VECadherin^{-/low}SCA1^{+}EPCR^{+}$ cells from E13.5 and E15.5 FL-HSC were sorted and transplanted into lethally irradiated mice. Donor chimerism in peripheral blood from secondary recipients at 24 weeks in E13.5 (left) and in E15.5 (right). 100 cells or 1,000 cells per recipient were transplanted. N=5 per cohort.

(D) Frequency of $GR1^{-}F4/80^{-}SCA1^{+}EPCR^{+}$ cells (amongst total viable $CD45^{+}$ cells). Single $CD150^{+}SE^{hi}$ cells from E15.5 FL were sorted and cultured with FL-AKT-EC. Colonies visually emerging at each timepoint were assessed by flow cytometry. All remaining colonies were analyzed on Day 14. n=9 (Day 7), n=21 (Day 12), n=49 (Day 14), n= 17 (no colony observed on Day14).

(E) The distribution of HSC-like colonies and total number of cells sorted from each fraction of SE^{hi} FL-HSCs based on expression of ESAM and CD150. (n=32 HSC-like colonies from a total of 181 wells at E13.5, from 3 independent experiments; n=95 HSC-like colonies from a total of 250 wells in E15.5/16.5, from 5 independent experiments).

(F) Expression of ESAM and CD150 by index analysis of E13.5 (left) and E15.5 (right) SE^{hi} FL-HSCs giving rise to immunophenotypic HSC-like colonies with serial multilineage engraftment (serial-engrafting HSC-like colonies, red) or lacking serial multilineage engraftment (short-term or non-engrafting HSC-like colonies, gray). E13.5: 9 HSC-like colonies were used for the transplantation. 1 colony was transplanted into 2 mice. Short-term or non-engrafting=6, serial-engrafting=3. E15.5: 7 HSC-like colonies were used for transplantation. 3 colonies were transplanted into 2 mice. Short-term or non-engrafting=5, Serial-engrafting=2.

Figure S2

A

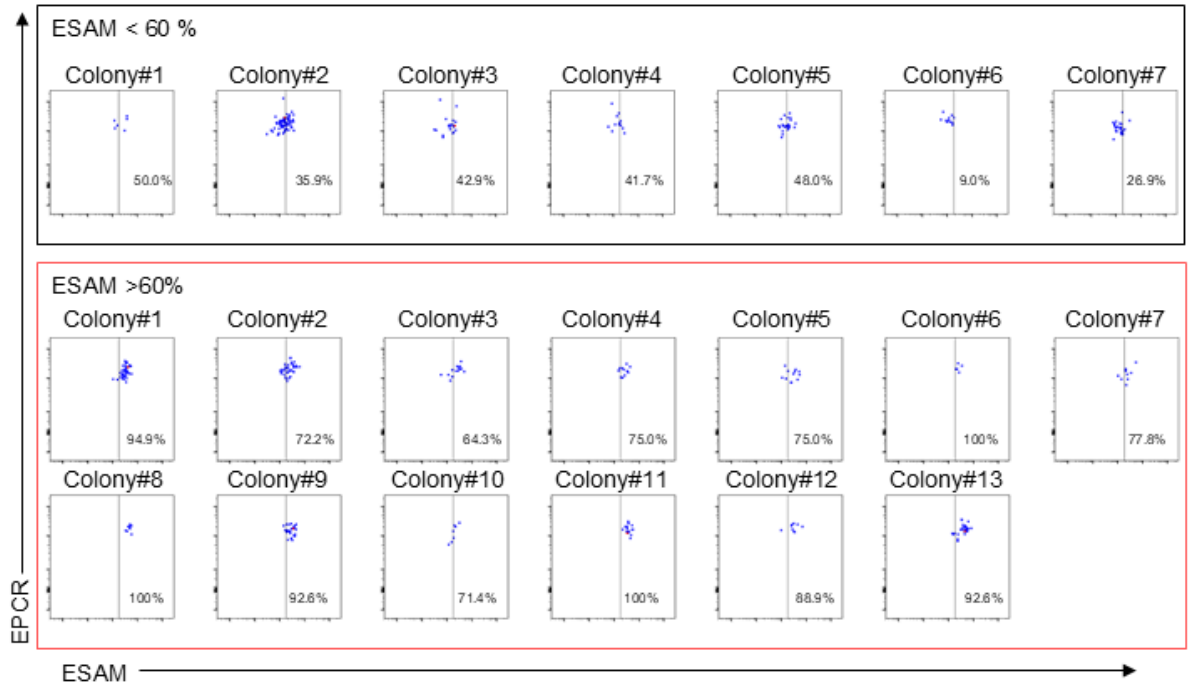
ESAM < 60 %
Colony#1
50.0%
Colony#2
35.9%
Colony#3
42.9%
Colony#4
41.7%
Colony#5
48.0%
Colony#6
9.0%
Colony#7
26.9%
ESAM >60%
Colony#1
94.9%
Colony#2
72.2%
Colony#3
64.3%
Colony#4
75.0%
Colony#5
75.0%
Colony#6
100%
Colony#7
77.8%
Colony#8
100%
Colony#9
92.6%
Colony#10
71.4%
Colony#11
100%
Colony#12
88.9%
Colony#13
92.6%
EPCR
ESAM

B

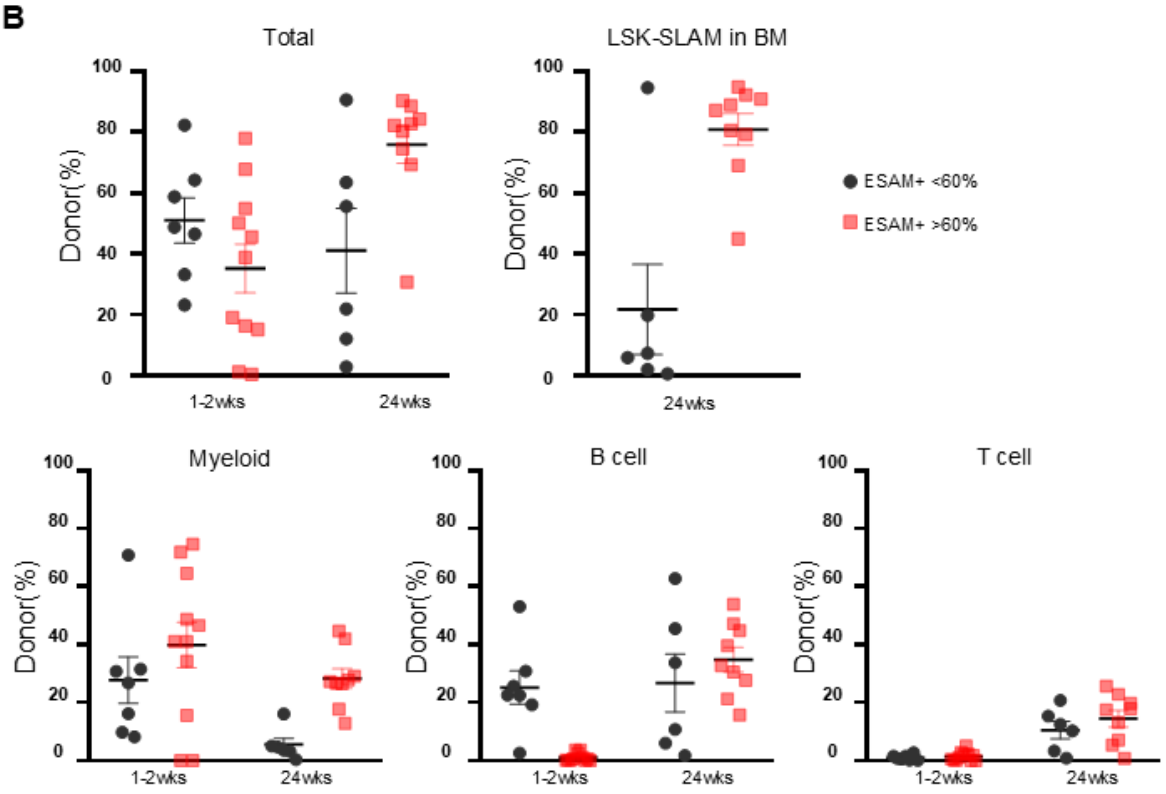
Total
LSK-SLAM in BM
Donor(%)
100
80
60
40
20
0
1-2wks
24wks
ESAM+ <60%
ESAM+ >60%
Myeloid
B cell
T cell

Figure S2: ESAM-expressing HSC-like colonies exhibit high-level contribution to immunophenotypic HSCs following transplantation. (Related to Figure 3)
(A) Expression of ESAM in HSC-like colonies analyzed by flow cytometry following coculture (after gating cells as $DAPI^{-}CD45^{+}CD48^{-}SCA1^{+}EPCR^{+}$). 50% of the cells from each colony were used for flow cytometry and the remaining cells from each of the 20 HSC-like colonies shown were used for transplantation. HSC-like colonies were divided based on ESAM expression (top: <60% $ESAM^{+}$ cells, n=7 or bottom: >60% $ESAM^{+}$ cells, n=13, in cells gated as $DAPI^{-}CD45^{+}CD48^{-}SCA1^{+}EPCR^{+}$).
(B) Donor chimerism (total, myeloid, B cell, and T cell in peripheral blood and LSK-SLAM: $Lin^{-}SCA1^{+}Kit^{+}CD48^{-}CD150^{+}$ HSCs in bone marrow) of primary recipients transplanted with cells from each of the HSC-like colonies defined based on ESAM expression as shown in A (black: <60% $ESAM^{+}$ cells, n=7; red: >60% $ESAM^{+}$ cells, n=13).

Figure S3.

A

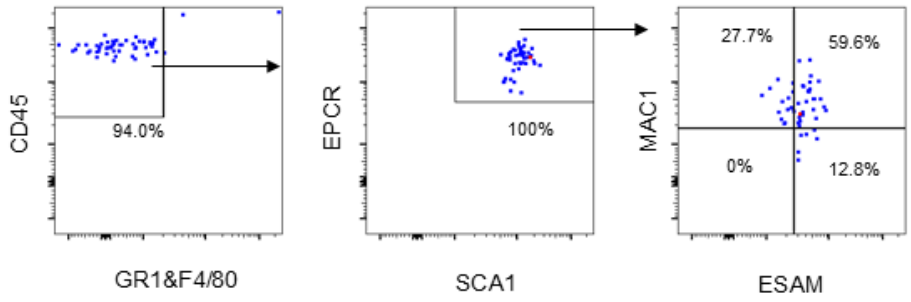

B

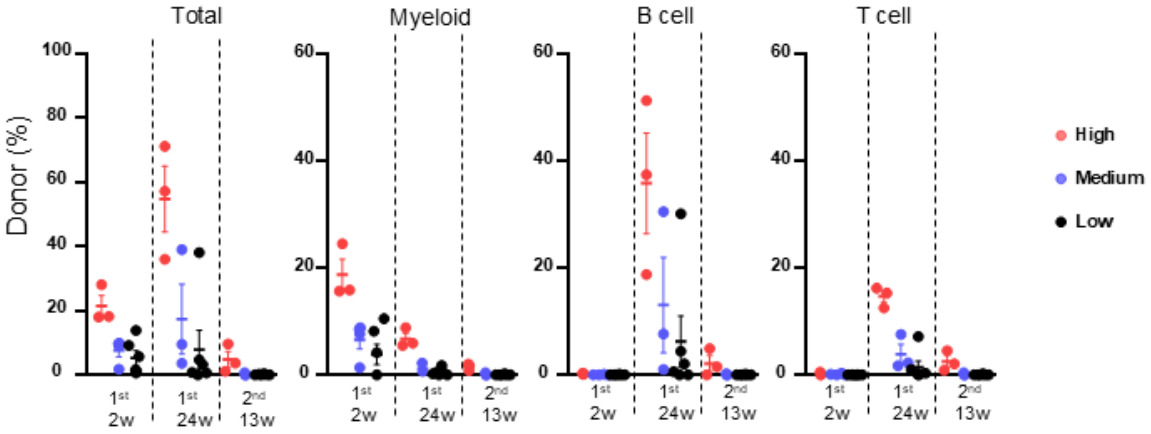

C

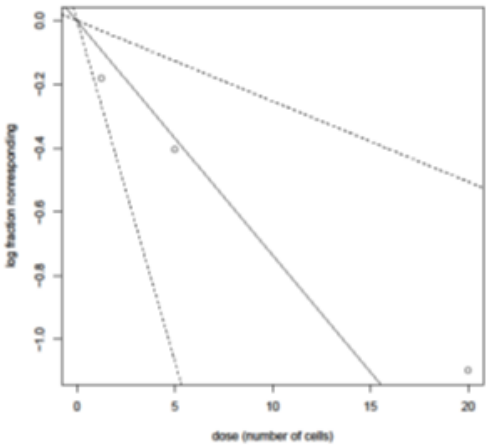

Group	Dose	Tested	Response
High dose	20	3	2
Medium dose	5	3*	1
Low dose	1.25	6	1

Figure S3: Limiting dilution transplantation demonstrates amplification of serial engrafting HSCs in an ESAM$^+$ HSC colony. (Related to figure 3).

(A) Immunophenotype of representative ESAM$^+$ HSC colony tested in limiting dilution transplantation (50% of cells were analyzed by flow cytometry on Day 15).

(B) Donor chimerism (total, myeloid, B cell, and T cell) in peripheral blood of primary and secondary recipients transplanted with limiting dilutions of cells from a single ESAM$^+$ HSC colony shown in (A) (High dose = 20 cells equivalent, Medium dose = 5 cells equivalent, Low dose = 1.25 cells equivalent).

(C) Limiting dilution calculation by ELDA (http://bioinf.wehi.edu.au/software/elda/) using the fraction of mice demonstrating serial engraftment of donor cells at each dilution[1]. Estimated HSC frequency: 1 in 13.6 cells (95% confidence interval 1 in 4.7 to 1 in 40). Estimated HSC generated: 15 (range 5-43). Engraftment was defined as >0.1% donor (CD45.2) contribution to the peripheral blood, with each of donor myeloid (Gr-1 and/or F4/80), B cell (CD19), and T cell (CD3) engraftment detected at >0.1% of peripheral blood at 13 weeks after secondary transplant. *3 out of 6 mice in medium dose cohort died before 2nd-13wks.

Figure S4.

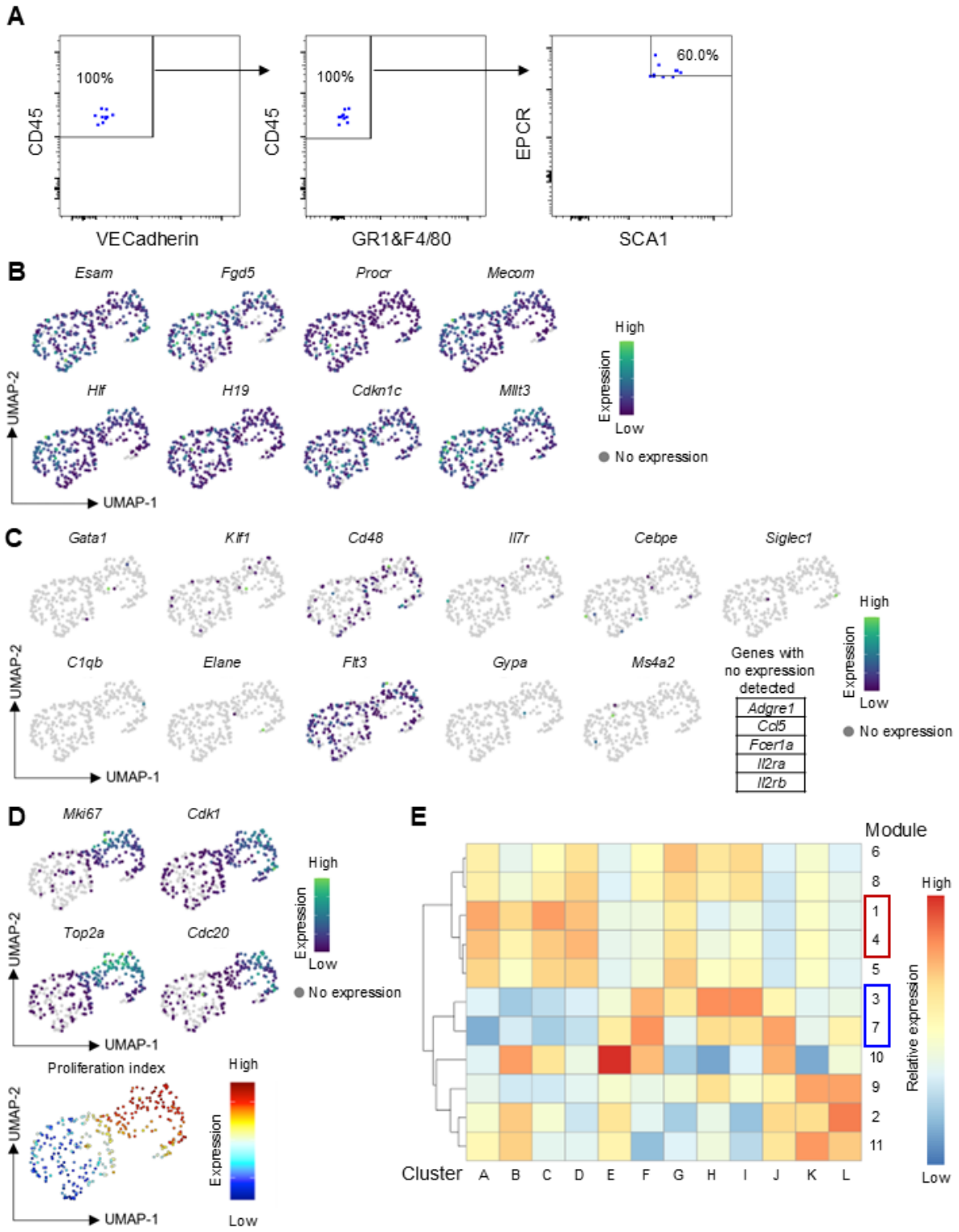
A
100%
CD45
VECadherin
100%
CD45
GR1&F4/80
60.0%
EPCR
SCA1
B
Esam
Fgd5
Procr
Mecom
Hlf
H19
Cdkn1c
Mllt3
UMAP-2
UMAP-1
High
Expression
Low
No expression
C
Gata1
Klf1
Cd48
Il7r
Cebpe
Siglec1
C1qb
Elane
Flt3
Gypa
Ms4a2
Genes with no expression detected
Adgre1
Ccl5
Fcer1a
Il2ra
Il2rb
UMAP-2
UMAP-1
High
Expression
Low
No expression
D
Mki67
Cdk1
Top2a
Cdc20
UMAP-2
UMAP-1
High
Expression
Low
No expression
Proliferation index
UMAP-2
UMAP-1
High
Expression
Low
E
Module
6
8
1
4
5
3
7
10
9
2
11
Cluster
A B C D E F G H I J K L
High
Relative expression
Low

Figure S4: Transcriptional heterogeneity of freshly isolated FL-HSCs by scRNAseq. (Related to Figure 4)

(A) Post-sort purity of E13.5 SE^{hi} FL-HSCs used for scRNAseq.

(B) Gene expression heatmap for HSC-specific genes.

(C) Gene expression heatmap for genes specific to differentiating hematopoietic progenitors and mature hematopoietic lineages.

(D) Gene expression heatmap for cell cycle genes and proliferation index [2-4].

(E) Heatmap of gene-module expression by cluster. Gene modules shown in figure 4E are highlighted in red (containing HSC-associated genes, modules 1 and 4) and blue (containing genes associated with biosynthetic/cell cycle activation, modules 3 and 7).

Figure S5.

A

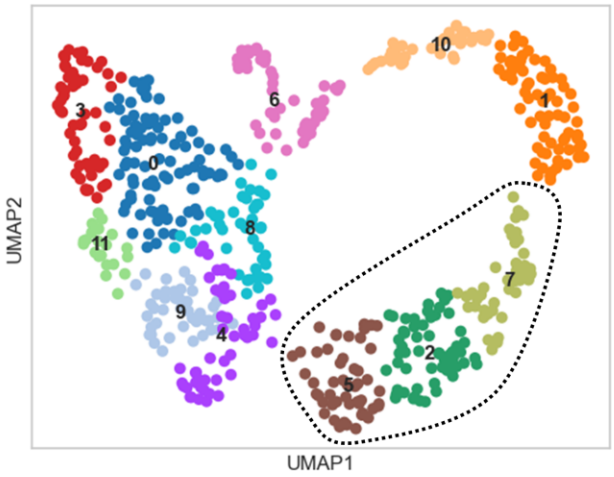
UMAP2
UMAP1
0
1
2
3
4
5
6
7
8
9
10
11

B

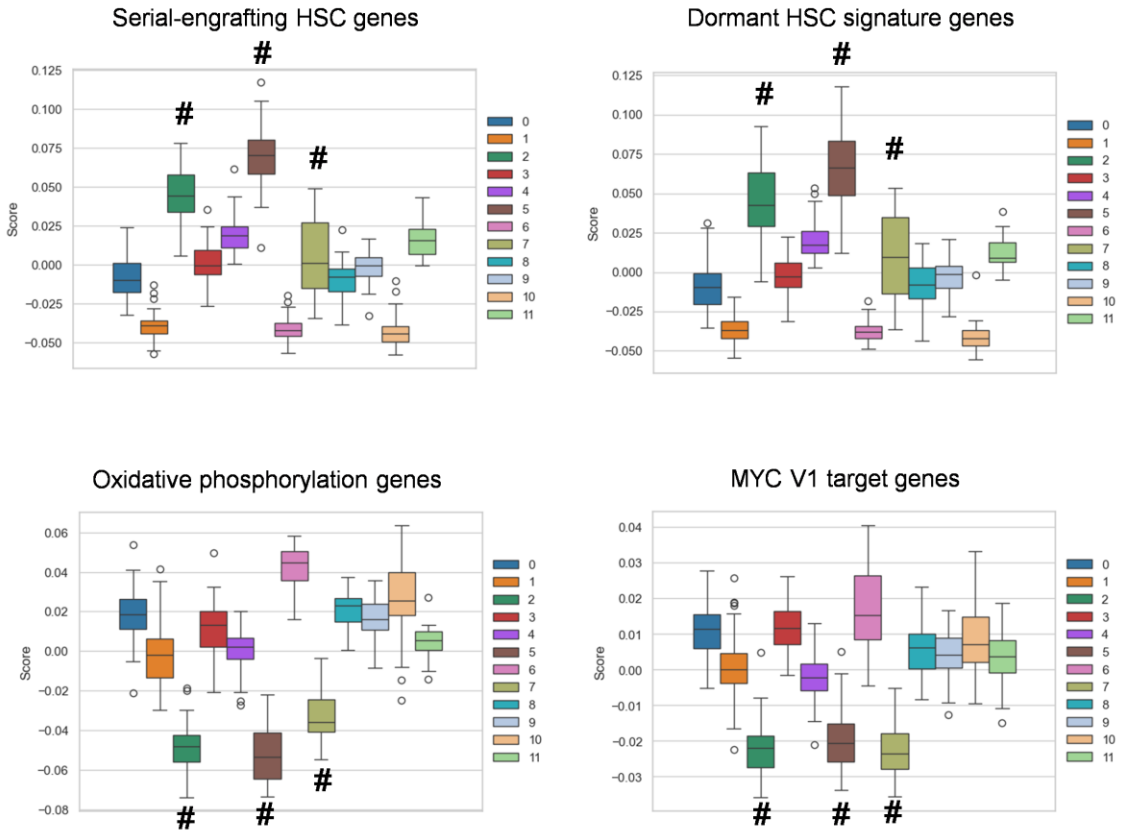
Serial-engrafting HSC genes
Dormant HSC signature genes
Oxidative phosphorylation genes
MYC V1 target genes
Score
#
0
1
2
3
4
5
6
7
8
9
10
11

Figure S5. LVM of sorted SE^{hi} primary FL-HSCs using select gene sets as Bayesian priors. (Related to Figure 4)

(A) UMAP plot of the cell clustering (leiden) in the inferred latent space representation. Numbers denote clusters, and dotted contour denotes the isolated island of cells composed of cluster 2, 5, and 7.

(B) Quantitation of latent factor loading among clusters for each gene set, comparing how each gene set (latent factor) explains the transcriptomic features of each cluster. Cluster 2, 5, 7 in A are marked by #.

Figure S6.

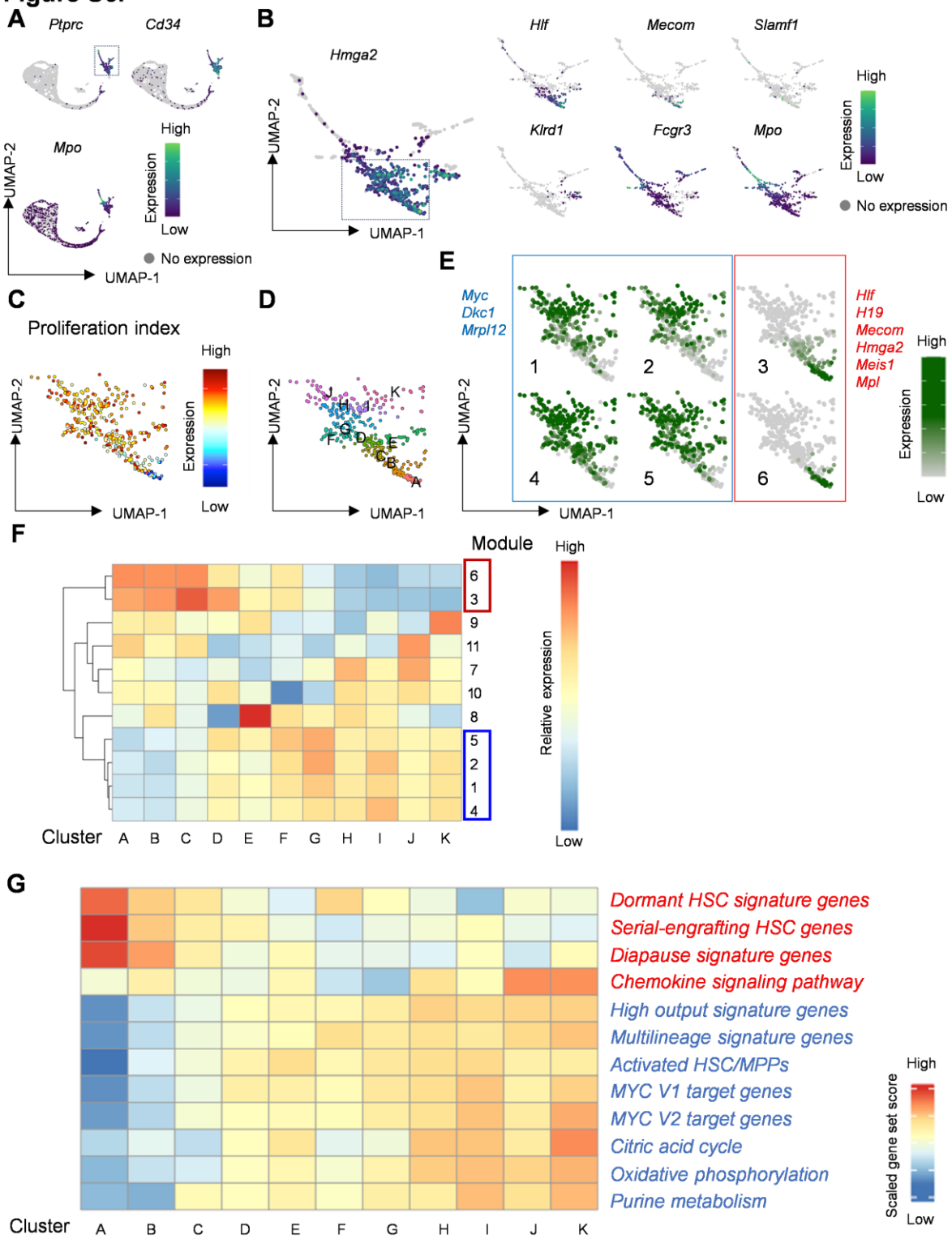
A
Ptprc
Cd34
Mpo
High
Expression
Low
No expression
UMAP-2
UMAP-1
B
Hmga2
Hlf
Mecom
Slamf1
Klrd1
Fcgr3
Mpo
High
Expression
Low
No expression
UMAP-2
UMAP-1
C
Proliferation index
High
Expression
Low
UMAP-2
UMAP-1
D
UMAP-2
UMAP-1
E
Myc
Dkc1
Mrpl12
Hlf
H19
Mecom
Hmga2
Meis1
Mpl
1
2
3
4
5
6
High
Expression
Low
UMAP-2
UMAP-1
F
Module
6
3
9
11
7
10
8
5
2
1
4
Cluster A B C D E F G H I J K
High
Relative expression
Low
G
Dormant HSC signature genes
Serial-engrafting HSC genes
Diapause signature genes
Chemokine signaling pathway
High output signature genes
Multilineage signature genes
Activated HSC/MPPs
MYC V1 target genes
MYC V2 target genes
Citric acid cycle
Oxidative phosphorylation
Purine metabolism
Cluster A B C D E F G H I J K
High
Scaled gene set score
Low

Figure S6: Transcriptional heterogeneity in freshly isolated E12.5 FL-HSCs from published scRNAseq data. (Related to Figure 4)

(A) Expression of *Ptprc* (CD45), *Mpo* and *Cd34* in scRNAseq data from GSE180050.[5] FL-HSPC expressing both *Ptprc* and *Cd34* (dashed square) were extracted for subsequent analysis (809 of 7,440 cells).

(B) Expression of HSC-associated and lineage-specific genes in extracted FL-HSPC fraction. FL-HSCs expressing *Hmga2* (dashed square) were extracted for subsequent analysis (372 of 809 cells).

(C) Gene expression heatmap for proliferation index.

(D) Unsupervised clustering in UMAP.

(E) Heatmaps for expression scores of gene modules. Gene modules 1-6 are shown with representative genes identified in each module.

(F) Heatmap of gene-module expression by cluster. Gene modules shown in (E) are highlighted in red (containing HSC-associated genes, modules 3 and 6) and blue (containing genes associated with metabolic/cell cycle activation, modules 1,2,4 and 5).

(G) Heatmap of gene-set scores by cluster for genes associated with HSC dormancy,[6] serial engrafting HSCs,[7,8] diapause,[9] and chemokine signaling (WP_CHEMOKINE_SIGNALING_PATHWAY) or genes associated with activated HSC/MPP states including high output and multilineage signatures,[6,8,10] Myc pathway activation (Hallmark Myc Target Genes V1, V2), and metabolic activity (WP_TCA_CYCLE, HALLMARK_OXIDATIVE_PHOSPHORY,LATION, WP_PURINE_METABOLISM). (See Table S1 for gene-sets)

Figure S7.

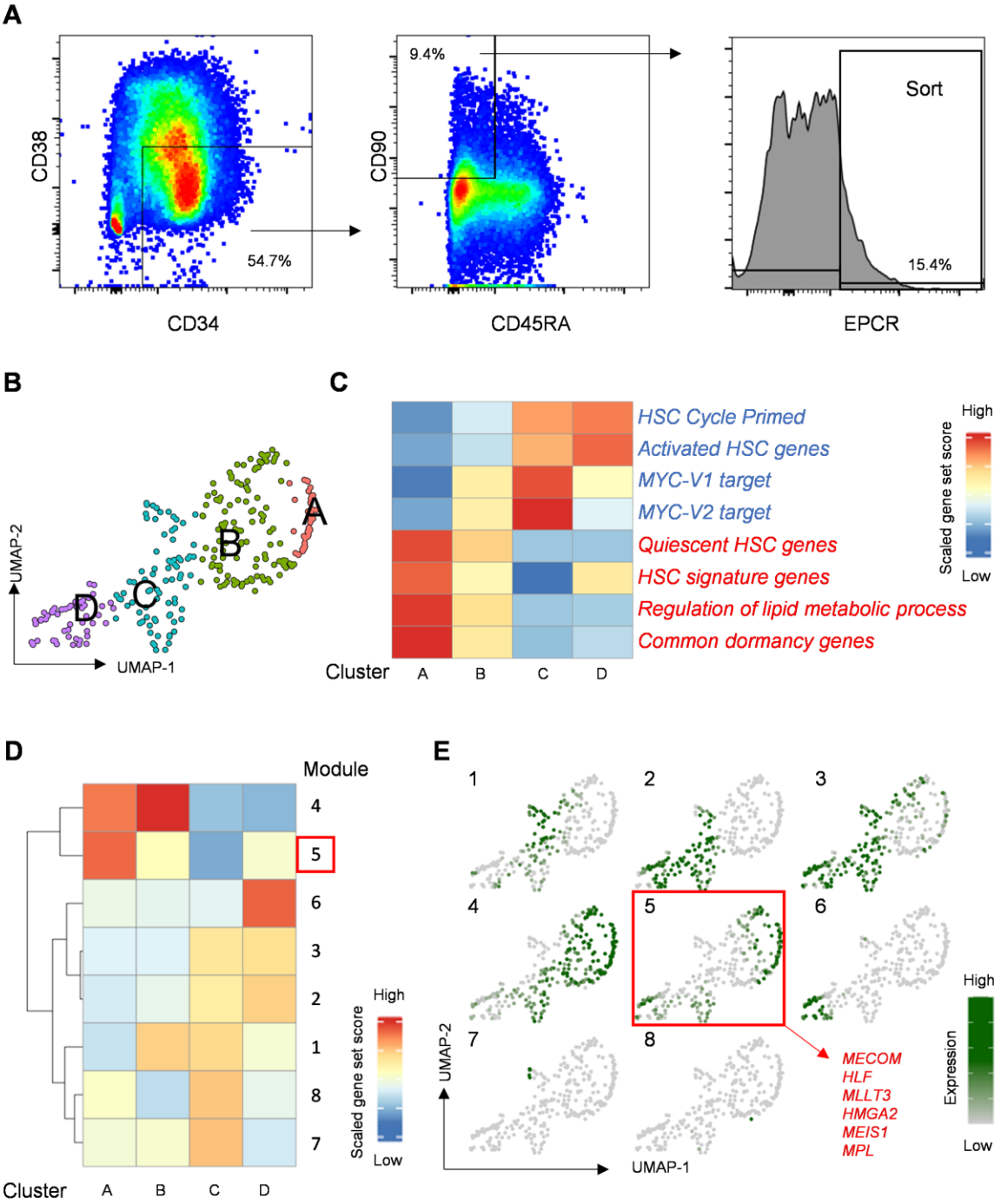
A
CD38
CD34
54.7%
9.4%
CD90
CD45RA
Sort
15.4%
EPCR
B
UMAP-2
UMAP-1
A
B
C
D
C
HSC Cycle Primed
Activated HSC genes
MYC-V1 target
MYC-V2 target
Quiescent HSC genes
HSC signature genes
Regulation of lipid metabolic process
Common dormancy genes
Cluster
A
B
C
D
Scaled gene set score
High
Low
D
Module
4
5
6
3
2
1
8
7
Cluster
A
B
C
D
Scaled gene set score
High
Low
E
1
2
3
4
5
6
7
8
UMAP-2
UMAP-1
MECOM
HLF
MLLT3
HMGA2
MEIS1
MPL
Expression
High
Low

Figure S7: Transcriptional heterogeneity of phenotypically purified human FL-HSCs. (Related to Figure 4)

(A) Gating strategy to sort $CD34^{+}38^{-}45RA^{-}90^{+}EPCR^{+}$ human FL-HSCs. Freshly isolated FL samples were subject to CD34 positive cell selection and cryopreserved. Thawed samples were pooled for FACS and scRNAseq.

(B) Unsupervised clustering in UMAP. (The number of cells in each cluster; A:116, B:80, C:55, D:41)

(C) Heatmap of gene-set scores by cluster for genes associated with HSC activation (HSC Cycle Primed,[11] Activated HSC[11], HALLMARK_MYC_TARGETS_V1 and V2), HSC dormancy/quiescence[11], HSC signature[12], lipid metabolism (GOBP_REGULATION_OF_LIPID_METABOLIC_PROCESS), and common stem cell dormancy genes[13] (See Table S1 for gene-sets).

(D) Heatmap of gene-module expression by cluster.

(E) Heatmaps for expression scores of gene modules. Gene modules 1-8 are shown. Representative HSC-associated genes are shown for module 5.

Figure S8.

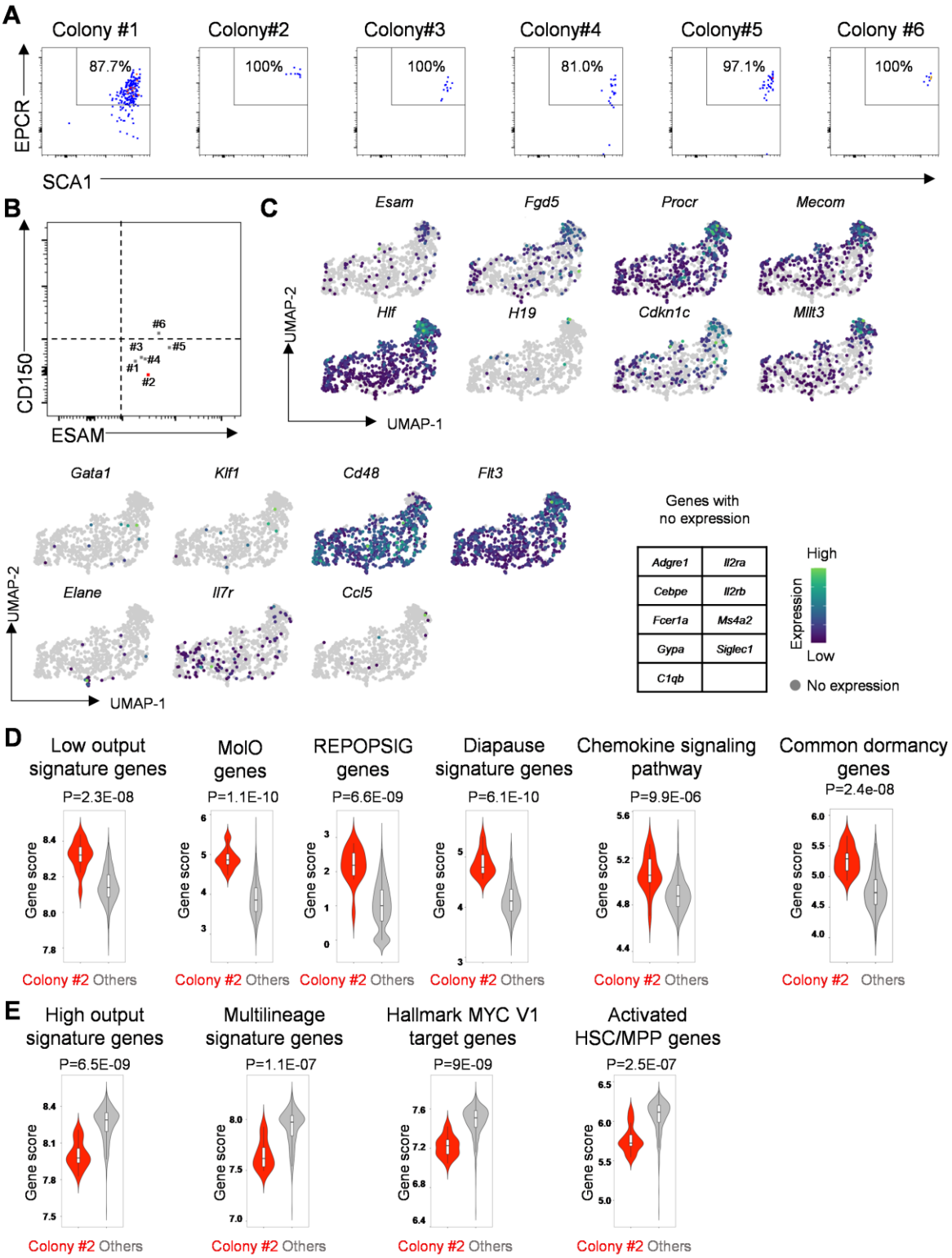
A
Colony #1
Colony#2
Colony#3
Colony#4
Colony#5
Colony #6
87.7%
100%
100%
81.0%
97.1%
100%
EPCR
SCA1
B
CD150
ESAM
#6
#3
#5
#4
#1
#2
C
Esam
Fgd5
Procr
Mecom
Hlf
H19
Cdkn1c
Mllt3
UMAP-2
UMAP-1
Gata1
Klf1
Cd48
Flt3
Elane
Il7r
Ccl5
Genes with no expression
Adgre1
Il2ra
Cebpe
Il2rb
Fcer1a
Ms4a2
Gypa
Siglec1
C1qb
High
Expression
Low
No expression
D
Low output signature genes
P=2.3E-08
MolO genes
P=1.1E-10
REPOPSIG genes
P=6.6E-09
Diapause signature genes
P=6.1E-10
Chemokine signaling pathway
P=9.9E-06
Common dormancy genes
P=2.4e-08
Gene score
Colony #2 Others
E
High output signature genes
P=6.5E-09
Multilineage signature genes
P=1.1E-07
Hallmark MYC V1 target genes
P=9E-09
Activated HSC/MPP genes
P=2.5E-07
Gene score
Colony #2 Others

Figure S8: Immunophenotype and scRNAseq analysis of HSC-like colonies. (Related to Figure 5)

(A) Flow cytometric analysis of EPCR and SCA1 expression in 6 HSC colonies used for simultaneous scRNAseq and transplantation. Cells are initially gated as viable (DAPI$^-$) CD45$^+$Gr1$^-$F4/80$^-$ after exclusion of VECadherin$^+$ FL-AKT-ECs. 15% of each colony was used for phenotyping.

(B) Index-sort profile showing surface expression of CD150 and ESAM in each of the originating SE^{hi} FL-HSCs giving rise to the indicated HSC-like colonies shown in (A).

(C) Gene expression heatmap for genes marking HSCs (top) and differentiating progenitors/mature hematopoietic lineages (bottom).

(D) Violin plots of gene-set scores by colony type. p values indicate Wilcoxon rank-sum test. Low output signature genes,[7] HSC Molecular overlap population (MolO) genes,[14] REPOPSIG genes,[15] diapause signature genes,[9,16] Chemokine signaling pathway (WP_CHEMOKINE_SIGNALING_PATHWAY) and common stem cell dormancy genes.[13] (See Table S1 for gene-sets).

(E) Violin plots of gene-set scores by colony type. p values indicate Wilcoxon rank-sum test. High output signature genes,[7] multilineage signature genes,[7] Myc target genes (HALLMARK_MYC_TARGETS_V1), and Activated HSC/MPP genes.[6,17] (See Table S1 for gene-sets).

Figure S9.

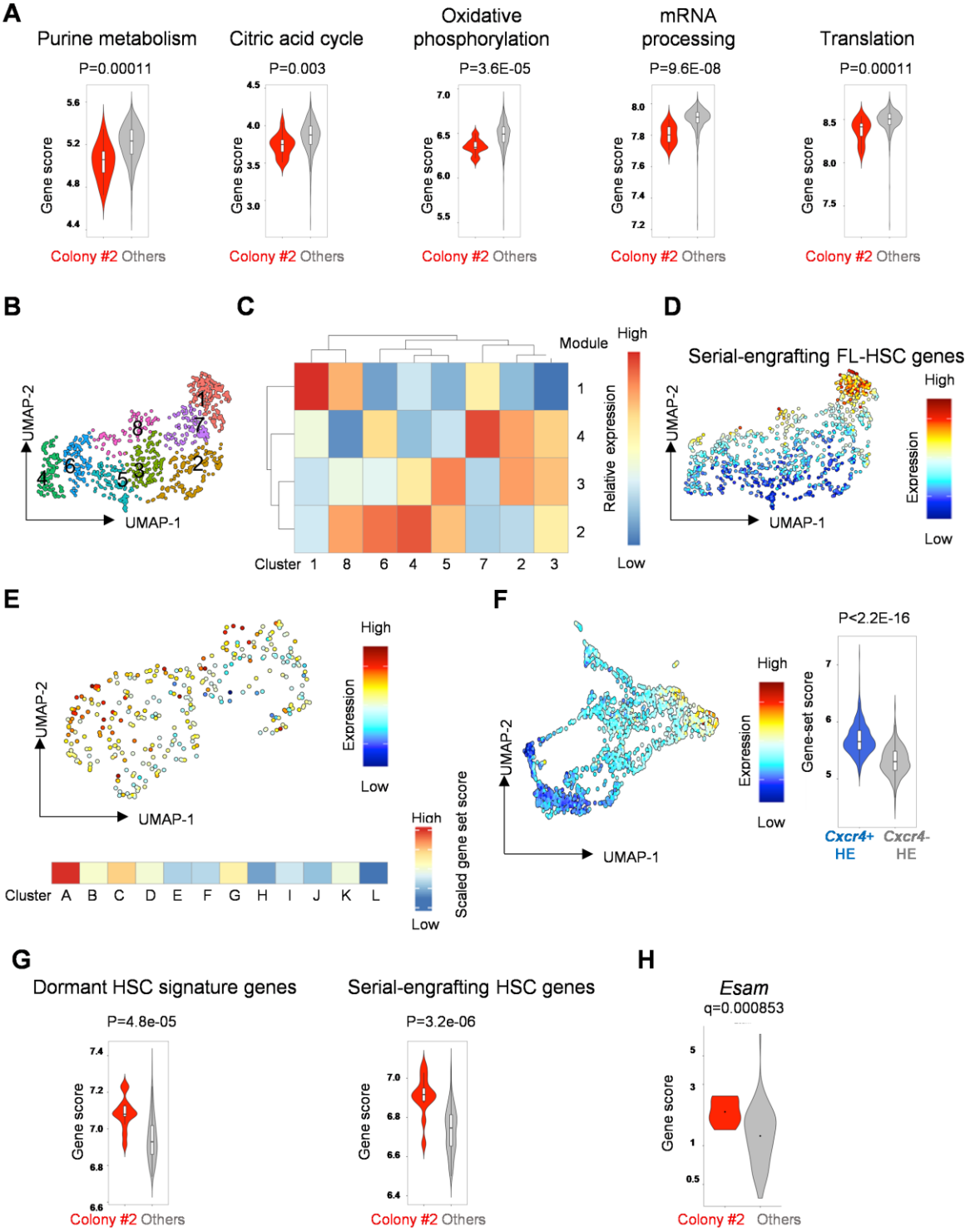
A
Purine metabolism
P=0.00011
Citric acid cycle
P=0.003
Oxidative phosphorylation
P=3.6E-05
mRNA processing
P=9.6E-08
Translation
P=0.00011
Gene score
Colony #2 Others
B
UMAP-2
UMAP-1
C
Module
High
Low
Relative expression
Cluster 1 8 6 4 5 7 2 3
D
Serial-engrafting FL-HSC genes
High
Low
Expression
E
Expression
Cluster A B C D E F G H I J K L
Scaled gene set score
F
P<2.2E-16
Gene-set score
Cxcr4+ HE
Cxcr4- HE
G
Dormant HSC signature genes
P=4.8e-05
Serial-engrafting HSC genes
P=3.2e-06
H
Esam
q=0.000853

Figure S9: scRNAseq analysis of HSC-like colonies and correlation with freshly isolated FL-HSCs and HSC-competent hemogenic endothelium. (Related to Figure 5)

(A) Violin plots of gene-set scores by colony type for genes associated with activated HSC/MPP metabolic states,[6] including purine metabolism (WP_PURINE_METABOLISM), citric acid cycle (WP_TCA_CYCLE), oxidative phosphorylation (HALLMARK_OXIDATIVE_PHOSPHORYLATION), mRNA processing (WP_MRNA_PROCESSING), and translation (REACTOME_TRANSLATION). p values indicate Wilcoxon rank-sum test. (See Table S1 for gene-sets).

(B) Unsupervised cluster analysis in UMAP.

(C) Heatmap of gene-module expression by cluster.

(D) Heatmap showing gene-set score of "Serially engrafting FL-HSC genes" in UMAP, identified by cross-referencing genes identified in module 1 to those identified by differential gene expression analysis (comparing colony #2 to other HSC-like colonies) (Table S1).

(E) Heatmap showing gene-set score of "Serially engrafting FL-HSC genes" applied to scRNAseq data from freshly isolated FL-HSCs at E13.5 (Figure 4) in UMAP (top) and scaled-gene set score in each cluster (bottom).

(F) Heatmap showing gene-set score of "Serially engrafting FL-HSC genes" applied to murine embryonic AGM hemogenic endothelium (HE) scRNAseq data[2] in UMAP. Violin plots of gene-set scores in *Cxcr4*-expressing HE (containing HSC-competent HE) versus *Cxcr4*-negative HE (lacking HSC potential). p values indicate Wilcoxon rank-sum test.

(G) Violin plots of gene-set scores within cluster 1 by colony type for genes associated with HSC dormancy[6] and serial-engraftment.[7] (See Table S1 for gene-sets).

(H) Violin plots of *Esam* gene expression by colony type. q value was calculated using the Benjamini and Hochberg correction method.

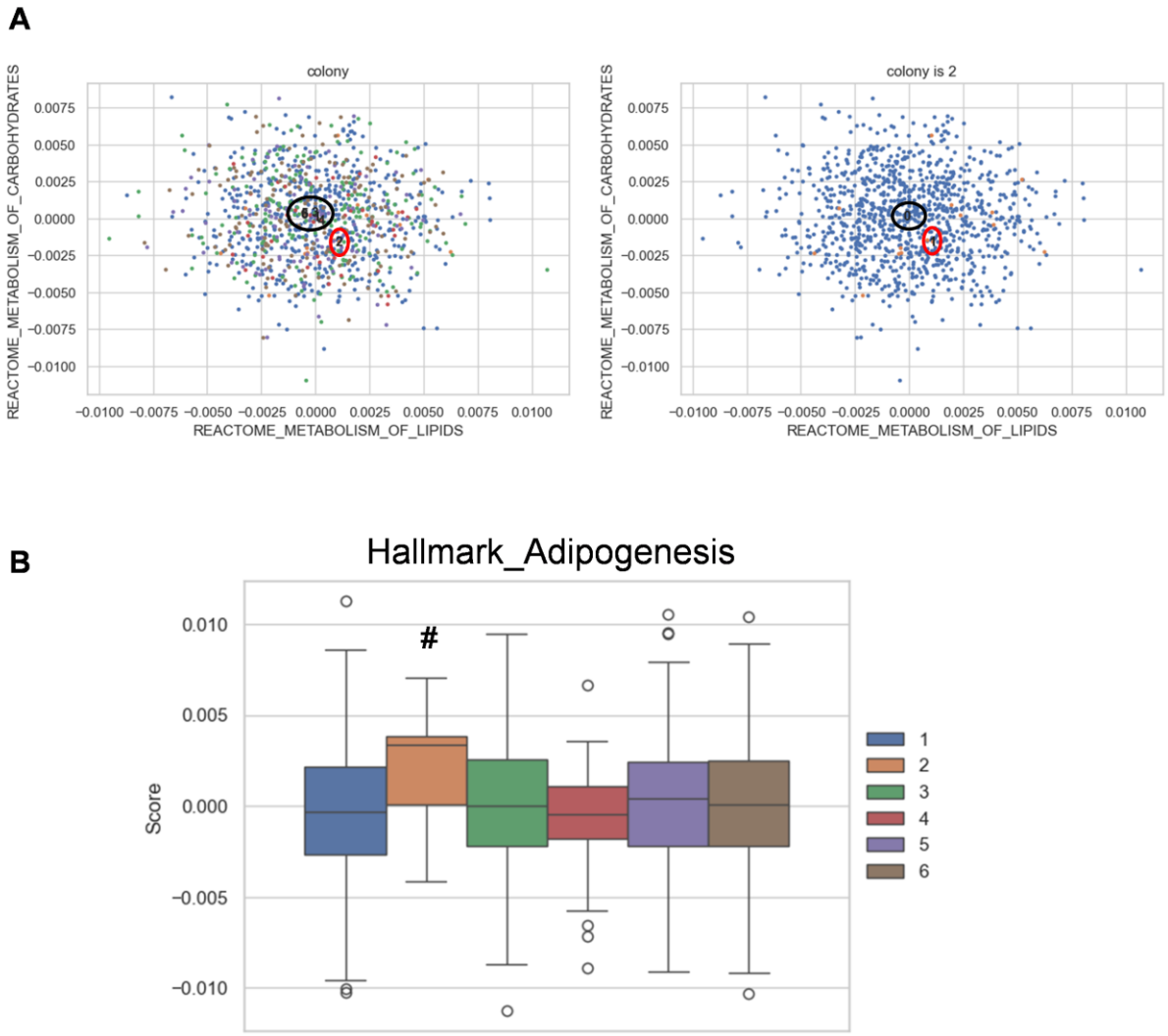

Figure S10: LVM analysis of scRNAseq data from HSC-like colonies using metabolism-related gene sets as Bayesian priors. (Related to Figure 5)

(A) Scatter plot of factor scores for gene signatures “metabolism of lipids” verses “metabolism of carbohydrates” amongst cells classified by colony. A positive factor score indicates positive association with the indicated gene signature. In the left panel, the colony numbers marked on the plots represent the centroids (density centers) among the cells of each colony. In the right panel, centroid of colony 2 is marked as “1”, and the centroid of all other colonies is marked as “0”. Colony 2 (red circle) separates from the remaining colonies (black circle), suggesting distinct metabolic features with a shift toward lipid metabolism.

(B) Quantitation of latent factor loading among colonies for the gene-set “Hallmark_Adipogenesis”. Colony 2 is marked by #.

Figure S11.

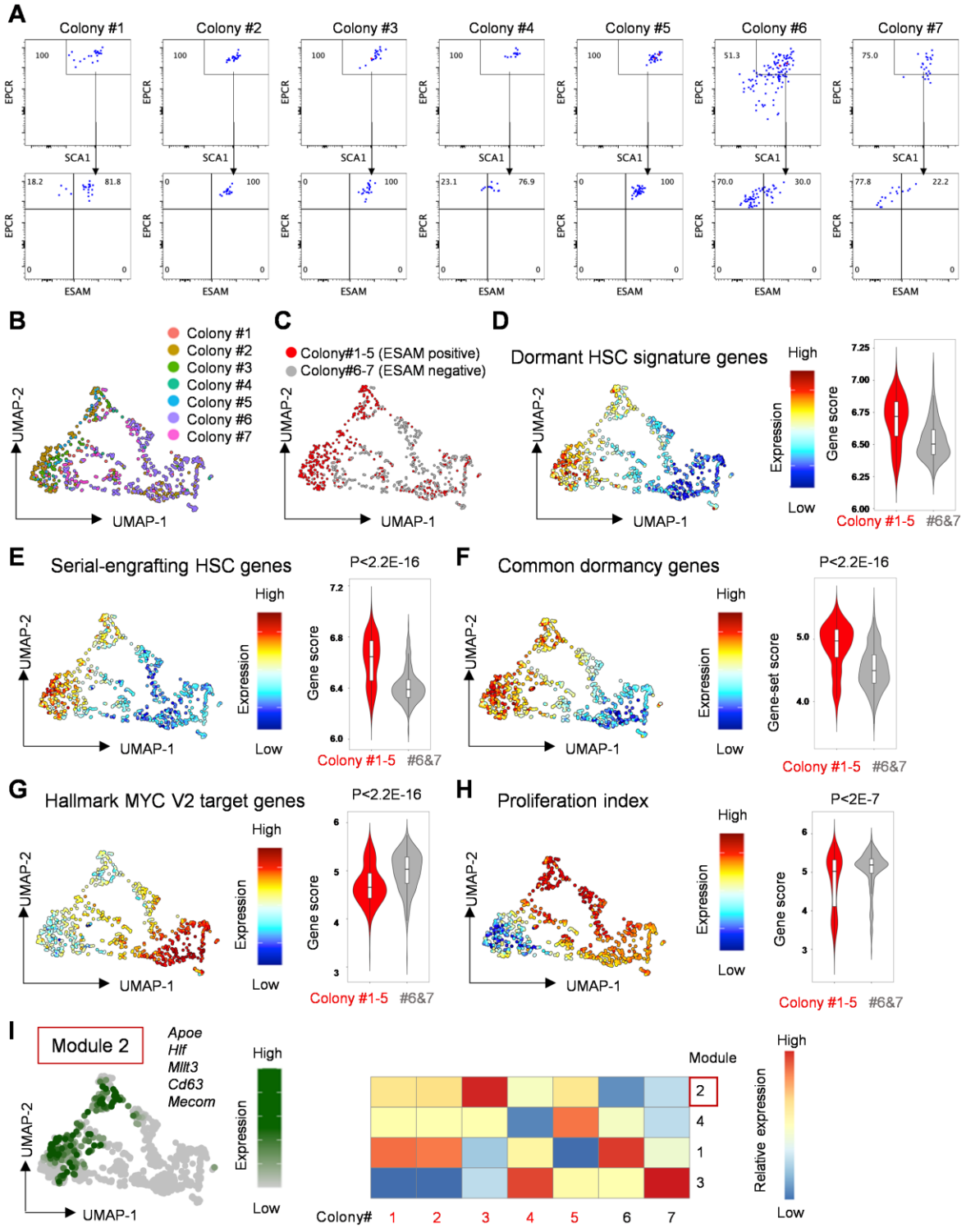
A
Colony #1
Colony #2
Colony #3
Colony #4
Colony #5
Colony #6
Colony #7
EPCR
SCA1
ESAM
B
Colony #1
Colony #2
Colony #3
Colony #4
Colony #5
Colony #6
Colony #7
UMAP-2
UMAP-1
C
Colony#1-5 (ESAM positive)
Colony#6-7 (ESAM negative)
D
Dormant HSC signature genes
High
Low
Expression
Gene score
Colony #1-5
#6&7
E
Serial-engrafting HSC genes
P<2.2E-16
F
Common dormancy genes
Gene-set score
G
Hallmark MYC V2 target genes
H
Proliferation index
P<2E-7
I
Module 2
Apoe
Hlf
Mllt3
Cd63
Mecom
Module
Colony#
Relative expression

Figure S11: scRNAseq analysis of ESAM$^+$ HSC colonies
(Related to Figure 5)

(A) Single E15.5 FL SE^{hi} cells were index sorted and cocultured with FL-AKT-EC. Flow cytometric analysis of colonies used for scRNAseq following coculture (n=7, day 13). Cells were initially gated as DAPI$^-$CD45$^+$Gr1$^-$F4/80$^-$. 25% of each colony was used for phenotyping and the remaining 75% were used for scRNAseq.

(B) UMAP of cells labeled by colony of origin (colony #1: 56 cells, colony #2: 212 cells, colony #3: 73 cells, colony #4: 16 cells, colony #5: 40 cells, colony #6: 319 cells, colony #7: 59 cells).

(C) UMAP of cells classified as ESAM$^+$ HSC colonies (#1-5, 397 cells) verses ESAM$^-$ colonies (#6-7, 378 cells).

(D) Heatmap of gene-set scores for dormant HSC signature genes.[6] Violin plots of gene-set scores by colony type. p values indicate Wilcoxon rank-sum test. (See Table S1 for gene-sets).

(E) Heatmap of gene-set scores for serial-engrafting HSC genes.[7] Violin plots of gene-set scores by colony type. p values indicate Wilcoxon rank-sum test.

(F) Heatmap of gene-set scores for common stem cell dormancy genes.[13] Violin plots of gene-set scores by colony type. p values indicate Wilcoxon rank-sum test.

(G) Heatmap of gene-set scores for Myc target genes (HALLMARK_MYC_TARGETS_V2). Violin plots of gene-set scores by colony type. p values indicate Wilcoxon rank-sum test.

(H) Heatmap of proliferation index. Violin plots of proliferation index by colony type. p values indicate Wilcoxon rank-sum test.

(I) Expression heatmaps for modules of co-regulated genes determined using Louvain community analysis. Gene modules 2 is shown in UMAP with representative genes (left). Heatmap of expression of gene modules by colony type (right).

Figure S12.

A

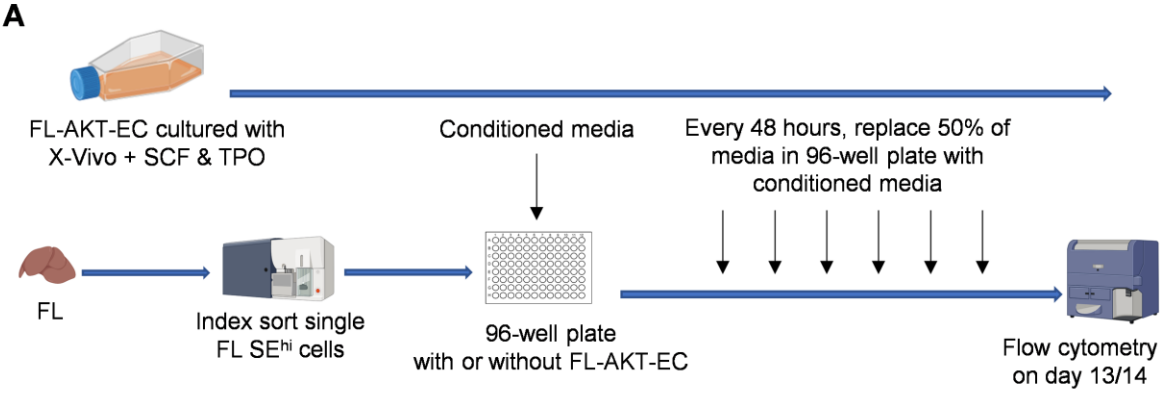

B

Experiment1

	Conditioned media with FL-AKT-EC	**Conditioned media without FL-AKT-EC**
ESAM⁺ HSC colonies	**20/48**	**1/48**

Experiment2

	Conditioned media with FL-AKT-EC	**Conditioned media without FL-AKT-EC**	**Standard media with FL-AKT-EC**	**Standard media without FL-AKT-EC**
ESAM⁺ HSC colonies	**18/48**	**0/48**	**23/48**	**0/48**

Figure S12: Conditioned media fails to support ESAM⁺ HSC colonies.
(A) Overview of the experimental design. Single index sorted E15.5/16.5 FL SE^{hi} cells were cultured in the presence or absence of FL-AKT-EC. FL-AKT-EC-conditioned media (or fresh standard media) was replenished every 48 hours during culture.
(B) The number of ESAM⁺ HSC colonies identified by flow cytometry in each experiment at end of culture (n=48 wells per cohort for each experiment).

Figure S13.

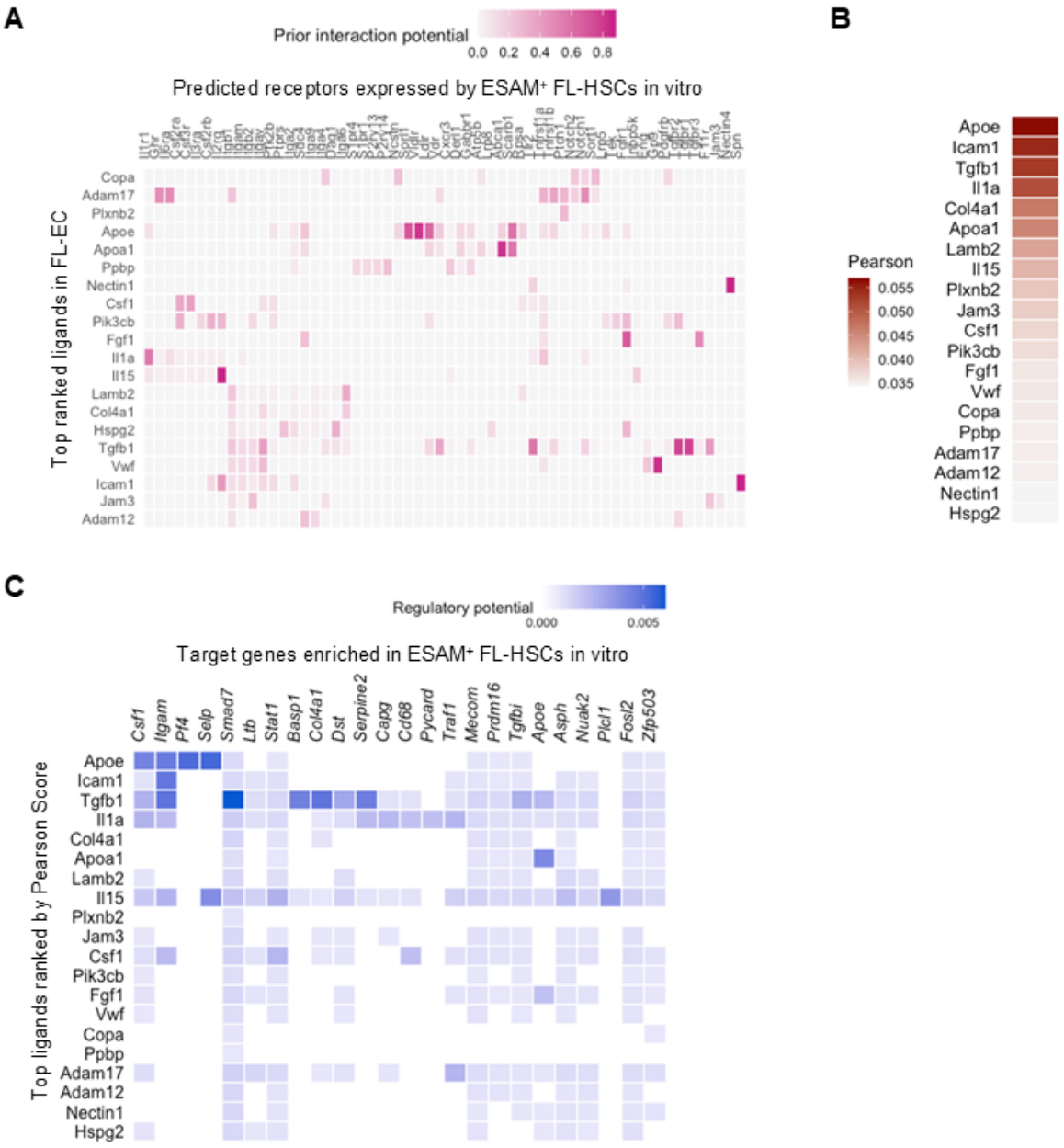
A
Prior interaction potential
0.0 0.2 0.4 0.6 0.8
Predicted receptors expressed by ESAM+ FL-HSCs in vitro
Top ranked ligands in FL-EC
Copa
Adam17
Plxnb2
Apoe
Apoa1
Ppbp
Nectin1
Csf1
Pik3cb
Fgf1
Il1a
Il15
Lamb2
Col4a1
Hspg2
Tgfb1
Vwf
Icam1
Jam3
Adam12
B
Pearson
0.055
0.050
0.045
0.040
0.035
Apoe
Icam1
Tgfb1
Il1a
Col4a1
Apoa1
Lamb2
Il15
Plxnb2
Jam3
Csf1
Pik3cb
Fgf1
Vwf
Copa
Ppbp
Adam17
Adam12
Nectin1
Hspg2
C
Regulatory potential
0.000
0.005
Target genes enriched in ESAM+ FL-HSCs in vitro
Csf1
Itgam
Pf4
Selp
Smad7
Ltb
Stat1
Basp1
Col4a1
Dst
Serpine2
Capg
Cd68
Pycard
Traf1
Mecom
Prdm16
Tgfbi
Apoe
Asph
Nuak2
Plcl1
Fosl2
Zfp503
Top ligands ranked by Pearson Score
Apoe
Icam1
Tgfb1
Il1a
Col4a1
Apoa1
Lamb2
Il15
Plxnb2
Jam3
Csf1
Pik3cb
Fgf1
Vwf
Copa
Ppbp
Adam17
Adam12
Nectin1
Hspg2

Figure S13: Analysis of scRNAseq data identifies candidate receptor-ligand interactions regulating self-renewal of serially engrafting FL-HSCs in the endogenous FL-EC niche. (Related to Figure 6).

scRNAseq data from E14 FL-EC were obtained from GEO (GSE174209).[18]

(A) Heatmap showing candidate ligands (expressed by FL-EC) interacting with receptors (expressed by cells in the serially engrafting HSC colony #2) inferred by NicheNet.

(B) Heatmap showing candidate ligands (expressed by FL-AKT-EC) ranked by Pearson correlation.

(C) Heatmap showing the regulatory potential between the top ranked ligands (expressed by FL-EC) and downstream genes whose expression is enriched in cells from the serially engrafting HSC colony (#2) compared to cells from other HSC colonies lacking serial engraftment.

Figure S14.

A

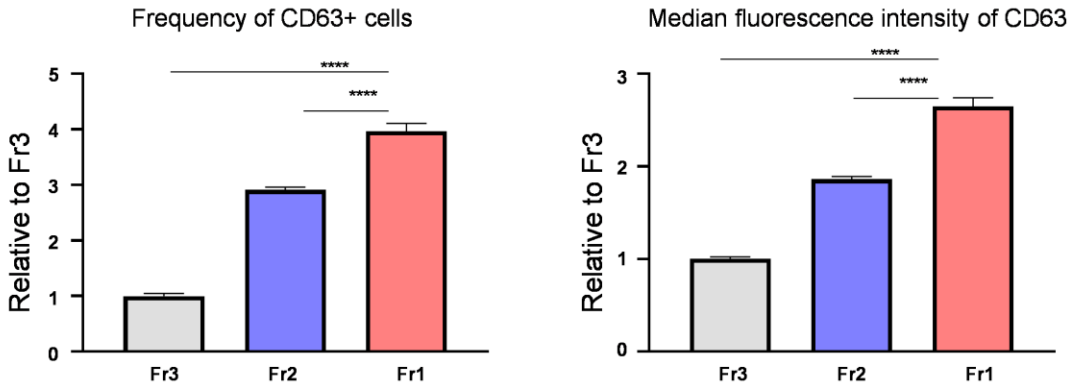

B

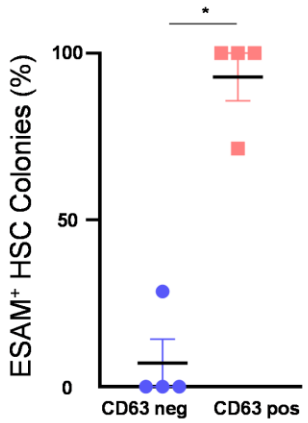

Experiment	ESAM+ HSC colonies from CD63+	ESAM+ HSC colonies from CD63-	CD63+ cells at sort	CD63- cells at sort
1	14	0	88	8
2	5	0	80	16
3	15	6	45	15
4	6	0	93	3

Figure S14: CD63 expression on FL-HSC colonies. (Related to Figure 7).
(A) Frequency of CD63 positive cells (left) and median fluorescence intensity of CD63 (right) in each fraction of cells from Figure 7D. 3 pooled FL samples from 4 different litters were used for analysis (total n=12) in 2 independent experiments. Values are normalized to Fr3 in each experiment. One-Way ANNOVA with Dunnett's multiple comparisons test was used for statistical comparison. **** P<0.0001
(B) Frequency of ESAM$^+$ HSC colonies arising from CD63 negative vs CD63 positive fraction of index sorted SE^{hi} FL cells, and summary of distribution of ESAM$^+$ HSC colonies based on CD63 expression at the time of index sorting. Total n=348 colonies from 4 independent experiments. Mann-Whitney testing was used for statistical analysis. *P<0.05.

Supplemental References

1. Hu, Y., and Smyth, G.K. (2009). ELDA: extreme limiting dilution analysis for comparing depleted and enriched populations in stem cell and other assays. J Immunol Methods *347*, 70-78. 10.1016/j.jim.2009.06.008.
2. Dignum, T., Varnum-Finney, B., Srivatsan, S.R., Dozono, S., Waltner, O., Heck, A.M., Ishida, T., Nourigat-McKay, C., Jackson, D.L., Rafii, S., et al. (2021). Multipotent progenitors and hematopoietic stem cells arise independently from hemogenic endothelium in the mouse embryo. Cell Reports *36*, 109675. https://doi.org/10.1016/j.celrep.2021.109675.
3. Srivatsan, S.R., McFaline-Figueroa, J.L., Ramani, V., Saunders, L., Cao, J., Packer, J., Pliner, H.A., Jackson, D.L., Daza, R.M., Christiansen, L., et al. (2020). Massively multiplex chemical transcriptomics at single-cell resolution. Science *367*, 45-51. 10.1126/science.aax6234.
4. Tirosh, I., Izar, B., Prakadan, S.M., Wadsworth, M.H., 2nd, Treacy, D., Trombetta, J.J., Rotem, A., Rodman, C., Lian, C., Murphy, G., et al. (2016). Dissecting the multicellular ecosystem of metastatic melanoma by single-cell RNA-seq. Science *352*, 189-196. 10.1126/science.aad0501.
5. Ceccacci, E., Villa, E., Santoro, F., Minucci, S., Ruhrberg, C., and Fantin, A. (2023). A Refined Single Cell Landscape of Haematopoiesis in the Mouse Foetal Liver. Journal of Developmental Biology *11*, 15.
6. Cabezas-Wallscheid, N., Buettner, F., Sommerkamp, P., Klimmeck, D., Ladel, L., Thalheimer, F.B., Pastor-Flores, D., Roma, L.P., Renders, S., Zeisberger, P., et al. (2017). Vitamin A-Retinoic Acid Signaling Regulates Hematopoietic Stem Cell Dormancy. Cell *169*, 807-823.e819. 10.1016/j.cell.2017.04.018.
7. Rodriguez-Fraticelli, A.E., Weinreb, C., Wang, S.W., Migueles, R.P., Jankovic, M., Usart, M., Klein, A.M., Lowell, S., and Camargo, F.D. (2020). Single-cell lineage tracing unveils a role for TCF15 in haematopoiesis. Nature *583*, 585-589. 10.1038/s41586-020-2503-6.
8. Weinreb, C., Rodriguez-Fraticelli, A., Camargo, F.D., and Klein, A.M. (2020). Lineage tracing on transcriptional landscapes links state to fate during differentiation. Science *367*. 10.1126/science.aaw3381.
9. Boroviak, T., Loos, R., Lombard, P., Okahara, J., Behr, R., Sasaki, E., Nichols, J., Smith, A., and Bertone, P. (2015). Lineage-Specific Profiling Delineates the Emergence and Progression of Naive Pluripotency in Mammalian Embryogenesis. Dev Cell *35*, 366-382. 10.1016/j.devcel.2015.10.011.
10. Schönberger, K., Obier, N., Romero-Mulero, M.C., Cauchy, P., Mess, J., Pavlovich, P.V., Zhang, Y.W., Mitterer, M., Rettkowski, J., Lalioti, M.E., et al.

(2022). Multilayer omics analysis reveals a non-classical retinoic acid signaling axis that regulates hematopoietic stem cell identity. Cell Stem Cell *29*, 131-148.e110. 10.1016/j.stem.2021.10.002.

11. García-Prat, L., Kaufmann, K.B., Schneiter, F., Voisin, V., Murison, A., Chen, J., Chan-Seng-Yue, M., Gan, O.I., McLeod, J.L., Smith, S.A., et al. (2021). TFEB-mediated endolysosomal activity controls human hematopoietic stem cell fate. Cell Stem Cell *28*, 1838-1850.e1810. 10.1016/j.stem.2021.07.003.
12. Calvanese, V., Capellera-Garcia, S., Ma, F., Fares, I., Liebscher, S., Ng, E.S., Ekstrand, S., Aguadé-Gorgorió, J., Vavilina, A., Lefaudeux, D., et al. (2022). Mapping human haematopoietic stem cells from haemogenic endothelium to birth. Nature. 10.1038/s41586-022-04571-x.
13. van der Weijden, V.A., Stötzel, M., Iyer, D.P., Fauler, B., Gralinska, E., Shahraz, M., Meierhofer, D., Vingron, M., Rulands, S., Alexandrov, T., et al. (2024). FOXO1-mediated lipid metabolism maintains mammalian embryos in dormancy. Nat Cell Biol *26*, 181-193. 10.1038/s41556-023-01325-3.
14. Wilson, N.K., Kent, D.G., Buettner, F., Shehata, M., Macaulay, I.C., Calero-Nieto, F.J., Sánchez Castillo, M., Oedekoven, C.A., Diamanti, E., Schulte, R., et al. (2015). Combined Single-Cell Functional and Gene Expression Analysis Resolves Heterogeneity within Stem Cell Populations. Cell Stem Cell *16*, 712-724. 10.1016/j.stem.2015.04.004.
15. Che, J.L.C., Bode, D., Kucinski, I., Cull, A.H., Bain, F., Becker, H.J., Jassinskaja, M., Barile, M., Boyd, G., Belmonte, M., et al. (2022). Identification and characterization of in vitro expanded hematopoietic stem cells. *23*, e55502. https://doi.org/10.15252/embr.202255502.
16. Duy, C., Li, M., Teater, M., Meydan, C., Garrett-Bakelman, F.E., Lee, T.C., Chin, C.R., Durmaz, C., Kawabata, K.C., Dhimolea, E., et al. (2021). Chemotherapy Induces Senescence-Like Resilient Cells Capable of Initiating AML Recurrence. Cancer Discovery *11*, 1542-1561. 10.1158/2159-8290.Cd-20-1375.
17. Schönberger, K., Obier, N., Romero-Mulero, M.C., Cauchy, P., Mess, J., Pavlovich, P.V., Zhang, Y.W., Mitterer, M., Rettkowski, J., Lalioti, M.E., et al. (2021). Multilayer omics analysis reveals a non-classical retinoic acid signaling axis that regulates hematopoietic stem cell identity. Cell Stem Cell. 10.1016/j.stem.2021.10.002.
18. Gómez-Salinero, J.M., Izzo, F., Lin, Y., Houghton, S., Itkin, T., Geng, F., Bram, Y., Adelson, R.P., Lu, T.M., Inghirami, G., et al. (2022). Specification of fetal liver endothelial progenitors to functional zonated adult sinusoids requires c-Maf induction. Cell Stem Cell *29*, 593-609.e597. 10.1016/j.stem.2022.03.002.